JSCSEN 88(5)467–575(2023)

ISSN 1820-7421(Online)

Journal of the Serbian Chemical Society

Electronic version

VOLUME 88

No 5

BELGRADE 2023

Available on line at

www.shd.org.rs/JSCS/

The full search of JSCS is available through

DOAJ DIRECTORY OF OPEN ACCESS JOURNALS

www.doaj.org

The **Journal of the Serbian Chemical Society** (formerly Glasnik Hemijskog društva Beograd), one volume (12 issues) per year, publishes articles from the fields of chemistry. The **Journal** is financially supported by the **Ministry of Education, Science and Technological Development of the Republic of Serbia.**

Articles published in the **Journal** are indexed in **Clarivate Analytics products: Science Citation Index-Expanded™** – accessed *via* **Web of Science®** and **Journal Citation Reports®**.

Impact Factor announced 2022: **1.100; 5-year Impact Factor**: **1.175**.

Articles appearing in the **Journal** are also abstracted by: **Scopus, Chemical Abstracts Plus (CAplus℠), Directory of Open Access Journals, Referativnii Zhurnal (VINITI), RSC Analytical Abstracts, EuroPub, Pro Quest** and **Asian Digital Library.**

Publisher:	**Serbian Chemical Society**, Karnegijeva 4/III, P. O. Box 36, 1120 Belgrade 35, Serbia tel./fax: +381–11–3370–467, E-mails: **Society** – shd@shd.org.rs; **Journal** – jscs@shd.org.rs Home Pages: **Society** – http://www.shd.org.rs/, **Journal** – http://www.shd.org.rs/JSCS/
Internet Service:	Contents, Abstracts and full papers (from Vol 64, No. 1, 1999) are available in the electronic form at the Web Site of the **Journal** (http://www.shd.org.rs/JSCS/).
Former Editors:	**Nikola A. Pušin** (1930–1947), **Aleksandar M. Leko** (1948–1954), **Panta S. Tutundžić** (1955–1961), **Miloš K. Mladenović** (1962–1964), **Đorđe M. Dimitrijević** (1965–1969), **Aleksandar R. Despić** (1969–1975), **Slobodan V. Ribnikar** (1975–1985), **Dragutin M. Dražić** (1986–2006).
Editor-in-Chief:	BRANISLAV Ž. **NIKOLIĆ**, Serbian Chemical Society (E-mail: jscs-ed@shd.org.rs)
Deputy Editor:	DUŠAN **SLADIĆ**, Faculty of Chemistry, University of Belgrade
Sub editors:	
Organic Chemistry	DEJAN **OPSENICA**, Institute of Chemistry, Technology and Metallurgy, University of Belgrade JÁNOS **CSANÁDI**, Faculty of Science, University of Novi Sad
Biochemistry and Biotechnology	OLGICA **NEDIĆ**, INEP – Institute for the Application of Nuclear Energy, University of Belgrade
Inorganic Chemistry	MILOŠ **ĐURAN**, Serbian Chemical Society
Theoretical Chemistry	IVAN **JURANIĆ**, Serbian Chemical Society
Physical Chemistry	LJILJANA **DAMJANOVIĆ-VASILIĆ**, Faculty of Physical Chemistry, University of Belgrade
Electrochemistry	SNEŽANA **GOJKOVIĆ**, Faculty of Technology and Metallurgy, University of Belgrade
Analytical Chemistry	SLAVICA **RAŽIĆ**, Faculty of Pharmacy, University of Belgrade
Polymers	BRANKO **DUNJIĆ**, Faculty of Technology and Metallurgy, University of Belgrade
Thermodynamics	MIRJANA **KIJEVČANIN**, Faculty of Technology and Metallurgy, University of Belgrade
Chemical Engineering	TATJANA **KALUĐEROVIĆ RADOIČIĆ**, Faculty of Technology and Metallurgy, University of Belgrade
Materials	RADA **PETROVIĆ**, Faculty of Technology and Metallurgy, University of Belgrade
Metallic Materials and Metallurgy	ANA **KOSTOV**, Mining and Metallurgy Institute Bor, University of Belgrade
Environmental and Geochemistry	VESNA **ANTIĆ**, Faculty of Agriculture, University of Belgrade
History of and Education in Chemistry	DRAGICA **TRIVIĆ**, Faculty of Chemistry, University of Belgrade
English Language Editors:	LYNNE **KATSIKAS**, Serbian Chemical Society VLATKA **VAJS**, Serbian Chemical Society JASMINA **NIKOLIĆ**, Faculty of Technology and Metallurgy, University of Belgrade
Technical Editors:	VLADIMIR **PANIĆ**, Institute of Chemistry, Technology and Metallurgy, University of Belgrade, MARIO **ZLATOVIĆ**, Faculty of Chemistry, University of Belgrade
Journal Manager & Web Master:	MARIO **ZLATOVIĆ**, Faculty of Chemistry, University of Belgrade
Office:	VERA **ĆUŠIĆ**, Serbian Chemical Society

Editorial Board

From abroad: **R. Adžić**, Brookhaven National Laboratory (USA); **A. Casini**, University of Groningen (The Netherlands); **G. Cobb**, Baylor University (USA); **D. Douglas**, University of British Columbia (Canada); **G. Inzelt**, Etvos Lorand University (Hungary); **J. Kenny**, University of Perugia (Italy); **Ya. I. Korenman**, Voronezh Academy of Technology (Russian Federation); **M. D. Lechner**, University of Osnabrueck (Germany); **S. Macura**, Mayo Clinic (USA); **M. Spiteller**, INFU, Technical University Dortmund (Germany); **M. Stratakis**, University of Crete (Grecce); **M. Swart**, University de Girona (Cataluna, Spain); **G. Vunjak-Novaković**, Columbia University (USA); **P. Worsfold**, University of Plymouth (UK); **J. Zagal**, Universidad de Santiago de Chile (Chile).

From Serbia: **B. Abramović**, **V. Antić**, **V. Beškoski**, **J. Csanadi**, **Lj. Damjanović-Vasilić**, **A. Dekanski**, **V. Dondur**, **B. Dunjić**, **M. Đuran, S. Gojković**, **I. Gutman**, **B. Jovančićević**, **I. Juranić**, **T. Kaluđerović Radoičić**, **L. Katsikas**, **M. Kijevčanin**, **A. Kostov**, **V. Leovac**, **S. Milonjić**, **V.B. Mišković-Stanković**, **O. Nedić**, **B. Nikolić**, **J. Nikolić**, **D. Opsenica**, **V. Panić**, **M. Petkovska**, **R. Petrović**, **I. Popović**, **B. Radak**, **S. Ražić**, **D. Sladić**, **S. Sovilj**, **S. Šerbanović**, **B. Šolaja**, **Ž. Tešić**, **D. Trivić**, **V. Vajs, M. Zlatović**.

Subscription: The annual subscription rate is **150.00 €** including postage (surface mail) and handling. For Society members from abroad rate is **50.00 €**. For the proforma invoice with the instruction for bank payment contact the Society Office (E-mail: shd@shd.org.rs) or see JSCS Web Site: http://www.shd.org.rs/JSCS/, option Subscription.

Godišnja pretplata: Za članove SHD: **2.500,00 RSD**, za penzionere i studente: **1000,00 RSD**, a za ostale: **3.500,00 RSD**:za organizacije i ustanove: **16.000,00 RSD**. Uplate se vrše na tekući račun Društva: **205-13815-62**, poziv na broj **320**, sa naznakom "pretplata za JSCS".

Nota: Radovi čiji su svi autori članovi SHD prioritetno se publikuju.

Odlukom Odbora za hemiju Republičkog fonda za nauku Srbije, br. 66788/1 od 22.11.1990. godine, koja je kasnije potvrđena odlukom Saveta Fonda, časopis je uvršten u kategoriju međunarodnih časopisa (**M-23**). Takođe, aktom Ministarstva za nauku i tehnologiju Republike Srbije, 413-00-247/2000-01 od 15.06.2000. godine, ovaj časopis je proglašen za publikaciju od posebnog interesa za nauku. **Impact Factor** časopisa objavljen 2022. godini iznosi **1,100**, a petogodišnji **Impact Factor 1,175**.

Journal of the Serbian Chemical Society
JSCS-info@shd.org.rs • www.shd.org.rs/JSCS

J. Serb. Chem. Soc. Vol. 88, No. 5 (2023)

CONTENTS*

Organic Chemistry

V. Kojić, *M. Svirčev*, *S. Djokić*, *I. Kovačević*, *M. V. Rodić*, *B. Srećo Zelenović*, *V. Popsavin* and *M. Popsavin*: Synthesis and antiproliferative activity of new thiazole hybrids with [3.3.0]furofuranone or tetrahydrofuran scaffolds 467

L. M. Breberina, *M. R. Nikolić*, *S. Đ. Stojanović* and *M. V. Zlatović*: On the importance of π–π interactions in the structural stability of phycocyanins 481

Biochemistry and Biotechnology

M. R. Alias, *C.-B. Ong* and *M. S. M. Annuar*: Adsorption of tannase from *Aspergillus ficuum* to carboxyl-functionalized multi-walled carbon nanotubes 495

Theoretical Chemistry

M. Aissaoui, *B. Belhani*, *A. Boulebnane*, *A. Bouzina* and *S. Eddine Djilani*: Diversifying the chloroquinoline scaffold against SARS-CoV-2 main protease: Virtual screening approach using cross-docking, SiteMap analysis and molecular dynamics simulation 505

Electrochemistry

O. C. Bodur, *M. Keskin*, *B. A. Avan* and *H. Arslan*: Designing an electrochemical biosensor based on tyrosinase for highly sensitive and rapid detection of bisphenol A and its derivatives 521

Materials

A. G. Krkobabić, *J. D. Stojičić*, *M. M. Radetić* and *D. D. Marković*: Biosynthesis of silver-based nanoparticles on polypropylene non-woven material for efficient antimicrobial activity 537

Environmental

M. Kašanin-Grubin, *G. Veselinović*, *N. Antić*, *G. Gajica*, *S. Stojadinović*, *A. Šajnović* and *S. Štrbac*: The influence of geological setting and land use on the physical and chemical properties of the soil at the Fruška Gora Mountain 551

History of and Education in Chemistry

A. Naumoska, *H. Dimeski* and *M. Stojanovska*: Using the Escape Room game-based approach in chemistry teaching 563

Published by the Serbian Chemical Society
Karnegijeva 4/III, P.O. Box 36, 11120 Belgrade, Serbia
Printed by the Faculty of Technology and Metallurgy
Karnegijeva 4, P.O. Box 35-03, 11120 Belgrade, Serbia

* For colored figures in this issue please see electronic version at the Journal Home Page: http://www.shd.org.rs/JSCS/

Journal of the Serbian Chemical Society
JSCS@tmf.bg.ac.rs • www.shd.org.rs/JSCS
J. Serb. Chem. Soc. *88* (5) 467–479 (2023)
JSCS–5639
Original scientific paper
Published 14 April 2023

Synthesis and antiproliferative activity of new thiazole hybrids with [3.3.0]furofuranone or tetrahydrofuran scaffolds

VESNA KOJIĆ[1], MILOŠ SVIRČEV[2#], SANJA DJOKIĆ[2#], IVANA KOVAČEVIĆ[2#], MARKO V. RODIĆ[2#], BOJANA SREĆO ZELENOVIĆ[2#], VELIMIR POPSAVIN[2,3*#] and MIRJANA POPSAVIN[2#]

[1]*University of Novi Sad, Faculty of Medicine, Oncology Institute of Vojvodina, Put Dr Goldmana 4, 21204 Sremska Kamenica, Serbia,* [2]*University of Novi Sad, Faculty of Sciences, Department of Chemistry, Biochemistry and Environmental Protection, Trg Dositeja Obradovića 3, 21000 Novi Sad, Serbia and* [3]*Serbian Academy of Sciences and Arts, Kneza Mihaila 35, 11000 Belgrade, Serbia*

(Received 30 November 2022, accepted 11 January 2023)

Abstract: New thiazole hybrids were synthesized and evaluated for their *in vitro* cytotoxicity against a panel of human malignant cell lines. The key steps in the synthesis of hybrids **3**–**7** involved the initial condensation of appropriate aldononitriles with cysteine ethyl ester hydrochloride, followed by subsequent treatment of resulting thiazolines with diazabicycloundecene to form the thiazole ring. Bioisosteres **8** and **14** have been prepared after the stereoselective addition of 2-(trimethylsilyl)thiazole to the hemiacetals obtained by periodate cleavage of terminal diol functionality in the suitably protected d-glucose derivatives. The obtained analogues showed various antiproliferative activities in the cultures of several tumour cell lines. Hybrid **6** was the most potent in HeLa cells, exhibiting more than 10 and 4 times stronger activity than both leads **1** and **2**, respectively. The most active compound in Raji cells was hybrid **12**, which was nearly 2-fold more potent than the clinical antitumour drug doxorubicin. All analogues were more potent in A549 cells with respect to lead **1**, while compounds **6** and **7** were slightly more active than doxorubicin. Preliminary structure–activity relationship analysis revealed that the presence of a cinnamate group at the C-3 position in analogues of type **7** increases the activity of resulting molecular hybrids.

Keywords: molecular hybridization; pseudo-*C*-nucleosides; goniofufurone; tiazofurin; analogues; antiproliferative activity.

* Corresponding author. E-mail: velimir.popsavin@dh.uns.ac.rs
# Serbian Chemical Society member.
https://doi.org/10.2298/JSC221130002K

INTRODUCTION

Molecular hybridization is a strategy of rational drug design based on the combination of pharmacophoric moieties of different bioactive substances to produce a new hybrid compound with improved affinity and efficacy, when compared to the parent drugs. In addition, this strategy may provide access to compounds with modified selectivity profiles, different or dual modes of action, and reduced unfavourable side effects.[1–3] Thiazole ring is a pharmacophore nucleus with various pharmaceutical applications. Its derivatives have a wide range of biological activities including anticancer activity.[4,5] We have recently reported on the synthesis of several thiazole bioisosteres of goniofufurone that exhibited *in vitro* antitumour activity against some human tumour cell lines.[6] Goniofufurone (**1**, Fig. 1) is natural styryl lactone with [3.3.0]furofuranone core,[7] which was isolated from the stem bark of tropical plant *Goniothalamus giganteus* (Annonaceae), and showed potent antiproliferative activity against several tumour cell lines.[8] This work describes the synthesis and *in vitro* antitumour screening of several new thiazole hybrids with furofuranone or tetrahydrofuran scaffolds. Compounds **3**–**5** might be considered pseudo-*C*-nucleosides related to tiazofurin (**2**), the oncolytic *C*-nucleoside with potent antileukaemic activity.[9,10] Pseudo-*C*--nucleosides are nucleoside analogues having a C–C bond between C-4 of the carbohydrate moiety and the heterocyclic aglycone.[11] Compound **8** represents a goniofufurone analogue with a thiazole replacing the phenyl ring at the C-7 position.

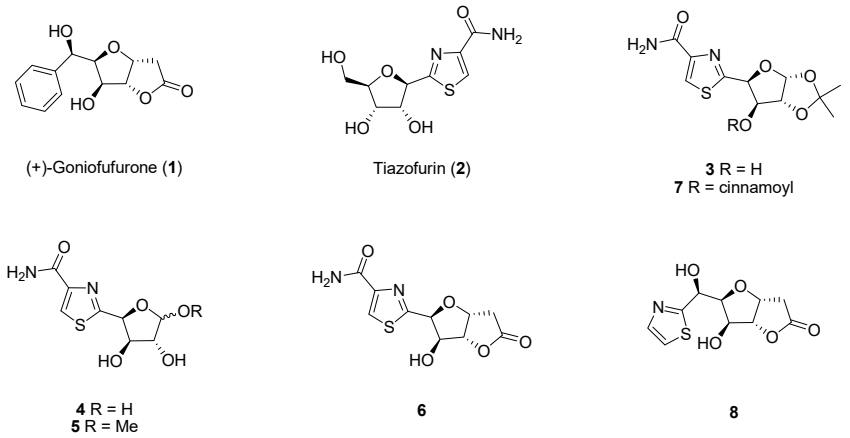

Fig. 1. Structures of (+)-goniofufurone (**1**), tiazofurin (**2**) and the corresponding analogues **3**–**8**.

EXPERIMENTAL

General procedures

Melting points were determined on a Büchi 510, or a hot stage microscope Nagema PHMK 05 apparatus, and were not corrected. Optical rotations were measured on a Rudolph

Research Analytical automatic polarimeter, Autopol IV. IR spectra were recorded on a FTIR Nexus 670 (Thermo-Nicolet) spectrophotometer. ^{1}H- and ^{13}C-NMR spectra were recorded on a Bruker AC 250 E (at 250 and 62.5 MHz, respectively) or a Bruker Avance III spectrometer (at 400 and 100 MHz, respectively) employing indicated solvents (*vide infra*) using TMS as the internal standard. Chemical shifts were expressed in ppm (δ) values and coupling constants in Hz (J). High-resolution mass spectra were taken on a Micromass LCT KA111 spectrometer or LTQ Orbitrap XL (Thermo Fisher Scientific Inc.) mass spectrometer. TLC was performed on DC Alufolien Kieselgel 60 F254 (E. Merck). Flash column chromatography was performed using Kieselgel 60 (0.040–0.063, E. Merck). All organic extracts were dried with anhydrous Na_2SO_4. Organic solutions were concentrated in a rotary evaporator under reduced pressure at a bath temperature below 35 °C. The purity of tested compounds was determined by HRMS and they were found to be > 95 % pure (errors were less than 5 ppm).

Synthetic procedures

*(*E,Z*)-1,2*-O-*Isopropylidene-α-D*-xylo-*pentodialdo-1,4-furanose-5-oxime (**10**).* To a stirred and cooled (0 °C) solution of triol **9** (2.032 g, 9.23 mmol) in a mixture of 2:1 MeOH/H_2O (54 mL) was added $NaIO_4$ (1.795 g, 10.49 mmol) in one portion. After 5 min, the cooling was stopped, and the reaction continues at room temperature for the next 4.5 h. The mixture was filtered through a Celite pad, the adsorbent was washed with MeOH, the filtrate was evaporated, and the residue was suspended in H_2O (10 mL) and extracted with EtOAc (3×50 mL). The extract was dried (Na_2CO_3 and Na_2SO_4), filtered, and evaporated to give the crude aldehyde **9a** (1.13 g) which was dried under a high vacuum overnight.

Suspension of crude aldehyde **9a** (1.631 g), sodium acetate (1.677 g, 20.40 mmol), and hydroxylamine hydrochloride (2.236 g, 32.10 mmol) in EtOH (40.75 mL) was vigorously stirred at room temperature for 24 h. The reaction mixture was evaporated, and the residue was purified by flash column chromatography (1:1 toluene/EtOAc). A mixture of *E*- and *Z*--oximes **10** (1.463 g, 78 % from **9**) was obtained as an amorphous powder, R_f = 0.27 (12:1 $CHCl_3$/ /MeOH). The ratio of isomers (from ^{1}H-NMR): *E*/*Z* = 1:0.8.

3-O-*Acetyl-1,2*-O-*isopropylidene*-α-*D*-xylo-*furanoseurononitrile (**11**).* A solution of compound **10** (1.463 g, 7.20 mmol) in acetic anhydride (29 mL) was stirred at reflux temperature for 1 h, and then evaporated. The residue was purified by flash column chromatography (19:1 toluene/EtOAc) to afford pure **11** (1.502 g, 92 %), as a colourless syrup, $[\alpha]_D$ = = +7.7 (*c* 1.0, $CHCl_3$), R_f = 0.53 (9:1 toluene/EtOAc).

3-O-*Acetyl-1,2*-O-*isopropylidene-4*-C-*(4'-ethoxycarbonylthiazol-2'-yl)*-α-*D*-xylo-*tetrofuranose (**12**).* To a stirred solution of **11** (0.999 g, 4.39 mmol) in absolute ethanol (85 mL) L--cysteine ethyl ester hydrochloride (1.217 g, 6.56 mmol) and anhydrous Et_3N (0.91 mL, 6.55 mmol) were added. The reaction mixture was stirred at room temperature for 3.5 h and then evaporated. The residue was dissolved in CH_2Cl_2 (50 mL), the organic phase was washed with water (15 mL), a saturated solution of $NaHCO_3$ (15 mL), and a saturated solution of NaCl (15 mL) then dried, filtered, and evaporated. A mixture of crude thiazoline derivatives **11a** (1.3279 g) was obtained.

To a solution of crude thiazolines **11a** (1.328 g, 3.70 mmol) in dry CH_2Cl_2 (27 mL) was added DBU (1.11 mL, 7.44 mmol). To the cooled solution (0 °C) was added $BrCCl_3$ (0.31 mL, 3.14 mmol), the reaction mixture was stirred at 0 °C for 2.5 h and then left at 4 °C for another 43 h and then evaporated. The residue was purified on a column of flash silica (9:1 → 4:1 toluene/EtOAc) to give pure product **12** (1.100 g, 87 % based on reacted **11**) as a yellow syrup. Recrystallization from CH_2Cl_2/hexane gave white needles, mp 141 °C, $[\alpha]_D$ = −23.0 (*c* 0.1, $CHCl_3$), R_f = 0.50 (7:3 toluene/EtOAc).

4-C-*(4'-(Carbamoyl)thiazol-2'-yl)-1,2-O-isopropylidene*-α-*D*-xylo-*tetrofuranose (**3**).* A solution of protected thiazole **12** (1.100 g, 3.08 mmol) in saturated methanolic ammonia (25 ml) was kept at room temperature for 7 days. The reaction mixture was then evaporated and purified by flash column chromatography ($CHCl_3$ → 12:1 $CHCl_3$/MeOH), to give pure **3** (0.498 g, 93 %) as a colourless syrup, $[\alpha]_D = -46.5$ (*c* 0.2, MeOH), $R_f = 0.30$ (12:1 $CHCl_3$/MeOH).

4-C-*(4'-(Carbamoyl)thiazol-2'-yl)-D*-xylo-*tetrofuranose (**4**).* A solution of **3** (0.312 g, 1.09 mmol) in 90 % aq TFA (18 mL) was stirred at 0 °C for 0.5 h and then at room temperature for 4.5 h. The reaction mixture was evaporated by azeotropic distillation with toluene. The remaining oily mixture was treated with EtOAc (2 mL) and saturated $NaHCO_3$ (2 mL) and evaporated again whereby a mixture of anomeric lactols **4** was obtained as a syrup. The residue was purified on a column of flash silica (5:1 → 25:6 → 10:3 $CHCl_3$/MeOH) to give pure product **4** (0.240 g, 89 %) in the form of pale yellow syrup, $R_f = 0.34$ (5:1 $CHCl_3$/MeOH). Anomeric ratio (from ^{1}H-NMR): α/β = 1:1.

Methyl 4-C-*(4'-(carbamoyl)thiazol-2'-yl)-D*-xylo-*tetrofuranoside (**5**)*. A solution of **3** (0.100 g, 0.35 mmol) in 90 % aq TFA (5.80 mL) was stirred at 0 °C for 0.5 h and then at room temperature for 4.5 h. The reaction mixture was evaporated by azeotropic distillation with toluene and methanol. The residue was purified by preparative thin-layer chromatography (2 preparative plates, 5:1 $CHCl_3$/MeOH, eluted with 7:3 EtOAc/^{i}PrOH), whereby a mixture of anomeric glycosides **5** (0.048 g, 52 %) was obtained, in the form of white powder, $R_f = 0.38$ (5:1 $CHCl_3$/MeOH). Anomeric ratio (from ^{1}H-NMR): α/β = 2:1.

3,6-Anhydro-2-deoxy-6-C-*(4'-(carbamoyl)thiazol-2'-yl)-D-ido-hexono-1,4-lactone (**6**)*. A) To a solution of compound **4** (0.202 g, 0.82 mmol) in anhydrous DMF (3.5 mL) was added Meldrum's acid (0.394 g, 2.73 mmol) and dry Et_3N (0.36 mL, 2.583 mmol). The reaction mixture was stirred at 46 °C for 69 h and then evaporated. The crude product was purified by preparative thin-layer chromatography (10 preparative plates, 6:1 $CHCl_3$/MeOH, eluted with 12:1 $CHCl_3$/MeOH), whereby impure **6** was obtained. After additional purification on a column of flash silica (20:1 → 12:1 $CHCl_3$/MeOH) and then by preparative thin-layer chromatography (2 preparative plates, 6:1 $CHCl_3$/MeOH, eluted with 12:1 $CHCl_3$/MeOH), pure product **6** was obtained as a white powder (0.015 g, 7 %), $R_f = 0.22$ (12:1 $CHCl_3$/MeOH). Analytical sample **6** was obtained by crystallization from MeOH in the form of white needles, m.p. 143 °C. B) To a cooled (0 °C) solution of **4** (0.204 g, 0.83 mmol) in dry MeOH (23 mL) was added MCMP (0.7923, 2.37 mmol) and the resulting solution was stirred at room temperature for 1 h. The reaction mixture was evaporated, and the residue was purified on a column of flash silica (20:1 → 12:1 $CHCl_3$/MeOH to give pure **6** as a yellow oil (0.050 g, 22 %), $[\alpha]_D$ = = −9.4 (*c* 0.13, DMSO), $R_f = 0.22$ (12:1 $CHCl_3$/MeOH). Analytical sample **6** was obtained by crystallization from MeOH as colourless needles, m.p. 143 °C.

4-C-*(4'-Carbamoyl)thiazol-2'-yl)-3*-O-*cinnamoyl-1,2*-O-*isopropylidene*-α-*D*-xylo-*tetrofuranose (7)*. To a stirred solution of compound **3** (0.0757 g, 0.2644 mmol) in a mixture of anhydrous MeCN (2 mL) and anhydrous CH_2Cl_2 (14.5 mL) was added cinnamic acid (0.088 g, 0.59 mmol), DCC (0.132 g, 0.64 mmol) and DMAP (0.130 g, 1.07 mmol). After stirring at room temperature for 24 h, the reaction mixture was filtered through a pad of quartz sand, the filtrate concentrated and purified by preparative thin-layer chromatography (5 preparative plates, 12:1 $CHCl_3$/MeOH, eluted with 7:3 EtOAc/^{i}PrOH), to give pure **7** as a white powder (0.103 g, 94 %). Analytical sample **7**, obtained by crystallization from a mixture of MeOH/$^i Pr_2O$ showed mp 180 °C, $[\alpha]_D = -157.1$ (*c* 0.40, $CHCl_3$), $R_f = 0.66$ (12:1 $CHCl_3$/MeOH).

3,6-Anhydro-2-deoxy-7-C-*(thiazol-2'-yl)-D-glycero-D*-ido-*heptono-1,4-lactone (**8**)*. To a stirred solution of compound **10**[12] (0.145 g, 0.71 mmol) in anhydrous MeCN (15 mL) was

added H_5IO_6 (0.146 g, 0.64 mmol). After stirring at room temperature for 22 h, the reaction mixture was evaporated with silica gel and purified by flash chromatography (9:1 CH_2Cl_2/ /Me_2CO). This gave pure **7a** (0.108 g, 75 %).

To the solution of **7a** (0.069 g, 0.34 mmol) in anhydrous THF (3 mL) 2-TST solution (0.081 mL, 0.51 mmol) in THF (1 mL) is added dropwise. The reaction mixture was stirred at room temperature for 48 h and then evaporated. The residue was dissolved in THF (3 mL) and treated with 1 M tetrabutylammonium fluoride in THF (0.4 mL), while stirring at room temperature for 2 h. The reaction mixture was evaporated, and the oily residue was purified by preparative thin-layer chromatography (10 preparative plates, 17:3 CH_2Cl_2/Me_2CO, second development 4:1 CH_2Cl_2/Me_2CO) to afford pure **8** (0.007 g, 7.5 %) in the form of an oil, $[\alpha]_D$ = = +10.0 (*c* 0.1, $CHCl_3$), R_f = 0.30 (9:1 CH_2Cl_2/Me_2CO, three successive developments).

1,2-O-*Isopropylidene-5*-C-*(thiazol-2'-yl)*-α-*D*-gluco-*pentofuranose (14)*. To a solution of compound **13** (2.166 g, 8.32 mmol) in anhydrous EtOAc (80 mL) was added H_5IO_6 (3.103 g, 13.61 mmol). The reaction mixture was stirred at room temperature for 6 h, then filtered and evaporated, leaving a light-pink reaction mixture. The residue was purified on a column of flash silica (11:9 Et_2O/light petroleum), whereby a mixture of alcohols **13a** was obtained (0.876 g, 56 %) in the form of a colourless syrup, R_f = 0.37 (1:1 Et_2O/light petroleum). IR (film): ν_{max} 3371 cm^{-1} (OH). (+)ESI-HRMS (*m*/*z*): calculated for [$C_{10}H_9O_5$ + NH_4^+] 236.11286, observed 236.11285.

To a solution of purified compound **13a** (0.161 g, 0.74 mmol) in anhydrous CH_2Cl_2 (6 mL) a 2-TST (0.174 g, 1.09 mmol) solution in CH_2Cl_2 (3 mL) was added dropwise at room temperature**.** After stirring at room temperature for 12 h, the solvent was evaporated and to the residue was added THF (10 mL) and tetrabutylammonium fluoride (0.886 mmol in 8.86 mL THF). After stirring at room temperature for 2 h, the reaction mixture was concentrated to a smaller volume, and after the addition of aq. $NaHCO_3$ solution, extracted with EtOAc. The combined extracts were dried and evaporated, and the remaining crude product **14** was purified on a column of flash silica (light petroleum/EtOAc 1:1), whereby pure product **14** (0.048 g, 24 %) was obtained, which crystallized from a mixture of CH_2Cl_2/hexane as white crystals, m.p. 120 °C, $[\alpha]_D$ = −12.5 (*c* 0.2, acetone).

Cytotoxic activity

Test cells. The *in vitro* cytotoxicities of test compounds were evaluated against seven human malignant cell lines: K562 (ATCC CCL-243, chronic myeloid leukaemia), HL-60 (ATCC CCL-240, promyelocytic leukaemia), Jurkat (ATCC CCL-1435, T cells leukaemia), Raji (ATCC CCL-86, Burkitt's lymphoma), MCF-7 (ATCC HTB-22, ER^+ breast adenocarcinoma), HeLa (ATCC CCL2, human cervix adenocarcinoma) and A549 (ATCC HTB-38, lung carcinoma). Cytotoxic activity against one normal human cell line, MRC-5 (ATCC CCL--185, foetal lung fibroblasts), was also estimated.

MTT test. Cytotoxic activity was evaluated by using standard MTT assay,[13] after exposure of cells to the tested compounds for 72 h.

Crystal structure determination

Diffraction experiments were performed on an Oxford Diffraction Gemini S diffractometer. Crystal structures were solved and refined as reported previously[14]. All hydrogen atoms are introduced in idealized positions are refined using a riding model. Pertinent crystallographic and refinement data are listed in Table S-III of the Supplementary material to this paper. CCDC 2218113 and CCDC 2218112 contain supplementary crystallographic data for

this paper. These data can be obtained free of charge from The Cambridge Crystallographic Data Centre *via* http://www.ccdc.cam.ac.uk/structures.

RESULTS AND DISCUSSION

Chemistry

Synthesis of compounds **3**–**7** is shown in Scheme 1 and commenced from the commercially available monoacetone-D-glucose (**9**).

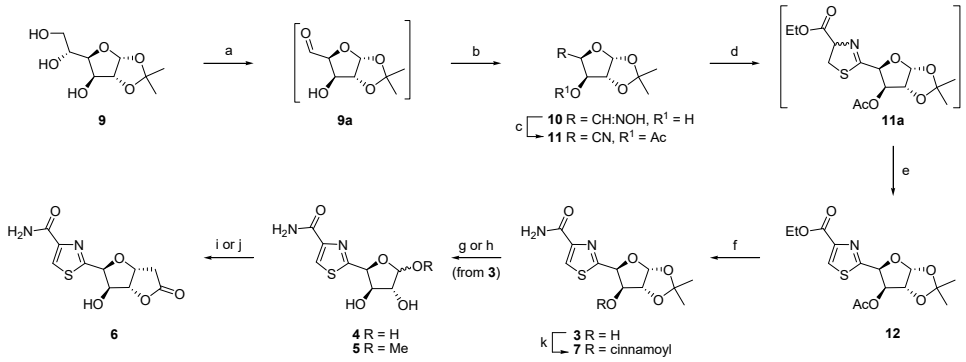

Scheme 1. a) $NaIO_4$, MeOH/H_2O, rt, 4.5 h; b) $NH_2OH{\times}HCl$, NaOAc, EtOH, rt, 24 h, 78 % from **9**; c) Ac_2O, reflux, 1 h, 92 %; d) L-cysteine ethyl ester hydrochloride, Et_3N, EtOH, CH_2Cl_2, rt, 3.5 h; e) $BrCCl_3$, DBU, CH_2Cl_2, 0 °C, 2.5 h, then 4 °C, 43 h, 87 % from **11**; f) saturated NH_3, MeOH, rt, 7 days, 93 %; g) 90 % aq TFA, 0 °C, 0.5 h, then rt, 4.5 h, 89 %; h) 90% aq TFA, MeOH, 0 °C, 0.5 h, then rt, 4.5 h, 52 %; i) Meldrum's acid, Et_3N, DMF, 46 °C, 69 h, 7 %; j) MCMP, MeOH, rt, 1 h, 22 %; k) cinnamic acid, DCC, DMAP, MeCN, CH_2Cl_2, rt, 24 h, 94 %.

Terminal diol cleavage in **9** was achieved with sodium periodate in aqueous MeOH to afford the unstable aldehyde **9a**. The resulting aldehyde **9a** was not purified but was rather immediately treated with hydroxylamine hydrochloride to yield the expected oxime **10** as a mixture of the corresponding *E*- and *Z*-isomers. The mixture was not separated but was further treated with refluxing acetic anhydride to give the corresponding nitrile **11** in 92 % yield. Nitrile **11** was allowed to react with ethyl ester of cysteine hydrochloride, in the presence of triethylamine at room temperature, to afford thiazoline **11a** as an inseparable mixture of C-4 epimers. The crude mixture was not separated but was immediately oxidized with bromotrichloromethane and DBU to give the thiazole **12** in an overall yield of 87 % from two steps. Treatment of **12** with methanolic ammonia provided the amide **3** (93 %) as a result of successive ester ammonolysis and *O*-deacetylation at the C-3 position. Hydrolytic removal of the isopropylidene protective group in **3** gave the expected lactol **4**, which upon treatment with Meldrum's acid in the presence of triethylamine gave a low yield (7 %) of target **6**. A better yield of **6** (22 %) was obtained by using the *Z*-selective Wittig olefination

of **4** with a stabilized C_2-ylide ($Ph_3P{=}CHCO_2Me$, MCMP).[15] Apart from spectroscopic methods, the structure of compound **6** was confirmed by X-ray analysis (see Supplementary material for details). Finally, compound **3** was esterified with cinnamic acid, under the Steglich conditions,[16] to afford the corresponding 3-*O*--cinnamoyl derivative **7** in 94 % yield. The reason for the preparation of cinnamate **7** lies in the fact that a significant number of cinnamic acid hybrids show antitumour activity.[17–19]

The preparation of bioisostere **8** is shown in Scheme 2. D-Glucose was first converted to the protected aldehyde **7a** using the procedure recently developed in our laboratory[20] (see the Supplementary Material for details).

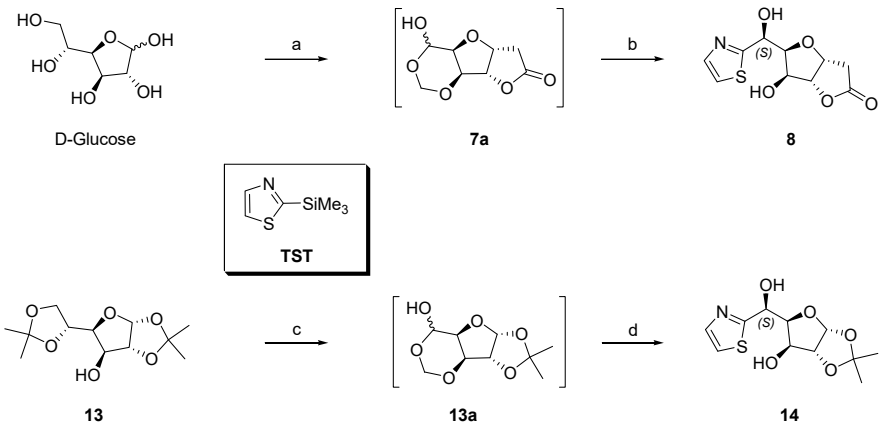

Scheme 2. a) See Supplementary material and/or Ref.[20]; b) (*i*) TST, THF, rt, 48 h, (*ii*) TBAF, THF, rt, 2 h, 7.5 %; c) Ref.[21]; d) (*i*) TST, CH_2Cl_2, rt, 12 h, (*ii*) TBAF, THF, rt, 2 h, 24 %.

The addition of 2-(trimethylsilyl)thiazole (TST) to hemiacetal **7a** (Scheme 2) in THF using the adopted procedure developed by Dondoni *et al.*[22] occurred with high diastereofacial selectivity affording, after desilylation with tetrabutylammonium fluoride, a low yield of thiazole **8** (7.5 %). This two-step transformation involves the initial unmasking of hemiacetal function with the subsequent addition of reagents to the liberated aldehyde group. Given that compound **8** showed relatively weak antiproliferative activity against tumour cells, the yield of this reaction was not optimized. To resolve the stereochemistry at the C-7 position in product **8**, the above-described addition reaction was repeated with the known[23] hemiacetal derivative **13a**. The corresponding thiazole derivative **14** was obtained in a yield of 24 %. The stereochemistry of **14** was unambiguously established by X-ray crystallographic analysis (see Supplementary material for details). Based on this result, as well as the observations of Dondoni *et al.*,[22] we concluded that the newly introduced stereocenter of product **8** has (7*S*)-stereochemistry.

Antiproliferative activity

Table I shows *in vitro* cytotoxicities of synthesized compounds against a panel of human cell lines (K562, HL-60, Jurkat, Raji, MCF-7, HeLa, A549 and MRC-5), using the standard MTT assay. Apart from the final products (**5**–**8**), intermediates, **3**, **4** and **12** were also included in the assay since they can be considered pseudo-*C*-nucleosides related to tiazofurin.

TABLE I. *In vitro* cytotoxicity (IC_{50}* / μM; values are means of three independent experiments. Coefficients of variation were less than 10 %) of (+)-goniofufurone (**1**), tiazofurin (**2**), DOX and analogues **3**–**8** and **12** after 72 h

Compound	Cell line							
	K562	HL-60	Jurkat	Raji	MCF-7	HeLa	A549	MRC-5
(+)-Goniofufurone (**1**)	0.41	201.32	32.45	18.45	16.59	8.32	35.21	>100
Tiazofurin (**2**)	2.06	0.67	0.09	5.28	2.03	3.26	5.92	0.36
3	21.01	7.64	7.09	15.64	10.52	4.36	18.21	>100
4	2.55	8.51	11.36	14.32	8.65	8.31	24.64	>100
5	17.50	7.79	11.36	7.63	18.36	8.64	5.46	>100
6	1.63	1.02	18.52	9.02	2.61	0.75	4.64	97.12
7	3.54	12.63	4.32	12.64	10.02	1.25	3.45	>100
8	3.05	3.54	25.02	25.41	7.62	9.06	11.59	>100
12	3.47	9.10	7.52	1.58	15.20	3.70	10.35	>100
DOX	0.25	0.92	0.03	2.98	0.20	0.07	4.91	0.10

The results in Table I show that five compounds exhibited micromolar activity in the culture of K562 cells, although only compound **6** was more potent than tiazofurin (**2**). Almost all synthesized compounds were more active than **1** against MCF-7 and HL-60 cells, with lactone **6** being the most potent. It is noteworthy that analogue **6** exhibited a prominent potency (IC_{50} = 1.02 μM) against promyelocytic leukaemia cells (HL-60) with activity similar to DOX. Among all synthesized molecules, which showed moderate activity in Jurkat and Raji cell cultures where they were more active than **1** (except **8** against Raji cells), the isopropylidene derivative **12** stands out, which was almost twice as active as DOX and 3 times as active as tiazofurin (**2**) against Raji cells. Against alveolar basal adenocarcinoma cells (A549), all compounds were more active than **1**, while two compounds (**6** and **7**) were slightly more active than DOX. Molecules **6** and **7** showed higher potency than both leads **1** and **2** against HeLa cells of which compound **6** showed submicromolar activity (IC_{50} = 0.75 μM), the best activity recorded in this assay. Like natural product **1**, none of the synthesized analogues were active against normal MRC-5 cells, in contrast to tiazofurin (**2**) and DOX, which showed high potencies against these cells in the submicromolar range.

* IC_{50} is the concentration of compound required to inhibit the cell growth by 50 % compared to an untreated control.

In an attempt to determine the structural features important to the activity of this series of compounds, we compared the activities of: a) compound **7** with a cinnamoyl ester group at the C-3 position, with **3** (which has an OH group at C-3); b) the activity of lactol **4**, with free OH groups at C-1 and C-2, with the activity of compounds **6** and **3** with a lactone or isopropylidene ring; c) the activity of lactol **4** with the activity of the methyl glycoside **5**; d) the activity of the C-7 thiazole hybrid **8** with the natural product **1** having a phenyl group at the C-7 position (Fig. S-1 of the Supplementary material). The results of this brief SAR analysis showed that the presence of the cinnamoyl group at C-3 is beneficial for the activity of this type of compound; the absence of OH groups at C-1 and C-2 and the structural architecture of a five-membered lactone or isopropylidene ring (the analysis also showed that pseudo-*C*-nucleoside **5** is more active against 50 % of the tested cell lines) and that the introduction of a thiazole ring at the C-7 position of the natural product **1** instead of the phenyl ring, increases the activity against four of seven cell lines.

*Crystal structure of pseudo-*C*-nucleoside **6***

The molecular structure of **6** is depicted in Fig. 2. Absolute configuration of all stereocenters is determined both from resonant scattering effects, and findings are in line with assumed absolute configurations of stereocenters whose stereochemistries remain unchanged during the synthetic route.

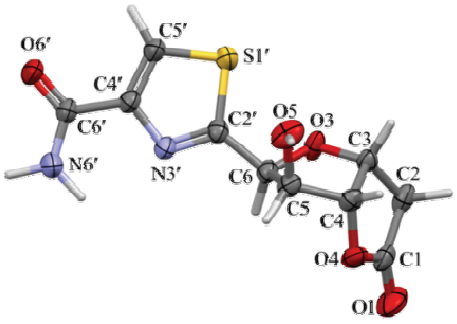

Fig. 2. Molecular structure of **6** (CCDC 2218113) with the atom numbering scheme.

From the structural point of view, **6** is the first structurally characterized compound that bears a furofuranone ring core coupled to a thiazole ring. The search of the CSD[24] resulted in only ten structures that contain a thiazole ring coupled to the C1′ atom of a tetrahydrofuran ring substructure depicted in Fig. 3a. All these structures can be regarded as tiazofurin analogues. Since **6** can also be regarded as a tiazofurin analogue, where a furanose ring is fused to a lactone ring, it is of interest to compare the furanose ring conformation in **6** and these tiazofurin analogues. For this purpose, atom numbering nomenclature established for furanose rings in nucleotides is used,[25,26] as shown in Fig. 3a.

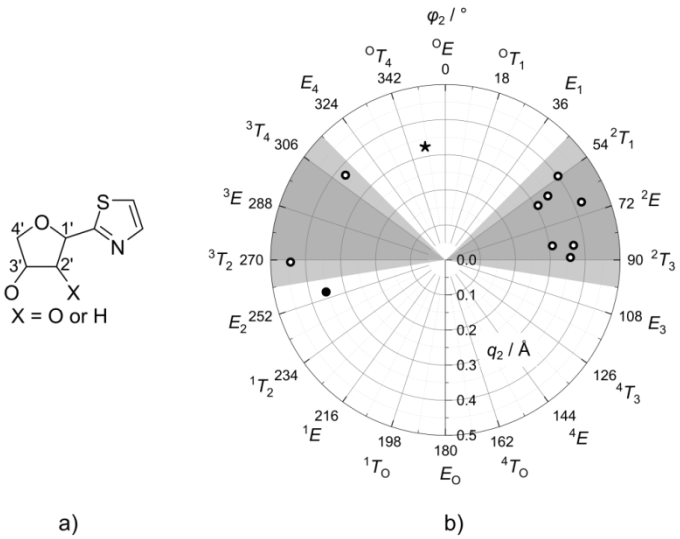

Fig. 3. a) Substructure fragment used in CSD search. Substituents at C4′ were unspecified. b) Pseudorotational circle for furanose ring conformations found in CSD hits. Conformation of **6** is indicated by a filled circle, and that of YIHCAT with a star. Preferred conformational ranges are shaded.

Conformations of the furanose rings are analysed *via* Cremer–Pople formalism.[27] It is found that in seven structures furanose rings adopt conformations that spread in pseudorotation regions demarcated by $^{2}T_1$ and $^{2}T_3$ conformations, while for two structures the range is enclosed between $^{3}T_2$ and $^{3}T_4$ conformations. These conformational ranges have been established as preferred for ribose and deoxyribose in nucleosides.[28,29] Structure YIHCAT,[30] with the furanose ring in conformation between $^{O}T_4$ and ^{O}E is the only outlier. The conformation of the furanose ring in the **6** is very close to E_2, which is also an aberration. What separates YIHCAT and **6** from other structures is the presence of fused rings – isopropylidene in YIHCAT and furofuranone in **6**, which may explain their different conformations. Notably, for all investigated structures, including **6**, ring puckering amplitude falls in the range from 0.30 to 0.45 Å. A graphical representation of ring conformation space for the investigated structures is given in Fig. 3b, while details are summarized in Table S-III of the Supplementary material.

Relative to the sugar moiety, the aglycone fragment of the nucleoside can adopt two main orientations about the glycosyl C1′–N link called *syn* and *anti*.[25,26] In analogy to that, for *C*-nucleosides such as tiazofurin and its derivatives, a torsion angle χ (O–C1′–C–S) can be defined to assess thiazole ring orientation. It is found that the thiazole ring orients in such a way that sugar O and thiazole S atoms are in *syn* orientation, with a restricted range of $|\chi|$ (0–60°), and the peak of the distribution at *ca.* 30° (see Fig. S-3 of the Supplementary material). The cor-

responding torsion angle for **6** amounts to −24.3(2)°, indicating that the mutual disposition of the studied rings in **6** is in line with the literature data.

Two intermolecular hydrogen bonds were found in the crystal structure of **6**. Hydroxyl O5–H5 group is bonded to carboxamide oxygen O6′ of the neighbouring molecule. Interestingly, only one of the carboxamide hydrogen atoms is involved in hydrogen bonding, with carbonyl oxygen O1 of the lactone ring being the hydrogen bond acceptor. Details of hydrogen bonding are listed in Table S-V of the Supplementary material.

CONCLUSION

In conclusion, seven new thiazole hybrids with furofuranone or tetrahydrofuran scaffolds have been synthesized and evaluated for their *in vitro* cytotoxicity against a panel of human malignant cell lines (K562, HL-60, Jurkat, Raji, MCF-7, HeLa and A549), as well as toward a single normal cell line (MRC-5). The key steps in the synthesis of pseudo-*C*-nucleosides **3**–**7** and **12** involved the initial cyclocondensation of the corresponding aldononitriles with cysteine ethyl ester hydrochloride, followed by subsequent treatment of the resulting C-4′ epimeric thiazolines with DBU to form the thiazole ring. Goniofufurone bioisosteres **8** and **14** have been prepared by stereoselective addition of 2-(trimethylsilyl)thiazole to partially protected hemiacetals, obtained by periodate cleavage of the terminal diol function in the appropriate D-glucose derivatives. The synthesized analogues showed moderate to strong antiproliferative activity in cultures of several malignant cell lines. The strongest activity was shown by hybrid **6** (HeLa cells, IC_{50} 0.75 μM) which was more than 10 or 4 times more active than both control compounds **1** and **2**, respectively. The most active compound in Raji cell culture was hybrid **12**, which was nearly two times more potent than the commercial antitumour drug doxorubicin (DOX). Lung adenocarcinoma cells (A549) were the most sensitive against the synthesized compounds. All were more active than lead **1**, while two compounds (**6** and **7**) were slightly more active than DOX. A brief SAR study revealed that the presence of the cinnamoyl group at C-3 may enhance the activity of this type of analogues.

SUPPLEMENTARY MATERIAL

Additional data and information are available electronically at the pages of journal website: https://www.shd-pub.org.rs/index.php/JSCS/article/view/12157, or from the corresponding author on request.

Acknowledgments. This work was supported by the Ministry of Education, Science and Technological Development of the Republic of Serbia (Grant No. 451-03-47/2023-01/200125). The work was also funded by the Serbian Academy of Sciences and Arts through a research grant, number F-130.

ИЗВОД

СИНТЕЗА И АНТИПРОЛИФЕРАТИВНА АКТИВНОСТ НОВИХ ТИАЗОЛНИХ ХИБРИДА СА [3.3.0]ФУРОФУРАНОНСКИМ ИЛИ ТЕТРАХИДРОФУРАНСКИМ СКЕЛЕТОМ

ВЕСНА КОЈИЋ[1], МИЛОШ СВИРЧЕВ[2], САЊА ЂОКИЋ[2], ИВАНА КОВАЧЕВИЋ[2], МАРКО В. РОДИЋ[2], БОЈАНА СРЕЋО ЗЕЛЕНОВИЋ[2], ВЕЛИМИР ПОПСАВИН[2,3] и МИРЈАНА ПОПСАВИН[2]

[1]Универзитет у Новом Саду, Медицински факултет, Институт за онкологију Војводине, пут Др Голдмана 4, 21204 Сремска Каменица, [2]Универзитет у Новом Саду, Природно–математички факултет, Департман за хемију, биохемију и заштиту животне средине, Трг Доситеја Обрадовића 3, 21000 Нови Сад и [3]Српска академија наука и уметности, Кнеза Михаила 35, 11000 Београд

Синтетизовани су нови тиазолни хибриди и одређена је њихова *in vitro* цитотоксичност према панелу хуманих малигних ћелијских линија. Кључни кораци у синтези хибрида **3**–**7** подразумевали су иницијалну кондензацију одговарајућих алдононитрила са хидрохлоридом етилестра цистеина, након чега је уследио третман резултујућих тиазолина са DBU при чему је формиран тиазолни прстен. Биоизостере **8** и **14** су добијене након стереоселективне адиције 2-(триметилсилил)тиазола на хемиацетале добијене перјодатним раскидањем терминалне диолне функције погодних деривата D-глукозе. Добијени тиазолни аналози су показали различите антипролиферативне активности у културама појединих туморских ћелијских линија. Најјачу активност према HeLa ћелијама показао је хибрид **6**, који је био више од десет, односно четири пута активнији од контролних молекула **1** и **2**, редом. Најактивније једињење према Raji ћелијама био је хибрид **12**, који је скоро два пута активнији од клиничког антитуморског лека доксорубицина. Сви аналози су били активнији према A549 ћелијама у односу на контролу **1**, док су једињења **6** и **7** била нешто активнија од доксорубицина. Прелиминарна SAR анализа је открила да присуство цинаматне групе на положају C-3, у аналозима типа **7**, повећава активност резултујућих хибрида.

(Примљено 30. новембра 2022, прихваћено 11. јануара 2023)

REFERENCES

1. H. M. Sampath Kumar, L. Herrmann, S. B. Tsogoeva, *Bioorg. Med. Chem. Lett*. **30** (2020) 127514 (https://doi.org/10.1016/j.bmcl.2020.127514)
2. V. Ivasiv, C. Albertini, A. E. Gonçalves, M. Rossi, M. L. Bolognesi, *Curr. Top. Med. Chem*. **19** (2019) 1694 (https://doi.org/10.2174/1568026619666190619115735)
3. C. Viegas-Junior, A. Danuello, V. da Silva Bolzani, E. J. Barreiro, C. A. Manssour Fraga, *Curr. Med. Chem*. **14** (2007) 1829 (https://doi.org/10.2174/092986707781058805)
4. A. Petrou, M. Fesatidou, A. Geronikaki, *Molecules* **26** (2021) 3166 (https://doi.org/10.3390/molecules26113166)
5. D. S. Bhagat, P. A. Chawla, W. B. Gurnule, S. K. Shejul, G. S. Bumbrah, *Curr. Org. Chem*. **25** (2021) 819 (https://doi.org/10.2174/1385272825999210101234704)
6. M. Sviržev, M. Popsavin, A. Pavić, B. Vasiljević, M. V. Rodić, S. Djokić, J. Kesić, B. Srećo Zelenović, V. Popsavin, V. Kojić, *Bioorg. Chem*. **121** (2022) 105691 (https://doi.org/10.1016/j.bioorg.2022.105691)
7. X.-S. Peng, R. M. P. Ylagan, Y. M. Siu, H. N. C. Wong, *Chem. Asian J*. **10** (2015) 2070 (https://doi.org/10.1002/asia.201500288)
8. X. Fang, J. E. Anderson, C. Chang, P. E. Fanwick, J. L. McLaughlin, *J. Chem. Soc. Perkin Trans. I* (1990) 1655 (https://doi.org/10.1039/P19900001655)
9. K. Malek, M. S. Boosalis, K. Waraska, B. S. Mitchell, D. G. Wright, *Leukemia Res*. **28** (2004) 1125 (https://doi.org/10.1016/j.leukres.2004.03.003)

10. D. G. Wright, M. Boosalis, K. Malek, K. Waraska, *Leukemia Res*. **28** (2004) 1137 (https://dx.doi.org/10.1016/j.leukres.2004.03.004)
11. A. P. Rauter, J. A. Figueiredo, I. M. Ismael, *Carbohydr. Res.* **188** (1989) 19 (https://dx.doi.org/10.1016/0008-6215(89)84054-6)
12. P. Köll, A. Wernicke, J. Kovács, A. Lützen, *J. Carbohydr. Chem*. **19** (2000) 1019 (http://dx.doi.org/10.1080/07328300008544132)
13. D. A. Scudiero, R. H. Shoemaker, K. D. Paull, A. Monks, S. Tierney, T. H. Nofziger, M. J. Currens, D. Seniff, M. R. Boyd, *Cancer Res*. **48** (1988) 4827 (https://cancerres.aacrjournals.org/content/48/17/4827)
14. I. Kovačević, M. Popsavin, G. Benedeković, J. Kesić, V. Kojić, D. Jakimov, T. Srdić-Rajić, G. Bogdanović, V. Divjaković, V. Popsavin, *Eur. J. Med. Chem*. **134** (2017) 293 (http://dx.doi.org/10.1016/j.ejmech.2017.03.088)
15. S. Valverde, M. Martin-Lomas, B. Herradon, S. Garcia-Ochoa, *Tetrahedron* **43** (1987) 1895 (https://doi.org/10.1016/S0040-4020(01)81502-7)
16. B. Neises, W. Steglich, *Angew. Chem. Int. Ed. Engl*. **17** (1978) 522 (https://doi.org/10.1002/anie.197805221)
17. P. De, M. Baltas, F. Bedos-Belval, *Curr. Med. Chem*. **18** (2011) 1672 (https://doi.org/10.2174/092986711795471347)
18. E. Pontiki, A. Peperidou, I. Fotopoulos, D. Hadjipavlou-Litina, *Curr. Pharm. Biotechnol*. **19** (2018) 1019 (https://doi.org/10.2174/1389201019666181112102702)
19. L.-S. Feng, J.-B. Cheng, W.-Q. Su, H.-Z. Li, T. Xiao, D.-A. Chen, Z.-L. Zhang, *Arch. Pharm*. **355** (2022) 2200052 (https://doi.org/10.1002/ardp.202200052)
20. G. Benedeković, J. Francuz, I. Kovačević, M. Popsavin, B. Srećo Zelenović, V. Kojić, G. Bogdanović, V. Divjaković, V. Popsavin, *Eur. J. Med. Chem*. **82** (2014) 449 (http://dx.doi.org/10.1016/j.ejmech.2014.05.081)
21. M. Svirčev, G. Benedeković, I. Kovačević, M. Popsavin, V. Kojić, D. Jakimov, T. Srdić-Rajić, M. V. Rodić, V. Popsavin, *Tetrahedron* **74** (2018) 4761 (https://doi.org/10.1016/j.tet.2018.07.046)
22. A. Dondoni, G. Fantin, M. Fogagnolo, A. Medici, *Tetrahedron* **43** (1987) 3533 (https://doi.org/10.1016/S0040-4020(01)81646-X)
23. T. D. Inch, *Carbohydr. Res.* **5** (1967) 53 (https://doi.org/10.1016/0008-6215(67)85007-9)
24. C. R. Groom, I. J. Bruno, M. P. Lightfoot, S. C. Ward, *Acta Crystallogr., B* **72** (2016) 171 (https://doi.org/10.1107/S2052520616003954)
25. M. Sundaralingam, *Biopolymers* 7 (1969) 821 (https://doi.org/10.1002/bip.1969.360070602)
26. W. Seanger, *Principles of Nucleic Acid Structure*, Springer-Verlag, New York, 1984
27. D. Cremer, J. A. Pople, *J. Am. Chem. Soc.* **97** (1975) 1354 (https://doi.org/10.1021/ja00839a011)
28. C. Altona, M. Sundaralingam, *J. Am. Chem. Soc.* **94** (1972) 8205 (https://doi.org/10.1021/ja00778a043)
29. H. P. M. de Leeuw, C. A. G. Hasnoot, C. Altona, *Isr. J. Chem.* **20**, (1980) 108 (https://doi.org/10.1002/ijch.198000059)
30. A. Dondoni, M.-C. Scherrmann, *J. Org. Chem.* **59** (1994) 6404 (https://doi.org/10.1021/jo00100a050).

Journal of the Serbian Chemical Society
JSCS@tmf.bg.ac.rs • www.shd.org.rs/JSCS
J. Serb. Chem. Soc. *88* (5) S126–S138 (2023) *Supplementary material*

SUPPLEMENTARY MATERIAL TO

Synthesis and antiproliferative activity of new thiazole hybrids with [3.3.0]furofuranone or tetrahydrofuran scaffolds

VESNA KOJIĆ[1], MILOŠ SVIRČEV[2], SANJA DJOKIĆ[2], IVANA KOVAČEVIĆ[2], MARKO V. RODIĆ[2], BOJANA SREĆO ZELENOVIĆ[2], VELIMIR POPSAVIN[2,3]* and MIRJANA POPSAVIN[2]

[1]*University of Novi Sad, Faculty of Medicine, Oncology Institute of Vojvodina, Put Dr Goldmana 4, 21204 Sremska Kamenica, Serbia,* [2]*University of Novi Sad, Faculty of Sciences, Department of Chemistry, Biochemistry and Environmental Protection, Trg Dositeja Obradovića 3, 21000 Novi Sad, Serbia and* [3]*Serbian Academy of Sciences and Arts, Kneza Mihaila 35, 11000 Belgrade, Serbia*

J. Serb. Chem. Soc. *88* (5) (2023) 467–479

PREPARATION OF STARTING INTERMEDIATES

*3,6-Anhydro-2-deoxy-D-glycero-D-ido-octono-l,4-lactone (**S1**)*

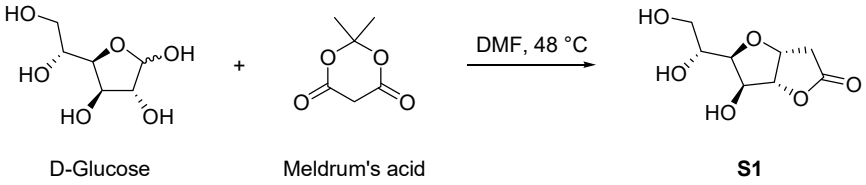

Scheme S-1. Preparation of **S1**.

To a suspension of D-Glucose (0.180 g, 1.00 mmol in anhydrous DMF (5 mL) was added anhydrous Et_3N (1.68 mL, 12.00 mmol) and Meldrum's acid (0.290 g, 2.00 mmol). The reaction mixture was stirred at 40 °C for 4 days and then evaporated. The residue was purified on a column of flash silica (19:1 EtOAc/MeOH) whereby pure **S1** (0.102 g, 50%) was obtained as a white powder. Recrystallization from a mixture of Me_2CO/light petroleum gave colourless needles, mp 119 °C, $[\alpha]_D$ = +32.2 (*c* 0.5, H_2O), lit.[1] $[\alpha]_D$ = +29.0 (*c* 0.5, H_2O), R_f = 0.27 (19:1 EtOAc/MeOH). Spectral data (IR, ^{1}H-NMR, ^{13}C-NMR and MS) were in good agreement with reported values.[1]

* Corresponding author. E-mail: velimir.popsavin@dh.uns.ac.rs

*(7S)-3,6-Anhydro-2-deoxy-7-C-hydroxy-5,7-O-methylidene-D-ido-heptono-1,4-lactone (**S2**)*

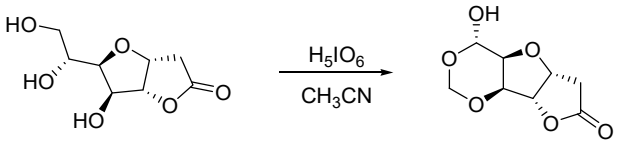

S1 **S2**

Scheme S-2. Preparation of **S2**

To a stirred solution of compound **S1** (0.145 g, 0.71 mmol) in anhydrous MeCN (15 mL) was added H_5IO_6 (0.146 g, 0.64 mmol). After stirring at room temperature for 22 h, the reaction mixture was evaporated with silica gel and purified by flash chromatography (9:1 CH_2Cl_2/Me_2CO). This gives a mixture of pure **S2** (0.108 g, 75 %) which crystallizes from Me_2CO/hexane in the form of cloudy needles, mp 152–153 °C, $[\alpha]_D$ = +130 (*c* 0.25, Me_2CO), R_f = 0.31 (9:1 CH_2Cl_2/Me_2CO). IR, NMR (^{1}H and ^{13}C) and MS data were in good agreement with previously recorded values.[2]

SPECTROSCOPIC DATA OF SYNTHESIZED COMPOUNDS

*(E,Z)-1,2-O-Isopropylidene-α-D-xylo-pentodialdo-1,4-furanose-5-oxime (**10**)*

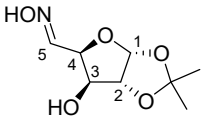

10

IR (film): ν_{max} 3390, 1637 cm^{-1}.

^{1}H NMR (250 MHz, DMSO-d_6, δ): 11.27 and 11.13 (2 × *s*, 1 H each, NOH both isomers), 7.26 (*d*, 1 H, $J_{4,5}$ = 7.2 Hz, H-5, *E* isomer), 6.67 (*d*, 0.8 H, $J_{4,5}$ = 4.6 Hz, H-5, *Z*-isomer), 5.88 (*m*, H-1 both isomers), 5.57 (*d*, 1 H, $J_{3,OH}$ = 4.3 Hz, OH, *E*-isomer), 5.43 (*d*, 0.8 H, $J_{3,OH}$ = 4.7 Hz, OH, *Z*-isomer), 4.50 (*m*, 0.8 H, H-4, *Z* isomer), 4.21–4.44 (*m*, H-2, both isomers, H-4, *E*-isomer), 4.21 (*br s*, 0.8 H, H-3, *Z*-isomer), 4.03 (*br s*, 1 H, H-3, *E*-isomer), 1.39 and 1.23 (2 × *s*, 3 H each, C*Me*$_2$). The ratio of isomers: *E*/*Z* = 1:0.8

^{13}C NMR (62.9 MHz, DMSO-d_6, δ): 147.38 (C-5, *Z*-isomer), 146.00 (C-5, *E*-isomer), 110.83 and 110.73 (Me$_2$*C*, both isomers), 104.55 (C-1, *E*-isomer), 104.15 (C-1, *Z*-isomer), 85.14, 78.18, 74. 98, (C-2 and C-4, both isomers), 75.50 and 74.24 (C-3, both isomers), 26.70, 26.07 and 26.04, (*Me*$_2$C, both isomers).

(+)ESI-HRMS (*m/z*): calculated for [$C_8H_{13}NO_5$ + Na^+] 226.06859, observed 226.06817.

*3-O-Acetyl-1,2-O-isopropylidene-α-D-xylo-furanoseurononitrile (**11**)*

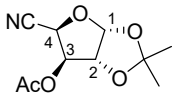

11

IR (film): ν_{max} 1754, 2260 cm^{-1}.

^{1}H NMR (250 MHz, $CDCl_3$, δ): 5.95 (*d*, 1 H, $J_{1,2}$ = 3.5 Hz, H-1), 5.40 (*d*, 1 H, $J_{3,4}$ = 3.4 Hz, H-3), 4.95 (*d*, 1 H, $J_{3,4}$ = 3.4 Hz, H-4), 4.55 (*d*, 1 H, $J_{1,2}$ = 3.5 Hz, H-2), 2.13 (*s*, 3 H, $COCH_3$), 1.45 and 1.27 (2 × *s*, 3 H each, CMe_2).

^{13}C NMR (62.9 MHz, $CDCl_3$, *δ*): 168.51 ($COCH_3$), 113.31 (CN), 112.93 (Me_2C), 104.94 (C-1), 81.89 (C-2), 75.06 (C-3), 68.03 (C-4), 26.23 and 25.52 (Me_2C), 19.91 ($COCH_3$).

(+)ESI-HRMS (*m/z*): calculated for [$C_{10}H_{13}NO_5$ + NH_4^+] 245.11229, observed 245.11320.

*3-O-Acetyl-4-C-(4'-(ethoxycarbonyl)thiazol-2'-yl)-1,2-O-isopropylidene-α-D-xylo-tetrofuranose (**12**)*

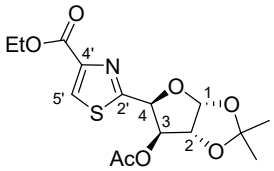

12

IR (KBr): ν_{max} 1755 and 1731 cm^{-1}.

^{1}H NMR (400 MHz, $CDCl_3$, δ): 8.20 (*s*, 1 H, H-5′), 6.09 (*d*, 1 H, $J_{1,2}$ = 3.6 Hz, H-1), 5.80 (*d*, 1 H, $J_{3,4}$ = 3.1 Hz, H-4), 5.52 (*d*, 1 H, $J_{3,4}$ = 3.1 Hz, H-3), 4.67 (*d*, 1 H, $J_{1,2}$ = 3.6 Hz, H-2), 4.43 (*q*, 2 H, J = 7.1 Hz, CH_2CH_3), 1.92 (*s*, 3 H, $COCH_3$), 1.42 (*t*, 3 H, CH_2CH_3), 1.58 and 1.37 (2 × *s*, 3 H each, CMe_2).

^{13}C NMR (100 MHz, $CDCl_3$, δ): 168.89 ($OCOCH_3$), 165.96 (CO_2Et), 161.28 (C-2′), 147.00 (C-4′), 133.41 129.48 128.32, and 127.99, (Ph), 128.32 (C-5′), 113.08 (Me_2C), 104.99 (C-1), 83.40 (C-2), 78.91 (C-4), 77.06 (C-3), 61.60 (CH_2CH_3), 26.78 and 26.34 (Me_2C), 20.60 ($OCOCH_3$), 14.39 (CH_2CH_3).

(+)ESI-HRMS (*m/z*): calculated for [$C_{15}H_{19}NO_7$ + H^+] 358.09482, observed 358.09550.

*4-C-(4′-(Carbamoyl)thiazol-2′-yl)-1,2-O-isopropylidene-α-D-xylo-tetrofuranose (**3**)*

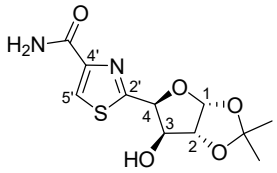

3

IR (film): ν_{max} 3348, 1668, 1590 cm^{-1}.

^{1}H NMR (250 MHz, acetone-d_6, δ): 8.16 (*s*, 1 H, H-5′), 7.46 and 6.89 (2 × *br s*, 1 H each, NH_2), 6.09 (*d*, 1 H, $J_{1,2}$ = 3.4 Hz, H-1), 5.43 (*d*, 1 H, $J_{3,4}$ = 2.7 Hz, H-4), 4.70 (*d*, 1 H, $J_{1,2}$ = 3.4 Hz, H-2), 4.64 (*d*, 1 H, $J_{3,4}$ = 2.4 Hz, H-3), 4.44 (*br s*, 1 H, OH), 1.50 and 1.33 (2 × *s*, 3 H each, CMe_2).

^{13}C NMR (62.9 MHz, acetone-d_6, δ): 167.94 (***C***ONH$_2$), 163.35 (C-2′), 150.78 (C-4′), 125.18 (C-5′), 112.57 (Me$_2$*C*), 106.12 (C-1), 86.27 (C-2), 81.76 (C-4), 76.59 (C-3), 27.17 and 26.37 (*Me*$_2$C).

(+)ESI-HRMS (*m/z*): calculated for [$C_{11}H_{13}N_2O_5S$ + H^+] 287.06962, observed 287.06946.

*4-C-(4′-(Carbamoyl)thiazol-2′-yl)-D-xylo-tetrofuranose (**4**)*

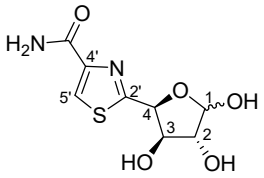

4

IR (film): ν_{max} 3354, 1674 cm^{-1}.

^{1}H NMR (400 MHz, methanol-d_4, δ): 8.22 and 8.19 (2 × *s*, 1 H, H-5′ both anomers), 5.63 (*d*, 1 H, $J_{1,2}$ = 3.6 Hz, H-1α), 5.49–5.55 (*m*, 2 H, H-4α and H-4β), 5.27 (*s*, 1 H, H-1β), 3.57–4.44 (*m*, H-2 and H-3, both anomers). Ratio of anomers: α/β = 1:1.

^{13}C NMR (100 MHz, methanol-d_4, δ): 172.07 and 171.49 (*C*ONH$_2$, both anomers), 166.16 and 160.01 (C-4′, both anomers), 150.40 and 150.24 (C-2′, both anomers), 126.13 and 125.32 (C-5′, both anomers), 105.01 (C-1β), 99.25 (C-1α).

(+)ESI-HRMS (*m/z*): calculated for [$C_8H_{10}N_2O_5S$ + H^+] 247.03832, observed 247.03747.

*Methyl 4-C-(4′-(carbamoyl)thiazol-2′-yl)-D-xylo-tetrofuranoside (**5**)*

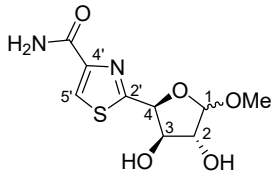

5

IR (film): ν_{max} 3340, 1668 cm^{-1}.

^{1}H NMR (400 MHz, DMSO-d_6 + D_2O, δ): 8.17 (*s*, 1.5 H, H-5′ both anomers), 7.78 and 7.42 (residual signals from CONH_2), 5.43 (*d*, 0.5 H, $J_{3,4}$ = 4.9 Hz, H-4β), 5.32 (*d*, 1 H, $J_{3,4}$ = 5.5 Hz, H-4α), 5.04 (*d*, 1 H, $J_{1,2}$ = 4.0 Hz, H-1α), 4.83 (*s*, 0.5 H, H-1β), 4.21 (*t*, 1 H, *J*=5.1 Hz, H-3α), 4.13 (*dd*, 0.5 H, $J_{2,3}$=1.1, $J_{3,4}$=4.7 Hz, H-3β), 3.97–4.02 (*m*, 1.5 H, H-2β,α), 3.37 and 3.35 (2 × *s*, OCH_3 β and α).

^{13}C NMR (62.9 MHz, DMSO-d_6 + D_2O, *δ*): 169.49 and 168.87 (CONH$_2$ β and α), 162.45 and 162.41 (C-2′ β and α), 149.68 and 149.59 (C-4′ β and α), 124.68 and 124.53 (C-5′ β and α), 110.30 (C-1β), 103.59 (C-1α), 82.22 (C-4 β), 80.41 (C-2 β), 78.59 (C-4 α), 76.67 (C-2 α), 76.20 (C-3 β and α), 55.63 and 55.13 (O*C*H$_3$ β and α).

(+)ESI-HRMS (*m/z*): calculated for [$C_9H_{12}N_2O_5S$ + H^+] 261.05397, observed 261.05441.

*3,6-Anhydro-6-C-(4′-(carbamoyl)thiazol-2′-yl)-2-deoxy-D-ido-hexono-1,4-lactone (**6**)*

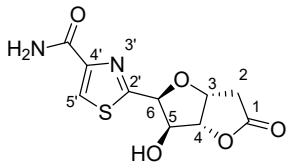

6

IR (KBr): ν_{max} 1781 cm^{-1}.

^{1}H NMR (250 MHz, DMSO-d_6, δ): 8.30 (*s*, 1 H, H-5′), 7.69 and 7.54 (2 × *br s*, 2 H, NH_2), 5.93 (*d*, 1 H, $J_{5,OH}$ = 5.1 Hz, OH), 5.26 (*d*, 1 H, $J_{5,6}$ = 3.0 Hz, H-6), 5.05 (*m*, 1 H, H-3), 5.00 (*d*, 1 H, $J_{3,4}$ = 4.2 Hz, H-4), 4.48 (*br s*, 1 H, H-5), 2.93 (*dd*, 1 H, $J_{2a,2b}$ = 18.7 Hz, $J_{2b,3}$ = 6.2 Hz, H-2b), 2.60 (*d*, 1 H, $J_{2a,2b}$ = 18.7 Hz, H-2a).

^{13}C NMR (62.9 MHz, DMSO-d_6, δ): 175.63 (C-1), 166.74 (*C*CONH$_2$), 162.37 (C-2′), 149.66 (C-4′), 124.97 (C-5′), 87.60 (C-4), 80.71 (C-6), 77.65 (C-3), 74.00 (C-5), 35.53 (C-2).

(+)ESI-HRMS (*m/z*): calculated for [$C_{10}H_{10}N_2O_5S$ + H^+] 271.03832, observed 271.03832.

*4-C-(4'-(Carbamoyl)thiazol-2'-yl)-3-O-cinnamoyl-1,2-O-isopropylidene-α-D-xylo-tetrofuranose (**7**)*

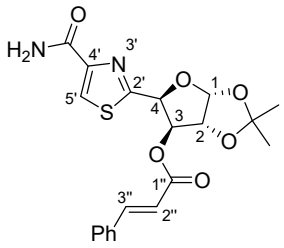

7

IR (KBr): ν_{max} 3466, 1725, 1690, 1634, 1578, 1524 cm^{-1}.

^{1}H NMR (400 MHz, $CDCl_3$, δ): 8.15 (*s*, 1 H, H-5′), 7.53 (*d*, 1 H, $J_{2'',3''}$ = 16.0 Hz, H-3″), 7.34–7.48 (*m*, 5 H, Ph), 6.22 (*d*, 1 H, $J_{2'',3''}$ = 16.0 Hz, H-2″), 6.18 (*d*, 1 H, $J_{1,2}$ = 3.6 Hz, H-1), 5.99 and 7.12 (2 × *br s*, 1 H each, NH_2), 5.73 (*d*, 1 H, $J_{3,4}$ = 3.1 Hz, H-4), 5.71 (*d*, 1 H, $J_{3,4}$ = 3.1 Hz, H-3), 4.78 (*d*, 1 H, $J_{1,2}$ = 3.6 Hz, H-2), 1.63 and 1.40 (2 × *s*, 3 H each, C*Me*$_2$).

^{13}C NMR (100 MHz, $CDCl_3$, δ): 165.32 and 164.87 ($CONH_2$ and CO from cinnamoyl), 162.81 (C-2′), 149.30 (C-4′), 146.53 (C-3″), 133.71 130.79, 128.90, 128.19, (Ph), 124.94 (C-5′), 116.16 (C-2″), 113.01 (Me$_2$*C*), 105.13 (C-1), 83.48 (C-2), 79.12 (C-4), 76.68 (C-3), 26.82 and 26.23 (*Me*$_2$C).

(+)ESI-HRMS (*m/z*): calculated for [$C_{20}H_{20}N_2O_6S$ + H^+] 417.11148, observed 417.11006.

*3,6-Anhydro-2-deoxy-7-C-(thiazol-2'-yl)-D-glycero-D-ido-heptono-1,4-lactone (**8**)*

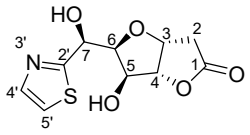

8

IR (film): ν_{max} 3451, 1789 cm^{-1}.

^{1}H NMR (400 MHz, $CDCl_3$, δ): 7.82 (*d*, 1 H, $J_{4',5'}$ = 3.3 Hz, H-4′), 7.43 (*d*, 1 H, $J_{4',5'}$ = 3.3 Hz, H-5′), 5.35 (*t*, 1 H, *J* = 5.0 Hz, H-7), 4.90–4.99 (*br s*, 3 H, H-3, H-4 and OH), 4.72 (*br s*, 1 H, H-5), 4.48 (*t*, 1 H, *J* = 4.4 Hz, H-6), 3.75 (*br s*, 1 H, OH), 2.65–2.85 (*m*, 2 H, H-2).

^{13}C NMR (100 MHz, $CDCl_3$, δ): 174.84 (C-1), 170.52 (C-2′), 142.26 (C-4′), 120.24 (C-5′), 88.32 (C-4), 83.56 (C-6), 77.84 (C-3), 75.55 (C-5), 71.29 (C-7), 36.25 (C-2).

(+)ESI-HRMS (*m/z*): calculated for [$C_{10}H_{11}NO_5S + H^+$] 258.04364, observed 258.04362.

*1,2-O-Isopropylidene-5-C-(thiazol-2'-yl)-α-D-gluco-pentofuranose (**14**)*

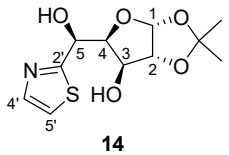

14

IR (film): ν_{max} 3340 cm^{-1}.

^{1}H NMR (500 MHz, methanol-d_4, δ): 7.75 (*d*, 1 H, $J_{4',5'}$ = 3.3 Hz, H-4′), 7.57 (*d*, 1 H, $J_{4',5'}$ = 3.3 Hz, H-5′), 5.88 (*d*, 1 H, $J_{1,2}$ = 3.6 Hz, H-1), 5.21 (*d*, 1 H, $J_{4,5}$ = 7.9 Hz, H-5), 4.51 (*d*, 1 H, $J_{1,2}$ = 3.6 Hz, H-2), 4.32 (*dd*, 1 H, $J_{3,4}$ = 2.8, $J_{4,5}$ = 7.9 Hz, H-4), 4.27 (*d*, 1 H, $J_{3,4}$ = 2.7 Hz, H-3), 1.43 and 1.28 (2 × *s*, 3 H each, C*Me*$_2$).

^{13}C NMR (125 MHz, methanol-d_4, δ): 175.51 (C-2′), 142.99 (C-4′), 121.18 (C-5′), 112.99 (Me$_2$*C*), 106.54 (C-1), 86.60 (C-2), 84.39 (C-4), 75.56 (C-3), 70.06 (C-5), 27.23 and 26.58 (*Me*$_2$C).

SAR ANALYSIS

TABLE S-I. Cytotoxicity data for SAR analysis.

Compounds	IC_{50} / μM[a], 72 h						
	K562	HL-60	Jurkat	Raji	MCF-7	HeLa	A549
(+)-Goniofufurone (**1**)	0.41	201.32	32.45	18.45	16.59	8.32	35.21
Tiazofurin (**2**)	2.06	0.67	0.09	5.28	2.03	3.26	5.92
3	21.01	7.64	7.09	15.64	10.52	4.36	18.21
4	2.55	8.51	11.36	14.32	8.65	8.31	24.64
5	17.50	7.79	11.36	7.63	18.36	8.64	5.46
6	1.63	1.02	18.52	9.02	2.61	0.75	4.64
7	3.54	12.63	4.32	12.64	10.02	1.25	3.45
8	3.05	3.54	25.02	25.41	7.62	9.06	11.59
12	3.47	9.10	7.52	1.58	15.20	3.70	10.35
DOX	0.25	0.92	0.03	2.98	0.20	0.07	4.91

[a]IC_{50} is the concentration of compound required to inhibit the cell growth by 50 % compared to an untreated control. Values are means of three independent experiments. Coefficients of variation were less than 10 %.

The structure-activity relationships were accessed as follows: the IC_{50} values of two compounds were compared, and the Δ log IC_{50} was calculated (Δ log IC_{50} is a difference between the log IC_{50} values of an analogue and the corresponding control compound). Positive Δ log IC_{50} values show a decrease of antiproliferative activity, whereas negative values indicate an increase in the activity upon the structural modification being considered. The results are presented in Fig. S-1.

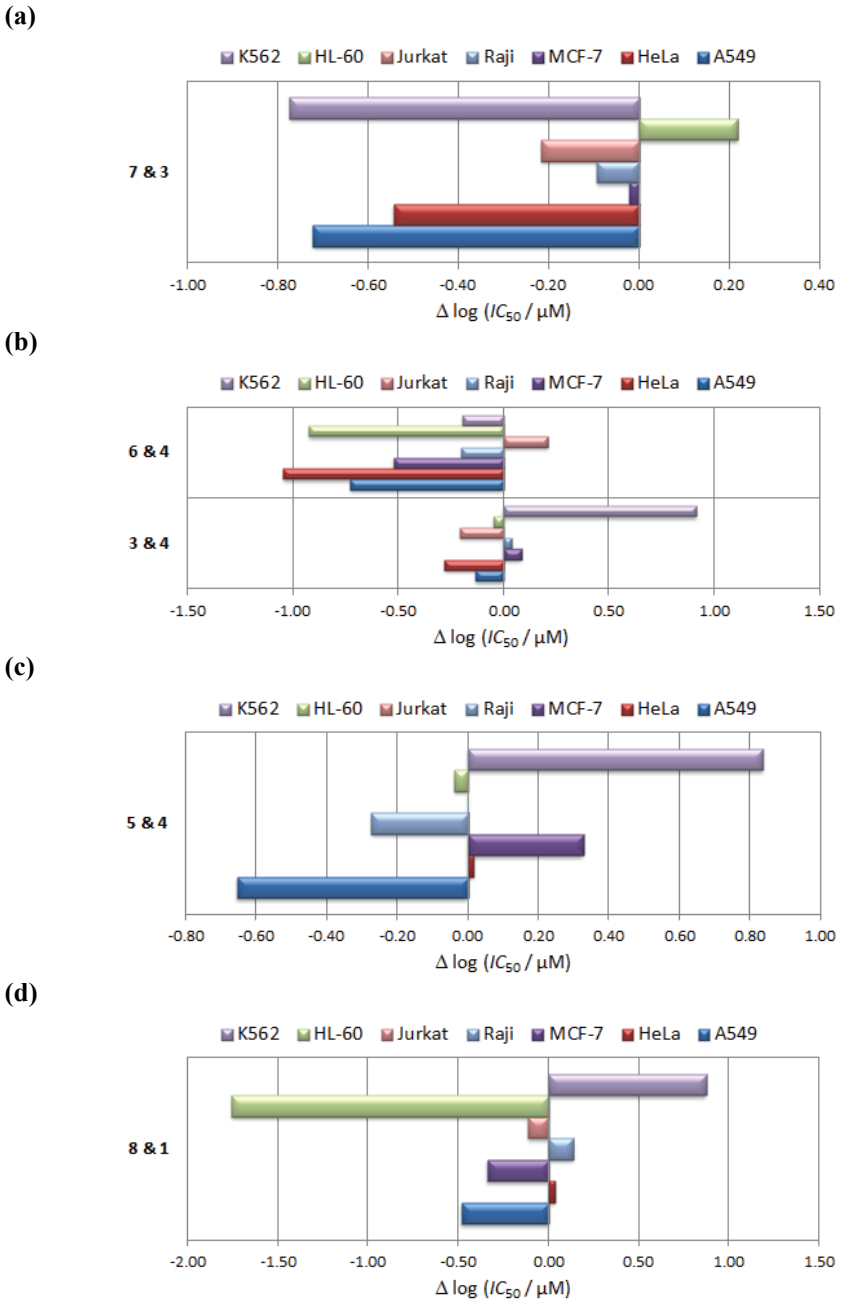

Fig. S-1. Influence of selected structural features on antitumour activities: (a) presence of cinnamoyl ester group; (b) presence of lactone/isopropyledene ring; (c) influence of methoxy group at C-1; (d) influence of thiazol *vs.* phenyl ring.

TABLE OF SYNTHESIZED COMPOUNDS

Table S-II. Chemical structures, numbering schemes and names (labels) of synthesised compounds

Entry	Structure	Name (label)
1	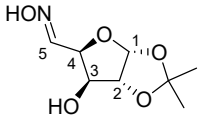	(*E,Z*)-1,2-*O*-Isopropylidene-α-D-*xylo*-pentodialdo-1,4-furanose-5-oxime (**10**)
2	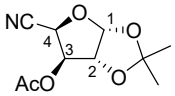	3-*O*-Acetyl-1,2-*O*-isopropylidene-α-D-*xylo*-furanoseurononitrile (**11**)
3	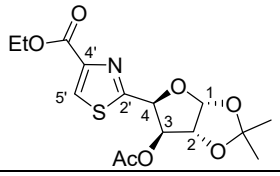	3-*O*-Acetyl-4-*C*-(4′-(ethoxycarbonyl)thiazol-2′-yl)-1,2-*O*-isopropilidene-α-D-*xylo*-tetrofuranose (**12**)
4	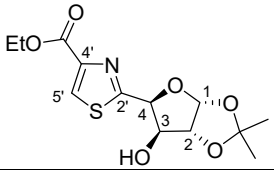	4-*C*-(4′-(Carbamoyl)thiazol-2′-yl)-1,2-*O*-isopropylidene-α-D-*xylo*-tetrofuranose (**3**)
5	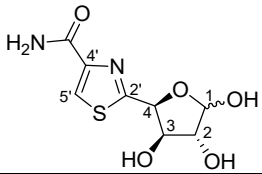	4-*C*-(4′-(Carbamoyl)thiazol-2′-yl)-D-*xylo*-tetrofuranose (**4**)
6	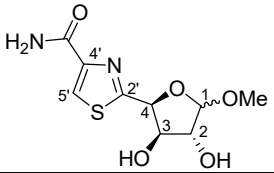	Methyl 4-*C*-(4′-(carbamoyl)thiazol-2′-yl)-D-*xylo*-tetrofuranoside (**5**)
7	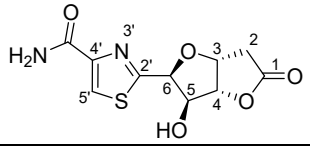	3,6-Anhydro-6-*C*-(4′-(carbamoyl)thiazol-2′-yl)-2-deoxy-D-*ido*-hexono-1,4-lactone (**6**)

Entry	Structure	Name (label)
8	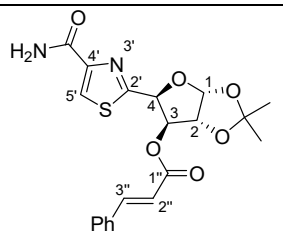	4-*C*-(4′-(Carbamoyl)thiazol-2′-yl)-3-*O*-cinnamoyl-1,2-*O*-isopropylidene-α-D-*xylo*-tetrofuranose (**7**)
9	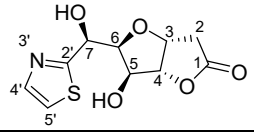	3,6-Anhydro-2-deoxy-7-*C*-(thiazol-2′-yl)-D-*glycero*-D-*ido*-heptono-1,4-lactone (**8**)
10	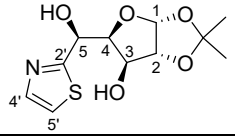	1,2-*O*-Isopropylidene-5-*C*-(thiazol-2′-yl)-α-D-*gluco*-pentofuranose (**14**)

X-RAY ANALYSIS

TABLE S-III. Crystallographic and refinement details of **6** and **14**

	6	**14**
Crystal data		
Chemical formula	$C_{10}H_{10}N_2O_5S$	$C_{11}H_{15}NO_5S$
M_r	270.26	273.30
Crystal system	Orthorhombic	Monoclinic
Space group	$P2_12_12_1$	$P2_1$
Temperature, K	295	295
a / Å	5.24495 (15)	9.3233 (3)
b / Å	9.6990 (3)	6.5430 (2)
c / Å	22.4217 (6)	11.4925 (4)
β / °	90	91.526 (3)
V / Å^3	1140.61 (5)	700.81 (4)
Z	4	2
Radiation type	Mo $K\alpha$	Mo $K\alpha$
μ / mm^{-1}	0.30	0.24
Crystal size, mm	0.67×0.15×0.09	0.67×0.56×0.33
Data collection		
Absorption correction type	Analytical	Analytical
T_{min}	0.892	0.743
T_{max}	0.978	0.937
Measured reflections	18935	10936
Independent reflections	2810	3288
Observed reflections [$I > 2\sigma(I)$]	2649	3030
R_{int}	0.024	0.018
$(\sin \theta/\lambda)_{max}$ / Å^{-1}	0.682	0.681
Refinement		
R [$F^2 > 2\sigma(F^2)$]	0.034	0.037
wR [F^2]	0.081	0.089
S	1.14	1.09
Reflections	2810	3288
Parameters	175	173

	6	**14**
Restraints	0	1
H-atom treatment	Mixed	Mixed
$\Delta\rho_{max}$ / e Å^{-3}	0.27	0.15
$\Delta\rho_{min}$ / e Å^{-3}	−0.26	−0.23
No. of $(I^+-I^-)/(I^++I^-)$ quotients[5]	980	1212
Absolute structure parameter[5]	0.04 (2)	−0.05 (2)

TABLE S-IV. Conformational analysis of tiazofurin derivatives and **6**. Cremer-Pople puckering parameters for furanose ring in tiazofurin derivatives and **6** are calculated for furanose ring atoms enumerated O→C1′→C2′→C3′→C4′, counting clockwise. Thiazole ring is coupled to C1′ atom.

CSD refcode	φ_2 / °	q_2 / Å	closest descriptor	$\lvert\chi\rvert$ / °	Reference
GAPCUV	53.5	0.401	C2'-*exo* – C1'-*endo*	55.5	[4]
FAFMOP	58.1	0.345	C2'-*exo* – C1'-*endo*	21.6	5
FAFMUV	59.7	0.307	major C2'-*exo* – minor C1'-*endo*	23.0	5
BOBNEL10	67.0	0.423	major C2'-*exo* – minor C1'-*endo*	30.7	6
VUNNUN	82.5	0.309	major C2'-*exo* – minor C3'-*endo*	34.5	7
BETKOA10	83.5	0.369	major C2'-*exo* – minor C3'-*endo*	40.8	6
FAFNAC	88.9	0.358	C2'-*exo* – C3'-*endo*	32.5	5
6	255.0 (4)	0.353 (2)	C2'-*endo*	24.3(2)	This work
BOBNOV10	269.2	0.443	major C3'-*exo* – minor C2'-*endo*	20.8	6
VUNPAV	310.2	0.374	C3'-*exo* – C4'-*endo*	27.2	7
YIHCAT	349.9	0.329	major *O*-*exo* – minor C4'-*endo*	16.2	8

TABLE S-V Parameters of hydrogen bonding in **6**

D—H···*A*	*d*(*D*—H) / Å	*d*(H···*A*) / Å	*d*(*D*···*A*) / Å	∠(*D*—H···*A*) / °
N6′—H6′*A*···O1 ^{i}	0.86 (4)	2.08 (4)	2.935 (3)	171 (3)
O5—H5···O6′ ^{ii}	0.92 (4)	1.78 (4)	2.696 (3)	176 (3)

Symmetry codes: (i) −*x*+1/2, −*y*+1, *z*+1/2; (ii) −*x*+2, *y*−1/2, −*z*+3/2.

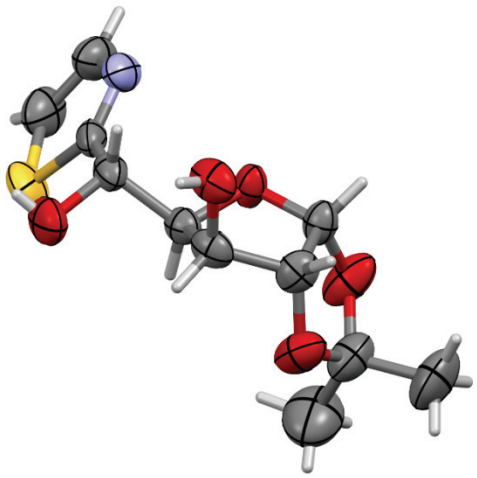

Fig. S-2. Molecular structure of compound **14** (CCDC 2218112)

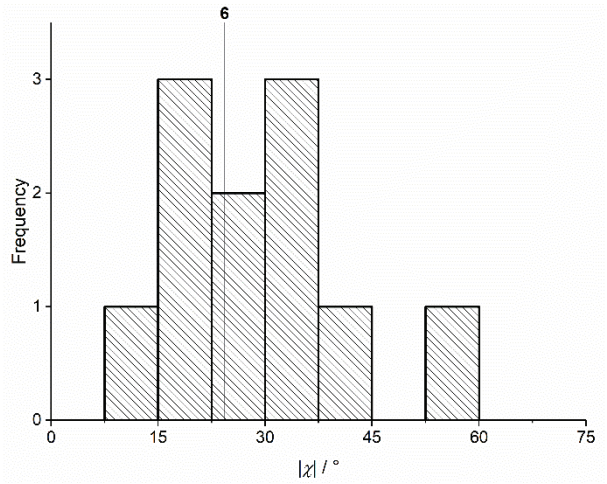

Fig. S-3. Distribution of torsion angle χ (O–C1′–C–S) for analyzed tiazofurin analogues

REFERENCES

1. P. Köll, A. Wernicke, J. Kovács, A. Lützen, *J. Carbohydr. Chem*. **19** (2000) 1019 (http://dx.doi.org/10.1080/07328300008544132)
2. G. Benedeković, J. Francuz, I. Kovačević, M. Popsavin, B. Srećo Zelenović, V. Kojić, G. Bogdanović, V. Divjaković, V. Popsavin, *Eur. J. Med. Chem*. **82** (2014) 449 (http://dx.doi.org/10.1016/j.ejmech.2014.05.081)
3. S. Parsons, H. Flack, T. Wagner, *Acta Crystallogr. Sect B* **69** (2013) 249 (https://doi.org/10.1107/S2052519213010014)
4. B. M. Goldstein, D. T. Mao, V. E. Marquez, *J. Med. Chem*. **31** (1988) 1026 (https://doi.org/10.1021/jm00400a024)
5. T. J. Miller, H. D. Farquar, A. Sheybani, C. E. Tallini, A. S. Saurage, F. R. Fronczek, R. P. Hammer, *Org. Lett*. **4** (2002) 877 (https://doi.org/10.1021/ol017003g)
6. B. M. Goldstein, F. Takusagawa, H. M. Berman, P. C. Srivastava, R. K. Robins, *J. Am. Chem. Soc*. **105** (1983) 7416 (https://doi.org/10.1021/ja00363a035)
7. F. T. Burling, W. H. Hallows, M. J. Phelan, B. Gabrielsen, B. M. Goldstein, *Acta Crystallogr. Sect. B* **48** (1992) 677 (https://doi.org/10.1107/S0108768192001101)
8. A. Dondoni, M.-C. Scherrmann, *J. Org. Chem*. **59** (1994) 6404 (https://doi.org/10.1021/jo00100a050).

Journal of the Serbian Chemical Society
JSCS-info@shd.org.rs • www.shd.org.rs/JSCS
J. Serb. Chem. Soc. *88* (5) 481–494 (2023)
JSCS–5640
Original scientific paper
Published 26 March 2023

On the importance of π–π interactions in the structural stability of phycocyanins

LUKA M. BREBERINA[1], MILAN R. NIKOLIĆ[1#], SRĐAN Đ. STOJANOVIĆ[2#] and MARIO V. ZLATOVIĆ[1*#]

[1]*University of Belgrade – Faculty of Chemistry, Belgrade, Serbia and* [2]*University of Belgrade – Institute of Chemistry, Technology and Metallurgy, Department of Chemistry, Belgrade, Serbia*

(Received 1 December 2022, revised 7 February, accepted 20 February 2023)

Abstract: The influences of π–π interactions in phycocyanin proteins and their environmental preferences were analyzed. The observations indicate that the majority of the aromatic residues in phycocyanin proteins are involved in π–π interactions. Phenylalanine (Phe) and tyrosine (Tyr) residues were found to be involved in π–π interactions much more frequently than tryptophan (Trp) or histidine (His). Similarly, the Phe–Phe and Tyr–Tyr π–π interacting pair had the highest frequency of occurrence. In addition to π-π interactions, the aromatic residues also form π-networks in phycocyanins. The π–π interactions are most favourable at the pair distance range of 5.5–7 Å, with a clear preference for T-shaped ring arrangements. Using *ab initio* calculations, we observed that most of the π–π interactions possess energy from 0 to −10 kJ mol^{-1}. Stabilization centres for these proteins showed that all residues found in π–π interactions are important in locating one or more such centres. π–π interacting residues are evolutionary conserved. The results obtained from this study will be beneficial in further understanding the structural stability and eventual development of protein engineering of phycocyanins.

Keywords: phycobiliproteins; aromatic interactions; stabilization centers; amino acid conservation; *ab initio* study.

INTRODUCTION

Phycobiliproteins (PBPs) are a family of water-soluble, intensely fluorescent holoproteins consisting of apoprotein and covalently bound linear tetrapyrrole chromophores called phycobilins that function as components in the photosynthetic apparatus of cyanobacteria and certain algae.[1] These organisms have been major contributors to the evolution of oxygen and the absorption of carbon diox-

* Corresponding author. E-mail: mario@chem.bg.ac.rs
# Serbian Chemical Society member.
https://doi.org/10.2298/JSC221201008B

ide from the atmosphere.[2] Most common PBPs, differing in their protein structure, phycobilin content attached to conserved cysteine residues, absorbance, and fluorescent properties, are phycoerythrins, with phycoerythrobilin as red chromophore and phycocyanins (C-phycocyanin and allophycocyanin) with blue-purple phycocyanobilin chromophore. They are efficiently used in various sectors, *e.g.*, as colourants in the food and cosmetics industries and pharmaceuticals.[3] In general, the stability of phycocyanin aggregates depends on their origin, amino acid composition, light, pH, temperature and some exogenous substances.[4] Interestingly, molecular forces (predominantly non-covalent interactions) responsible for the observed differences in thermal and chemical stability of different phycocyanin complexes are not entirely understood.[5] Understanding the nature of non-covalent interactions is thus extremely important to see what causes these variations in the properties.

Interaction between the arene systems (π–π) has been recognized as a key stabilizing force in supramolecular chemistry, drug design, biochemistry, crystal engineering, and molecular science.[6-10] The nature of π–π interaction was primarily thought to be dispersive with notable electrostatic contribution depending on the system in question.[11] Although π–π interactions are accepted as weak, they still play an important role in the folding and the thermal stability of proteins.[12,13] The calculated π–π interaction energies of the parallel, edge–face (T--shaped) and offset stacked are –6.19, –10.29 and –10.38 kJ mol^{-1}, respectively,[14] and the major source of attraction are not short-range (such as charge--transfer), but long-range interactions (quadrupole–quadrupole electrostatic and dispersion).[15] Aromatic residues show a high tendency towards forming clusters beyond the dimer, significantly influencing protein folding, structure and stability.[7,16]

The presented study expands on our previous work on the non-covalent interactions and cation–π interactions of phycocyanin crystal structures by analyzing the same protein group with respect to π–π interactions to better understand their stabilizing role.[17,18] We have focused our study on the phycocyanin interfaces and therefore the π–π interactions within a protein are not considered. Obtained results might contribute to the understanding of the structural stability of this class of evolutionary essential proteins with increased practical application and future designs of novel protein–bioactive compound interactions.

EXPERIMENTAL

Dataset

For this study, we used the Protein Data Bank (PDB), accessed on June 14th, 2022, at that moment, listing 191,308 resolved structures.[19] The selection criteria for phycocyanins to be included in the dataset were as follows: 1) structures of proteins containing phycocyanin alpha or beta subunit domain (SCOP Classification, version 1.75)[20] were accepted; 2) theoretical model structures and NMR structures were not included (these structures were not accepted as it was difficult to define the accuracy of the ensemble of structures in terms of dis-

placement that was directly comparable to the X-ray diffraction studies); 3) only crystal structures with the resolution of 2.0 Å or better and a crystallographic *R*-factor of 25.0 % or lower were accepted; 4) we included only representatives having at least 30 % sequence identity. After assembling the dataset, several structures containing ligands and mutant amino acids were rejected, leaving 20 proteins that were actually used as the dataset in our analysis. Hydrogen atoms were added and optimized, where needed, using the program REDUCE,[21] with default settings. REDUCE software adds hydrogen atoms to protein and/or DNA structures in standardized geometry, optimizing them to the orientations of OH, SH, NH_3^+, Met (methionine) methyls, Asn (asparagine) and Gln (glutamine) sidechain amides and His rings. The software determines the best hydrogen positions by selecting the best overall score from all of the possible combinations, taking into account single scores assigned for each individual residue and for groups containing movable protons partitioned in closed sets of local interacting networks. The PDB IDs of selected protein chain structures were as follows: 1all, 1b33, 1cpc, 1f99, 1gh0, 1jbo, 1kn1, 1phn, 2bv8, 2vjt, 2vml, 3dbj, 3o18, 4f0u, 4l1e, 4lm6, 4lms, 4po5, 4rmp and 4yjj.

π–π Interaction analysis

A computer program Discovery Studio Visualizer 2020[22] was used for the calculation of various types π–π interactions and their geometrical features with default settings (Fig. 1). π–π interactions are determined following the methodology of McGaughey.[23] This method finds stacked and staggered π–π interactions by performing the following tests: 1) the distance between the centroid of each pair of π rings is determined to find those which fall within the π–π centroid (R_{cen}) cutoff distance (7 Å by default). For these, an atom from each ring should be within the closest atom distance (R_{clo}) cutoff distance (default 7 Å). The angle θ between the normal of one or both rings and the centroid–centroid vector must fall between 0°, and ± the theta angle cutoff (default 90°), and the angle λ between the normal to each ring must fall between 0° and ± the lambda angle cutoff (default 90°) or greater. The aromatic systems include the aromatic side chains of the residues Trp, Tyr, Phe, and His. However, as His can act either as a cation or as an aromatic moiety depending on its protonation state, in our study, REDUCE software did not suggest protonated form presence in our set of proteins.

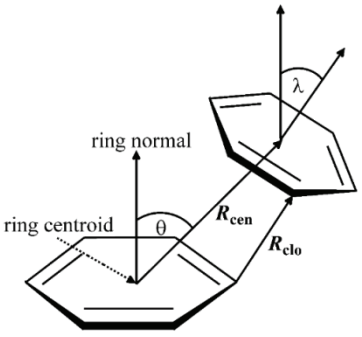

Fig. 1. Parameters for π–π interactions: R_{cen}, the distance between the centroid of each pair of π rings; R_{clo}, the distance between the closest atom of each π ring; θ, the angle between the normal of one or both rings and the centroid–centroid vector; λ, the angle between the normal to each ring.

Computation of π–π interaction energy

To apply *ab initio* methods in determining the energies of π–π pairs on the desired level of theory, with a sufficient level of accuracy and still in the satisfactory time frame, calculations were performed on the structurally reduced model systems: phenylalanine was simpli-

fied to toluene (**1**), histidine to 5-methyl-1*H*-imidazole (**2**), tryptophan to 3-methyl-1*H*-indole (**3**) and tyrosine was reduced to 4-methylphenol (**4**), Fig. 2.[24]

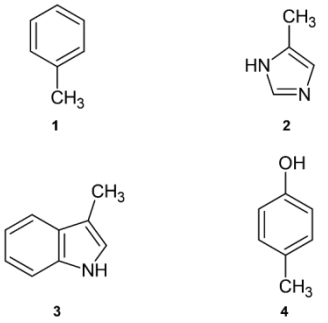

Fig. 2. Structurally reduced structures used for calculations of π–π interaction energy. **1** instead of Phe; **2** instead of His; **3** instead of Trp; **4** instead of Tyr.

Using reduced model systems in calculations of a specific intramolecular interaction in large systems is well known and already proven methodology,[25] producing accurate enough results and still significantly reducing computation times and strength needed. More extensive models, like whole amino acids or parts of the protein chain, will unnecessarily complicate calculations and probably even bring in errors. Numerous interaction mechanisms are possible in a larger protein structure, and a single binding energy computation cannot always correctly determine which of these interactions are present and to what amount they contribute to overall stabilization. As a result, it is difficult to separate the involvement of the π–π interaction and their energy contributions from the interacting pair residues involved in other non-covalent interactions.

Ab initio calculations were performed using Jaguar from Schrödinger Suite 2018-1,[26] using the LMP2 method with triple zeta Dunning's correlation consistent basis set[27] and ++ diffuse functions.[28] All calculations were performed in a vacuum. The LMP2 method applied to the study of π–π interactions, showed to be considerably faster than the MP2 method. Contrary to that, the calculated interaction energies and equilibrium distances were almost identical for both methods.[26] Several authors found that LMP2 represents an excellent method for calculating interaction energies in proteins.[29,30] Sometimes calculation results can be influenced mainly by BSSE, and taking that into account is mandatory for correct results, making the calculation times significantly longer. Local correlation methods (such as LMP2) not only reduce the cost of the calculations but the local Møller–Plesset second-order method LMP2 is well known for reducing intramolecular BSSE.[31-33]

Geometries of interacting structures were optimized using the LMP2/cc-pVTZ(-f)++ level of theory, and their single point energies were calculated at LMP2/cc-pVTZ++ level. We used a slightly smaller basis set for optimization than for SP calculations because the calculated geometries are almost identical as the ones produced with a larger basis set, and the calculations are more suitable for our equipment and almost twofold faster. The optimized geometries were placed in space to match corresponding complexes by superimposing heavy atoms onto their respective coordinates from the crystal structures. Then the energies of dimeric structures produced that way were calculated. The π–π interaction energies in dimers (π–π pairs) were calculated as the difference between the energy of the complex and the sum of the energies of the monomers in their optimized geometries.

As mentioned earlier, the energies in this work were calculated in the gas phase. When observing *in vivo* processes, we can expect that the water molecules and other atoms and

groups from the protein structure could be present in the vicinity, influencing the binding process. To correctly describe the binding, one must be well aware of the role of solvent in the complete process of binding to the proteins. To accurately depict the enthalpy of binding and calculate the interacting energy of bonded structures, high-level quantum mechanical calculations with extended basis sets, including a large number of atoms both in protein and ligand as well, together with water molecules, would be needed. But for a complete understanding of biological complexes and their behaviour, the free-energy changes (ΔG) have to be calculated using some statistical mechanics method.[34,35] However, this will exceed the main goal of this article, which is to point out the possible contribution and significance of the energies of π–π interactions to stability and orientation in protein complexes. Nevertheless, in the description of the complete biomolecular process of binding, accompanying entropies and solvation–desolvation processes are important and can be a dominant factor in the formation of complexes.

At this moment, our main focus was on the possible influence of the energy profile of π–π interactions on protein complexes. Therefore, we selected already-known structures of protein complexes and attempted to calculate energy contributions that originated just from specific π–π interactions whenever it was possible. The results relate only to gas-phase complexes, and the role of the solvent was disregarded. It should, however, be mentioned that the interactions inside the biomacromolecules correspond merely to the gas-phase model, and the gas-phase interactions thus play a vital role.[36]

Computation of stabilization centres

Stabilization centres (SC) are defined as the clusters of residues making cooperative, noncovalent long-range interactions.[37] Measured as individual interactions, stabilization forces resulting from noncovalent long-range interactions are not very strong. Still, since they are cooperative by their nature, in regions where they act in a group of SC, they could play an important role in maintaining the overall stability of protein structures. To analyse the SC of interaction-forming residues, we used the SCide program.[38] The criteria SCide uses for determining SC are as follows: 1) two residues are in contact if there is at least one heavy atom––atom distance smaller than the sum of their van der Waals radii plus 1 Å; 2) a contact is recognized as a "long-range" interaction if the interacting residues are at least ten amino acids apart; 3) two residues form stabilization centres if they are in long-range interaction and if it is possible to select one–one residue from both flanking tetrapeptides of these two residues that make at least seven contacts between these two triplets.[38]

Computation of conservation of amino acid residues

The conservation of amino acid residues in each protein was computed using the ConSurf server.[39] This server computes the conservation based on the comparison of the sequence of the given PDB chain with the proteins deposited in Swiss–Prot database.[40] It identifies ones that are homologous to the PDB sequence. The number of PSI–BLAST iterations and the *E*-value cutoff used in all similarity searches were 1 and 0.001, respectively. All the evolutionary sequences related to each of the proteins in the dataset were used in the subsequent multiple alignments. The residues were classified into nine categories based on these protein sequence alignments. Residues with a score of 1 are considered highly variable, and residues with a score of 9 are considered highly conserved.

RESULTS AND DISCUSSION

In this work, we studied the role of π–π interactions in the interfaces of phycocyanin proteins and their environmental preferences. We performed computat-

ional analysis of the 20 X-ray structures of phycocyanin-containing proteins and summarized π–π interactions to better understand the high stability of phycocyanin oligomers. Also, the relative preference of π–π interacting amino acids in interfaces, interaction geometries, and energetic contribution of π–π interactions, stabilization centres, and conservation score of amino acid residues were analysed.

Preference of aromatic residues for forming π–π interactions

We have analysed the frequency of occurrence of aromatic amino acid residues which are involved in π–π interactions. The results are given in Table 1. There are 158 π–π interactions in phycocyanin proteins in the data set we used. It is interesting to note that there is an average of 8 interactions per protein interface. We observed that in these proteins, Phe and Tyr have a higher occurrence than His and Trp. However, many amino acids are found in phycocyanin interfaces very rarely. Less than 1 % of the His and Trp residues in our database are in phycocyanin interfaces.[17] Considering the benzene ring in Phe and Tyr residues, the greater electro negativity of sp^2 C relative to H produces substantial C^{-}–H^{+} dipole. The C–H dipole accounts well for π–π interaction in phenylalanine.[41] In tyrosine, the hydroxyl group in the ortho position on the benzene ring increases the π-stacking by withdrawing the π-electron density from the substituted benzene, reducing the electrostatic repulsion with other the benzene ring.[42] We compared the occurrence of interacting pairs to find the preference for phycocyanin proteins (Table I). When homo-pairs of aromatic side chains are considered, the

TABLE I. Frequency of occurrence of π–π interaction-forming residues in active centers of phycocyanin proteins

Residue	Number[a]	Occurrence, %[b]
His	12	3.80
Phe	144	45.57
Trp	5	1.58
Tyr	155	49.05
Total	316	100
Interacting pair		
His–His	–	–
His–Phe	6	3.80
His–Trp	–	–
His–Tyr	6	3.80
Phe–Phe	63	39.87
Phe–Trp	–	–
Phe–Tyr	12	7.59
Trp–Trp	–	–
Trp–Tyr	5	3.16
Tyr–Tyr	66	41.78
Total	158	100

[a]The number of times a particular amino acid occurs in an appropriate interaction; [b]percent of amino acid occurs in an appropriate interaction

highest percentage of interactions is observed between Phe–Phe and Tyr–Tyr residues. Among the hetero-pairs, the occurrences of the Phe–Tyr pair are more frequent than other interacting pairs. Hence, these interaction pairs may be quite important in the structural stability of phycocyanin proteins.

We have also analysed the multiple π–π interactions (π-networks) in phycocyanin proteins. These π-networks might add more stability and play an important role in understanding the 3D structure of proteins.[43] The analysis showed that about 75 % of the total π–π interactions in the dataset are involved in the formation of multiple π interactions. The connectivity of the π-ring is found to increase along the length of a network from 2π to 7π. A large π-network can enhance the stability of a protein conformation and can have a considerable influence on protein–ligand interactions. It has also been shown that the addition of an aromatic pair on the protein surface increases its stability.[44] An illustrative example of a typical 7π-network of allophycocyanin B from *Synechocystis* PCC [PDB ID 4PO5] is shown in Fig. 3.

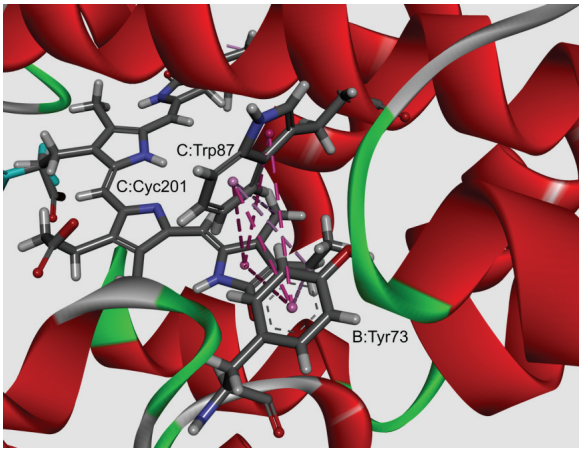

Fig. 3. The view of Trp–Tyr interacting pair and 7π network in allophycocyanin B from *Synechocystis* PCC [PDB ID 4PO5]. The interactions are marked with pink dashed lines.

Interaction geometries and energetic contribution of π–π interactions

The native structure is the compromise of many noncovalent interactions existing in proteins, and the geometrical features relating to the two residue-types are expected to be rather broad. However, based on the distribution of interplanar angles, it was suggested that there is nonrandomness in the packing of side chains.[45] On the basis of the orientation of the aromatic rings, the π–π interactions between two aromatic species have been broadly classified into three categories: edge to face (T-shaped), parallel displaced, and parallel stacked.[46] For example, McGaughey *et al.* analysed 505 proteins and determined that an offset parallel-

-stacked conformation was, on average, 4.18 kJ mol^{-1} more stabilizing than a T--shaped geometry.[23,47] The frequency distribution of the distance and angle parameters of π–π interacting pairs are analysed. These results are shown in Fig. 4. The π–π interacting pairs are most favourable in the distance range (R_{cen}) of 5.5––7 Å (Fig. 4a). At separation distances below 5 Å, aromatic pairs are rarely observed, a result of obvious physical constraints. The distribution of R_{clo} for π–π interactions was found to be a narrow peak at 4 Å (Fig. 4b), which is the optimal average distance between two aromatic rings in a T-shaped orientation. This is because T-shaped orientations have a shorter R_{clo} than parallel orientations. Regardless of the angle, the aromatic side chains orient in a fashion to minimize R_{clo} between the two rings and thus maximize the van der Waals attraction. The normal of one or both rings and the centroid–centroid vector (θ) was found to be bimodal with a prominent minimum between 40 and 60° (Fig. 4c) and it nearly equally prefers apical and equatorial ring orientations. Considering the plane––plane angle (λ), the angles were distributed between all angles (0–90° range) (Fig. 4d). While axial aromatic pairs (λ > 50°) are more frequent, there were a few interactions with angles below 40° (shows coplanarity), possibly to maximize π stacking and packing.[23] Overall, the preferred orientations are quite sim-

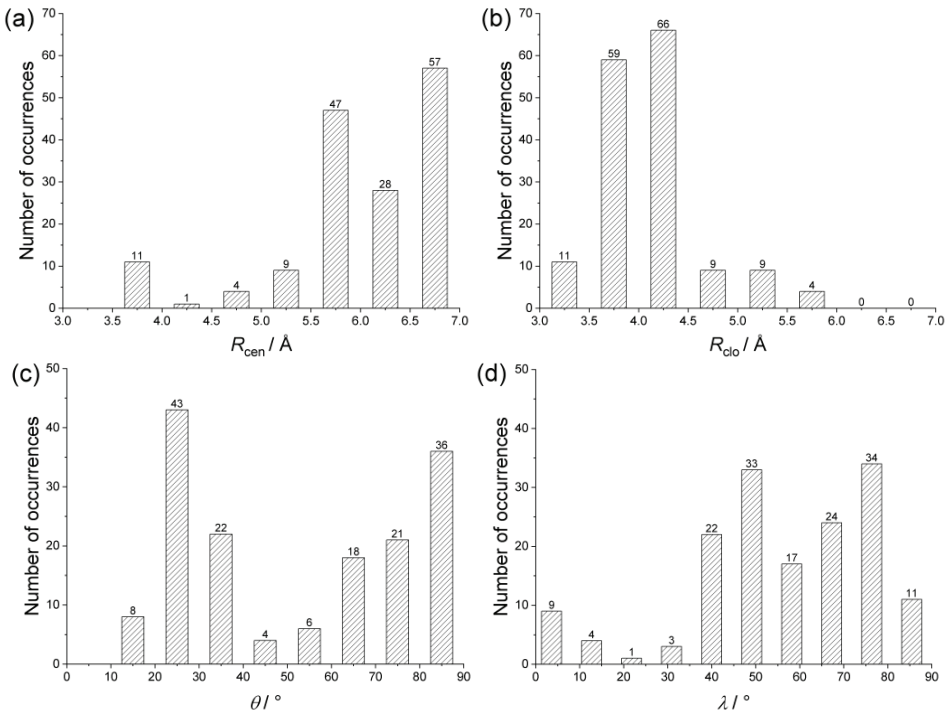

Fig. 4. Interaction geometries of π–π interactions in phycocyanins: a) R_{cen} distance distribution, b) R_{clo} distance distribution c) θ angle distribution, d) λ angle distribution.

ilar to those found with aromatic–aromatic interactions,[48] and the T-shaped orientation is observed. The geometries observed in abundance are not necessarily the ones that have the highest interaction energy between the two moieties in a pair, but the ones that can provide the maximum overall stability to the protein structure by the optimum use of all π interactions.

The quantification of non-covalent interactions is of great importance for a rational approach to biological systems, including protein structure and function, antibody binding, or drug design, as well as for the further development of supramolecular chemistry.[49] Therefore, the energetic contributions of residues involved in π–π interactions were computed using *ab initio* calculations at the LMP2 level. Within a large protein structure, numerous interactions are possible, and sometimes it is not easy to parse out the role of the π–π interaction in their energetics by a simple calculation. Therefore, the interacting pair residues participating in other non-covalent interactions were not analysed. The results for π–π interacting pairs are presented in Fig. 5. The energies calculated for many of the π–π interactions are substantially stabilizing, with 10 % of the total showing positive (repulsive) interaction energies. The repulsive nature of those interactions emerges from the unfavourable geometries of π–π interactions in the crystal structures and is usually counterbalanced by other stronger interactions (salt bridge, H-bonding, or similar).[24] Namely, we mentioned earlier that, when examined under isolated conditions, this type of interaction is considered unfavourable, but similar to other potentially unfavourable interactions, their influence can be compensated by other interactions from the rest of the polypeptide chain. In our database, it was found that π–π interactions showed energy less than −20 kJ mol^{-1}, and most of them have energy in the range 0 to −10 kJ mol^{-1}. The energies associated with π–π interactions may be important contributors to the overall protein stability. It should also be taken into account in supramolecular chemistry and protein engineering fields.[43]

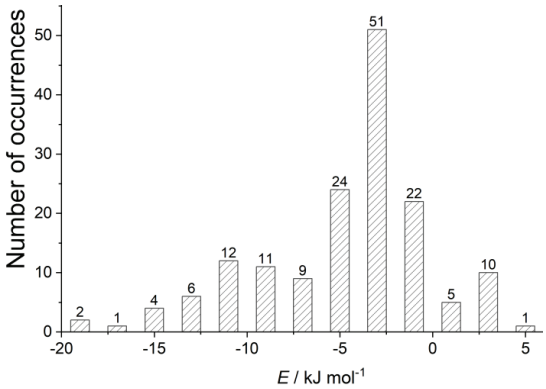

Fig. 5. Interaction energies of π–π interactions in phycocyanins.

The results of our *ab initio* calculations of optimized structures showed that the strongest attractive π–π interaction (−18.58 kJ mol^{-1}) exists between A:Tyr65–I:Tyr65 pair in the monoclinic structure of phycocyanin from *Gloeobacter violaceus* (PDB ID 2vml; Fig. 6).

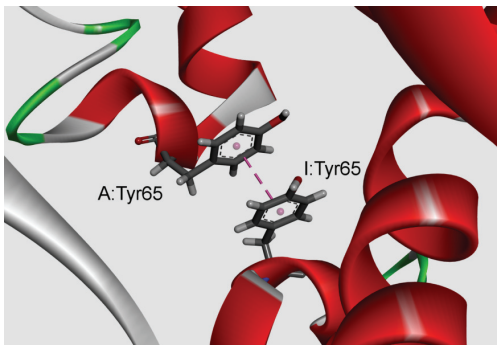

Fig. 6. Details of the strongest attractive π–π interaction of phycocyanin from *Gloeobacter violaceus* (PDB ID 2vml). The interaction is marked with a pink dashed line: A:Tyr65 – I:Tyr65; R_{cen} = 4.00 Å, R_{clo} = 3.55 Å, θ = 24.85°, λ = 5.53°, E = = –18.58 kJ mol^{-1}.

Stabilization centers and conservation of amino acid residues

The unit of stabilization centre is one pair of interacting residues that are far enough in the primary structure and the interactions of which are also supported by other interactions formed by residues located in their vicinity in the primary structure.[37] We have computed the stabilization centre for all π–π interaction forming residues in phycocyanins. Considering the whole data set, 41.4 % of all stabilizing residues are involved in building π–π interactions. It was interesting to note that all residues involved in π–π interactions were included in at least one stabilization centre. These observations strongly reveal that these residues may contribute significantly to the structural stability of these proteins in addition to participating in π–π interactions.

The level of evolutionary conservation was often used as an indicator of the importance of certain positions in maintaining the protein's structure and/or function.[50] Conservation score is a useful parameter for the identification of conserved residues in a protein sequence based on the phylogenetic relations between homologous sequences. Considering the conservation score of π-interacting residues, we found several residues with a conservation score of 9, and there are 57.8 % of residues with a conservation score higher or equal to 6. Our results assumed that most of the residues involved in π–π interactions are evolutionarily conserved. Therefore, we believe that π–π interacting residues have an additional role in maintaining the structure and function of phycocyanin proteins.

CONCLUSION

Even though many studies are done on the molecular aspects, there are no reports on the systematic analysis of π–π interactions in phycocyanin proteins. In the present study, the analysis of the role of π–π interactions in phycocyanin

proteins indicate that most of the aromatic residues are involved in π–π interactions and contribute significantly to the structural stability of these proteins. Considering the individual contribution of the aromatic residues towards π–π interactions, Phe and Tyr residues are found to have exceeded the other two aromatic amino acids. We compared the occurrence of interacting pairs to find the preference for phycocyanin proteins. The Phe–Phe and Tyr–Tyr pairs have a higher frequency of occurrence than other pairs. Furthermore, the multiple interaction patterns found in the present study indicate that around 75 % of the total interacting residues participate in multiple π–π interactions. We also find that all these interacting pairs are favourable in the distance range of 5.5–7 Å. Considering the angle distribution, effective π–π interactions can be realized above a wider area above the π ring, indicating a clear overall preference for T-shaped rings arrangements. The *ab initio* calculations of the optimized structures of interacting π–π pairs showed that favourable energy interactions were less than –20 kJ mol^{-1}, while most of them have energy from 0 to –10 kJ mol^{-1}. A significant percentage of the π–π interacting residues also are located as stabilization centres and thus might provide additional stability to these proteins. The conservation patterns in the present study indicate that more than half of the residues involved in these interactions are evolutionarily conserved. These results were comparable with our earlier observations in protein–porphyrin complexes and superoxide dismutases and show that the fundamental property of π–π interactions, namely non-randomness in the packing of side chains, holds by and large for all categories in macromolecular structures.

In conclusion, the observations obtained in this study identify π–π interactions and structural motifs that contribute to stabilizing the increasingly used phycocyanin proteins, are relevant to the understanding of structure-function relationships, and are helpful to the efforts made to design and engineer protein–protein complexes.

Acknowledgement. The authors would like to thank the Ministry of Education, Science and Technological Development of the Republic of Serbia (Grant No: 451-03-47/2023-01/ /200026 and 451-03-47/2023-01/200168) for financial support.

ИЗВОД

О ЗНАЧАЈУ π–π ИНТЕРАКЦИЈА У СТРУКТУРНОЈ СТАБИЛНОСТИ ФИКОЦИЈАНИНА

ЛУКА М. БРЕБЕРИНА[1], МИЛАН Р. НИКОЛИЋ[1], СРЂАН Ђ. СТОЈАНОВИЋ[2] и МАРИО В. ЗЛАТОВИЋ[1]

[1]Универзитет у Београду – Хемијски факултет, Београд и [2]Универзитет у Београду – Институт за хемију, технологију и металургију, Београд

Анализирани су утицаји π–π интеракција у протеинима фикоцијанинима и њихове преференције ка окружењу. Запажања показују да је већина ароматичних остатака у протеинима фикоцијанинима укључена у π–π интеракције. Утврђено је да су остаци фенилаланина (Phe) и тирозина (Tyr) много чешће укључени у π–π интеракције него триптофана (Trp) или хистидина (His). Слично томе, интерагујући π–π парови Phe–Phe и

Tyr–Tyr имали су највећу учесталост појављивања. Додатно, ароматични остаци такође стварају π-мреже у фикоцијанинима. π–π интеракције су најповољније у распону дистанци парова од 5,5–7 Å, с јасном склоношћу за распоред прстенова у облику слова T. Користећи *ab initio* прорачуне, приметили смо да већина π–π интеракција има енергију у распону од 0 до –10 kJ mol^{-1}. Стабилизациони центри ових протеина показали су да су сви остаци пронађени у π–π интеракцијама важни у лоцирању једног или више таквих центара. π–π интеракциони остаци су еволутивно конзервирани. Резултати добивени овом студијом биће од користи у даљем разумевању структурне стабилности и евентуалном развоју протеинског инжењеринга фикоцијанина.

(Примљено 16. децембра 2022, ревидирано 7. фебруара, прихваћено 20. фебруара 2023)

REFERENCES

1. N. Tandeau de Marsac, *Photosynth. Res*. **76** (2003) 193 (https://doi.org/10.1023/A:1024954911473)
2. P. Falkowski, R. J. Scholes, E. Boyle, J. Canadell, D. Canfield, J. Elser, N. Gruber, K. Hibbard, P. Hogberg, S. Linder, F. T. Mackenzie, B. Moore, III, T. Pedersen, Y. Rosenthal, S. Seitzinger, V. Smetacek, W. Steffen, *Science* **290** (2000) 291 (https://doi.org/10.1126/science.290.5490.291)
3. V. K. Kannaujiya, D. Kumar, V. Singh, R. P. Sinha, in *Natural Bioactive Compounds*, R. Sinha, D. P. Häder, Eds., Academic Press, New York, 2021, pp. 57—81 (ISBN: 0128206594)
4. M. G. de Morais, D. da Fontoura Prates, J. B. Moreira, J. H. Duarte, J. A. V. Costa, *Ind. Biotechnol*. **14** (2018) 30 (https://doi.org/10.1089/ind.2017.0009)
5. McGregor, M. Klartag, L. David, N. Adir, *J. Mol. Biol.* **384** (2008) 406 (https://doi.org/10.1016/j.jmb.2008.09.018)
6. D. Andersson, B. K. Mishra, N. Forsgren, F. Ekström, A. Linusson, *J. Phys. Chem., B* **124** (2020) 6529 (https://doi.org/10.1021/acs.jpcb.0c03778)
7. E. Lanzarotti, L. A. Defelipe, M. A. Marti, A. n. G. Turjanski, *J. Cheminform*. **12** (2020) 30 (https://doi.org/10.1186/s13321-020-00437-4)
8. K. S. Chatterjee, R. Das, *J. Biol. Chem*. **297** (2021) (https://doi.org/10.1016/j.jbc.2021.100970)
9. H. B. Gray, J. R. Winkler, *Chem. Sci.* **12** (2021) 13988 (https://doi.org/10.1039/D1SC04286F)
10. Z. Y. Yan, X. J. Xu, L. Fang, C. Geng, Y. P. Tian, X. D. Li, *Phytopathology Res.* **3** (2021) 10 (https://doi.org/10.1186/s42483-021-00088-9)
11. M. O. Sinnokrot, C. D. Sherrill, *J. Am. Chem. Soc.* **126** (2004) 7690 (https://doi.org/10.1021/ja049434a)
12. R. Bhattacharyya, U. Samanta, P. Chakrabarti, *Protein Eng. Des. Sel*. **15** (2002) 91 (https://doi.org/10.1093/protein/15.2.91)
13. N. Kannan, S. Vishveshwara, *Protein Eng. Des. Sel*. **13** (2000) 753 (https://doi.org/10.1093/protein/13.11.753)
14. S. Tsuzuki, K. Honda, T. Uchimaru, M. Mikami, K. Tanabe, *J. Am. Chem. Soc.* **124** (2002) 104 (https://doi.org/10.1021/ja0105212)
15. V. Morozov, K. M. S. Misura, K. Tsemekhman, D. Baker, *J. Phys. Chem. B*. **108** (2004) 8489 (https://doi.org/10.1021/jp037711e)

16. E. Lanzarotti, R. R. Biekofsky, D. o. A. Estrin, M. A. Marti, A. n. G. Turjanski, *J. Chem. Inf. Model.* **51** (2011) 1623 (https://doi.org/10.1021/ci200062e)
17. L. M. Breberina, M. V. Zlatović, M. R. Nikolić, S. Đ. Stojanović, *Mol. Inform.* **38** (2019) e1800145 (https://doi.org/10.1002/minf.201800145)
18. L. M. Breberina, M. R. Nikolić, S. Đ. Stojanović, M. V. Zlatović, *Comput. Biol. Chem.* **100** (2022) 107752 (https://doi.org/10.1016/j.compbiolchem.2022.107752)
19. P. W. Rose, B. Beran, C. Bi, W. F. Bluhm, D. Dimitropoulos, D. S. Goodsell, A. Prlic, M. Quesada, G. B. Quinn, J. D. Westbrook, J. Young, B. Yukich, C. Zardecki, H. M. Berman, P. E. Bourne, *Nucleic Acids Res*. **39** (2011) D392 (https://doi.org/10.1093/nar/gkq1021)
20. G. Murzin, S. E. Brenner, T. Hubbard, C. Chothia, *J. Mol. Biol*. **247** (1995) 536 (https://doi.org/10.1016/S0022-2836(05)80134-2)
21. J. M. Word, S. C. Lovell, J. S. Richardson, D. C. Richardson, *J. Mol. Biol*. **285** (1999) 1735 (https://doi.org/10.1006/jmbi.1998.2401)
22. *Discovery Studio Visualizer, release 2020*, Accelrys Software Inc., San Diego, CA, 2020
23. G. B. McGaughey, M. Gagné, A. K. Rappé, *J. Biol. Chem*. **273** (1998) 15458 (https://doi.org/10.1074/jbc.273.25.15458)
24. V. R. Ribić, S. Đ. Stojanović, M. V. Zlatović, *Int. J. Biol. Macromol*. **106** (2018) 559 (https://doi.org/10.1016/j.ijbiomac.2017.08.050)
25. J. Hostaš, D. Jakubec, R. A. Laskowski, R. Gnanasekaran, J. Řezáč, J. Vondrášek, P. Hobza, *J. Chem. Theory Comput.* **11** (2015) 4086 (https://doi.org/10.1021/acs.jctc.5b00398)
26. D. Bochevarov, E. Harder, T. F. Hughes, J. R. Greenwood, D. A. Braden, D. M. Philipp, D. Rinaldo, M. D. Halls, J. Zhang, R. A. Friesner, *Int. J. Quantum Chem.* **113** (2013) 2110 (https://doi.org/10.1002/qua.24481)
27. T. H. Dunning, *J. Chem. Phys*. **90** (1989) 1007 https://doi.org/10.1063/1.456153
28. T. Clark, J. Chandrasekhar, G. n. W. Spitznagel, P. V. R. Schleyer, *J. Comput. Chem.* **4** (1983) 294 (https://doi.org/10.1002/jcc.540040303)
29. K. E. Riley, J. A. Platts, J. Řezáč, P. Hobza, J. G. Hill, *J Phys. Chem., A* **116** (2012) 4159 (https://doi.org/10.1021/jp211997b)
30. G. J. Jones, A. Robertazzi, J. A. Platts, *J. Phys. Chem., B* **117** (2013) 3315 (https://doi.org/10.1021/jp400345s)
31. S. Saebø, W. Tong, P. Pulay, *J. Chem. Phys.* **98** (1993) 2170 (https://doi.org/10.1063/1.464195)
32. Reyes, L. Fomina, L. Rumsh, S. Fomine, *Int. J. Quantum Chem.* **104** (2005) 335 (https://doi.org/10.1002/qua.20558)
33. R. M. Balabin, *J. Chem. Phys.* **132** (2010) 231101 (https://doi.org/10.1063/1.3442466)
34. Y. Deng, B. t. Roux, *J. Phys. Chem., B* **113** (2009) 2234 https://doi.org/10.1021/jp807701h
35. J. C. Gumbart, B. t. Roux, C. Chipot, *J. Chem. Theory Comput.* **9** (2013) 794 https://doi.org/10.1021/ct3008099
36. J. Černý, P. Hobza, *Phys. Chem. Chem. Phys.* **9** (2007) 5291 https://doi.org/10.1039/B704781A
37. Z. Dosztányi, A. Fiser, I. Simon, *J. Mol. Biol*. **272** (1997) 597 (https://doi.org/10.1006/jmbi.1997.1242)
38. Z. Dosztányi, C. Magyar, G. Tusnady, I. Simon, *Bioinformatics* **19** (2003) 899 (https://doi.org/10.1093/bioinformatics/btg110)
39. H. Ashkenazy, E. Erez, E. Martz, T. Pupko, N. Ben-Tal, *Nucleic Acids Res.* **38** (2010) W529 (https://doi.org/10.1093/nar/gkq399)

40. B. Boeckmann, A. Bairoch, R. Apweiler, M. C. Blatter, A. Estreicher, E. Gasteiger, M. J. Martin, K. Michoud, C. O'Donovan, I. Phan, S. Pilbout, M. Schneider, *Nucleic Acids Res*. **31** (2003) 365 (https://doi.org/10.1093/nar/gkg095)
41. C. A. Hunter, J. Singh, J. M. Thornton, *J. Mol. Biol*. **218** (1991) 837 (https://doi.org/10.1016/0022-2836(91)90271-7)
42. F. Cozzi, M. Cinquini, R. Annunziata, T. Dwyer, J. S. Siegel, *J. Am. Chem. Soc.* **114** (1992) 5729 (https://doi.org/10.1021/ja00040a036)
43. S. Mahadevi, G. N. Sastry, *Chem. Rev*. **116** (2016) 2775 (https://doi.org/10.1021/cr500344e)
44. Ma, T. Elkayam, H. Wolfson, R. Nussinov, *Proc. Natl. Acad. Sci. USA* **100** (2003) 5772 (https://doi.org/10.1073/pnas.1030237100)
45. J. B. Mitchell, R. A. Laskowski, J. M. Thornton, *Proteins* **29** (1997) 370 (https://doi.org/10.1002/(SICI)1097-0134(199711)29:3%3C370::AID-PROT10%3E3.0.CO;2-K)
46. E. G. Hohenstein, C. D. Sherrill, *J. Phys. Chem., A* **113** (2009) 878 (https://doi.org/10.1021/jp809062x)
47. P. Chakrabarti, R. Bhattacharyya, *Prog. Biophys. Mol. Biol.* **95** (2007) 83 (https://doi.org/10.1016/j.pbiomolbio.2007.03.016)
48. B. P. Dimitrijević, S. Z. Borozan, S. Đ. Stojanović, *RSC Adv.* **2** (2012) 12963 (https://doi.org/10.1039/C2RA21937A)
49. P. A. Maury, D. N. Reinhoudt, J. Huskens, *Curr. Opin. Colloid Interface Sci*. **13** (2008) 74 (https://doi.org/10.1016/j.cocis.2007.08.013)
50. M. Landau, I. Mayrose, Y. Rosenberg, F. Glaser, E. Martz, T. Pupko, N. Ben-Tal, *Nucleic Acids Res*. **33** (2005) W299-W302 (https://doi.org/10.1093/nar/gki370).

Journal of the Serbian Chemical Society
JSCS-info@shd.org.rs • www.shd.org.rs/JSCS
J. Serb. Chem. Soc. *88* (5) 495–504 (2023)
JSCS–5641
Original scientific paper
Published 17 May 2023

Adsorption of tannase from *Aspergillus ficuum* to carboxyl--functionalized multi-walled carbon nanotubes

MATTHEW RAJ ALIAS[1], CHONG-BOON ONG[1]* AND MOHAMAD SUFFIAN MOHAMAD ANNUAR[2]

[1]*School of Science and Psychology, Faculty of Arts and Sciences, International University of Malaya-Wales, 50480 Kuala Lumpur, Malaysia and* [2]*Institute of Biological Sciences, Faculty of Science, Universiti Malaya, 50603 Kuala Lumpur, Malaysia*

(Received 21 November 2022, revised 3 January, accepted 1 March 2023)

Abstract: The immobilization of cross-linked tannase onto carboxyl-functionalized multi-walled carbon nanotubes (MWCNT–COOH) was achieved *via* physical adsorption. Glutaraldehyde was used to cross-link the enzyme molecules. Spectroscopic and morphological characterizations of the enzyme-nanotubes composite were carried out, which authenticated the successful adsorption event. Enzyme composite is proven equal to, or even superior than free tannase, in terms of catalytic activities and stabilities, when measured under different thermal, pH and recycling conditions. Whilst both free and immobilized tannase preparations exhibited optimum catalysis at pH 5.0 and 35 °C, tannase-nanotubes composite possesses better thermal stability. The immobilized preparation retained 75 % of its initial catalytic activity following ten consecutive uses. The study demonstrated a facile method to produce catalytically efficient nanobiocatalyst composite for biotechnological applications.

Keywords: MWCNT; MWCNT–COOH; nanobiocatalyst; enzyme immobilization; enzymes stability and reusability.

INTRODUCTION

The initial hydrolysis of tannin is mediated by tannase (tannin acyl hydrolases, EC 3.1.1.20), which catalyzes the hydrolysis of ester and depside bonds found in tannins to release, *e.g.*, gallic acid, catechin and glucose.[1] The enzyme also fulfills a number of applications for different industrial sectors, such as food and beverages, cosmetics, as well as biological remediation. However, the role of tannase in the production of gallic acid is the most often highlighted. The compound is a feedstock in the production of antibacterial drugs, and in the synthesis

* Corresponding author. E-mail: ongchongboon@yahoo.com
https://doi.org/10.2298/JSC221121009A

of esters such as propyl gallate, an important additive and antioxidant in the food industry.[2]

Recently, developments in nanomaterials and their applications have opened up numerous opportunities in the area of nanobiocatalysis.[3] Carbon nanomaterials have been promoted as versatile supports for enzyme immobilization due to their small size, large surface area, mechanical and thermal stabilities.[4] Enzyme attachment to a nanoscale support material allows for a much higher enzyme loading, and catalytic stability was exceedingly better than those of free enzyme.[5] Among the various nanostructured materials, such as nanoparticles, nanofibers or carbon nanotubes (CNT), the latter is considered markedly promising for enzyme immobilization.[6]

Two main types of CNT namely, single-walled carbon nanotubes (SWCNT), and multi-walled carbon nanotubes (MWCNT) have been utilized as a support in enzyme immobilization.[3,7] Whilst SWCNT are attractive because of their higher surface area/high enzyme loading capacity, MWCNT are preferred alternative due to their better dispersibility, environmental and health safety. MWCNT have been frequently reported as a popular choice of starting nanomaterial for potential developments in recent years owing to their unique properties such as biocompatibility, high mechanical stability, good dispersibility, and high surface-to-volume ratio, ordered, nonporous structure, and large surface area.[8] Recently, a wide variety of enzymes such as ferredoxin-NAD(P)$^+$ reductase (NAhAa),[9] lipase,[10] L-ribose isomerase,[11] L-asparaginase,[8] peroxidase[12] and cellulase[13] have been successfully immobilized on carboxyl-functionalized MWCNT (MWCNT–COOH) for various applications. The nanobiocatalyst composites obtained are stable and active at a relatively high temperature, providing a unique combination of useful attributes such as low mass transfer resistance, as well as recycling of the catalyst.[13]

In this study we have investigated the attachment of tannase from *Aspergillus ficuum* to carboxyl-functionalized multi-walled carbon nanotubes (MWCNT–COOH) *via* facile adsorption, hence its immobilization. The efficiency of immobilized enzyme preparation, along with its stability and reusability were compared to its free counterpart.

EXPERIMENTAL

Materials

Carboxyl-functionalized multi-walled carbon nanotubes (MWCNT–COOH, length of 1.5 μm×outer diameter of 9.5 nm, Cat. #755125), tannic acid, gallic acid, rhodanine, potassium hydroxide and tannase from *Aspergillus ficuum* (EC 3. 1. 1.20; ≥ 150 U g^{-1}) were purchased from Sigma–Aldrich. Citric acid and trisodium citrate dehydrate were procured from Merck. Ultrapure water (18.2 MΩ·cm resistivity at 25 °C) was used to prepare buffer and reagent solutions. All chemicals used are ACS reagent grade, and were used as received from the suppliers.

Immobilization of tannase onto MWCNT–COOH

The MWCNT–COOH (3 mg) was dispersed in 3.0 ml of 50 mM citrate buffer (pH 4.7) *via* sonication at 37 kHz frequency, and 0.8 W sonification power (Elmasonic P30H, Elma, Singen, Germany) for 30 min. To the suspension, 0.3 mg of tannase was added, followed by incubation at 25 °C for 60 min under constant shaking at 200 rpm. Subsequently, 0.18 ml glutaraldehyde (3 vol. %) was added to the mixture, followed by shaking at 200 rpm, 25 °C for 60 min. Afterwards, the suspension was centrifuged for 30 min (6153*g*), and the supernatant was decanted. The unbound proteins were removed by washing with citrate buffer (pH 4.7) for at least five times. Then, the recovered enzyme-nanotubes composite was lyophilized overnight, and stored at 4 °C prior to use.

The enzyme loading efficiency was estimated as reported by Ulu *et al.*:[8]

$$\text{Enzyme loading efficiency}(\%) = 100\frac{C_\text{i}V_\text{i} - C_\text{f}V_\text{f}}{C_\text{i}V_\text{i}} \quad (1)$$

where C_i is the initial enzyme protein concentration (mg ml^{-1}), V_i is the initial volume of enzyme solution (ml), C_f is the residual enzyme protein concentration in the total supernatant (mg ml^{-1}), and V_f is the total volume of total supernatant (ml). The enzyme protein concentrations in solutions were measured by the Bradford assay with Bovine Serum Albumin (BSA) as a standard protein.

Characterization of tannase–nanotubes composite

Fourier transform infrared spectroscopy (FTIR, Perkin Elmer, model: Spectrum™ 400) in the frequency range (450–4000 cm^{-1}) was employed to analyze the signature functional group signals of MWCNT–COOH and tannase-immobilized MWCNT–COOH composite from He–Ne laser that emits red light with a wavelength of 633 nm. Field emission scanning electron microscopy (FESEM, FEI, model: FEL Quanta™ 450 FEG, operating voltage 10 kV) and transmission electron microscope (TEM, Carl Zeiss, model: Libra® 120 FEG) operated at accelerating voltage of 120 kV were used to observe the fine morphologies of pristine MWCNT–COOH and tannase-nanotubes composite.

Tannase assay

Tannin hydrolysis was determined based on the formation of chromogen between gallic acid and rhodanine (2-thioxo-4-thiazolidinone), resulting in a colored product with strong absorption at λ_max 520 nm according to Sharma *et al.*[14] Tannic acid at a final concentration of 0.075 mM was used as the substrate, and different concentrations of gallic acid were applied in standard calibration. One unit (U) of tannase activity is defined as 1 μmol of gallic acid released per min at pH 4.7 and 30 °C.

Effects of pH and temperature on tannase activities

The optimum temperature for free- and immobilized tannase catalysis were determined by performing enzyme assay at different temperatures from 20 °C to 45 °C at pH 4.7. Another set of experiments was also carried out to examine the effects of pH on free and immobilized enzyme activities (at 30 °C) in 50 mM citrate buffer at different pH, *i.e.*, 3.5 to 5.5, and in 50 mM phosphate buffer at different pH, *i.e.*, 6.0 to 7.0. The ratio of enzyme activity-to-enzyme activity at optimal pH or temperature yields residual enzyme activity (%).

Thermal stability of free and immobilized tannase

Thermal stability of the free- and immobilized tannase was investigated by incubating the preparations at different temperatures (30, 40, 50, 60 and 70 °C) and pH 4.7 (50 mM citrate buffer) for 60 min in the absence of enzyme substrate. After 60 min, the residual tannase

activities were determined. The relative activities of the free and immobilized tannase without incubation were considered to be 100 %.

Reusability of immobilized tannase

The reusability of the immobilized preparation was evaluated according to the standard assay conditions. After each cycle, the immobilized tannase was recovered by centrifugation (6153*g*, 30 min). The pellet was washed thrice with assay buffer before the subsequent cycle. For the consecutive successive cycles, the immobilized preparation was resuspended in a fresh substrate solution, and the reaction was carried out as described earlier. The activity of the immobilized preparation in the first cycle was considered to be 100 %.

Statistical analysis

All experiments were performed in triplicates. The data obtained were expressed as mean ± standard deviation. Microsoft Office Excel (Microsoft Corporation, USA) was used to calculate the means and standard deviations, and graph plotting.

RESULTS AND DISCUSSION

The enzyme loading efficiency

In this study, 0.1 mg of MWCNT–COOH was found efficient for the immobilization of 0.1 mg tannase *via* adsorption mechanism with the protein loading efficiency of 81 % under the experimental conditions used.

Fourier transform infrared spectroscopy (FTIR)

From Table I, for MWCNT–COOH, the signal peaks at 1740 and 2922 cm^{-1} are due to C=O and O–H stretching of carboxylic groups (O=C–OH) from the side wall of the graphite structure.[15] For MWCNT–COOH–tannase composite, signal peaks at and 1543 cm^{-1} are attributed to the amine C–N stretching and amine N–H bending lend support that tannase enzyme was successfully attached to the MWCNT–COOH carrier,[10] presumably *via* non-specific interactions involving hydrogen bonding and van der Waals forces between the amino acids of the enzyme and MWCNT–COOH carrier. Stable non-specific, multipoint interactions between tannase molecules and MWCNT–COOH are hypothesized to minimize enzyme conformational changes hence preventing the distortion of its active site.

TABLE I. Signal assignments for: a) pristine MWCNT–COOH and b) MWCNT–COO–tannase composite

Sample	Frequency, cm-1	Functional group
MWCNT–COOH	1740	C=O stretching
	2922	O–H stretching
MWCNT–COOH-tannase	1168	Amine C–N stretching
composite	1543	Amine N–H bending

Morphologies of MWCNT–COOH and tannase-immobilized MWCNT–COOH

Figs. 1 and 2 show the FESEM and TEM micrographs of the MWCNT–COOH and tannase-immobilized MWCNT–COOH, respectively. As shown in Fig. 1a, the MWCNT–COOH sample exhibits a distinct, smoother strands of tubes. On the other hand, for tannase-immobilized MWCNT–COOH sample (Fig. 1b), the morphology is in contrast to pristine MWCNT–COOH, which indicates successful deposition of the enzyme molecules onto the carbon nanotubes. The observed increase in thickness dimension of the strands of the enzyme–nanotubes composite sample (Fig. 2b) compared to MWCNT–COOH sample (Fig. 2a) is ascribed to the adsorption of tannase onto the outermost wall of MWCNT–COOH. These morphological characteristics bear strong resemblance to the images reported in the previous study of lipase enzyme immobilization on MWCNT–COOH.[15]

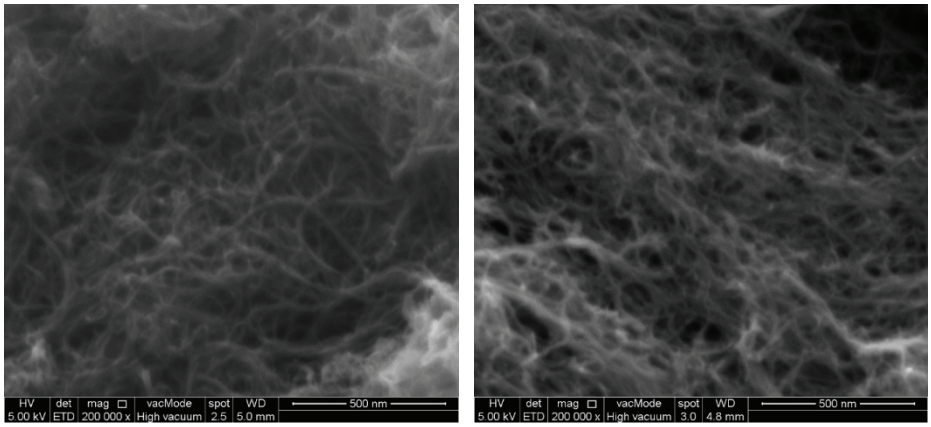

(a) (b)

Fig. 1. FESEM micrographs of the MWCNT–COOH: a) before and b) after tannase immobilization.

(a) (b)

Fig. 2. TEM micrographs of the MWCNT–COOH: a) before and b) after tannase immobilization. The increased thickness of the carbon nanotubes is due to deposition of enzyme molecules onto outermost wall *via* physical adsorption.

Optimum pH and temperature for free and immobilized tannase

Fig. 3 shows the effect of pH on the relative activities of free and immobilized tannase. The enzyme activities were highest at pH 5.0 for both free and immobilized preparation, hence, 5.0 is the optimum pH value. Immobilized tannase showed no observable alteration in its optimum pH and shared a similar pH-activity profile with its free counterpart. The finding is in general agreement to the previous study, *i.e.*, identical optimum pH at 5.0 for both free and immobilized tannase obtained from *Aspergillus ficuum*.[16,17] In contrast, Li *et al.*[18] reported that the optimal pH value for immobilized tannase (pH 4.5) was lower than that of the free tannase (pH 5.5) when sourced from *A. niger*.

The effects of temperature (20–45 °C) on the free and immobilized enzyme activities were studied in 50 mM citrate buffer (pH 4.7, Fig. 4). Both free and immobilized preparations showed identical optimum temperature at 35 °C. Although

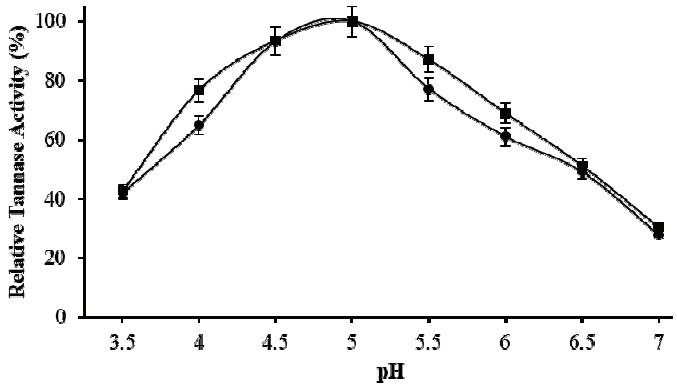

Fig. 3. Effects of pH on the enzyme activities. Square marker refers to the immobilized enzyme preparation while circle marker to free tannase.

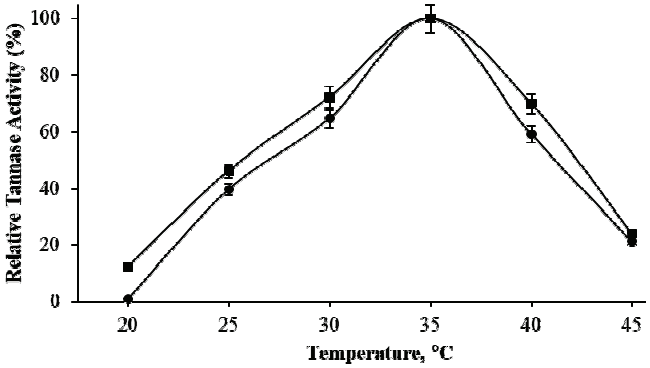

Fig. 4. Effects of temperature on the enzyme activities. Square marker refers to immobilized enzyme preparation while circle marker to free tannase.

temperature profiles of immobilized enzyme exhibited similar trend to those of free enzyme, significantly higher relative activities were observed for immobilized preparation over the temperature range studied. Similar observation was reported where free and immobilized *A. ficuum* tannase exhibited the same optimal temperature after immobilization onto pristine MWCNT.[16] It has been reported that immobilization may not necessarily alter the optimum temperature of tannase catalysis.[18,19]

Thermal stability of free and immobilized tannase

Fig. 5 shows the effect of temperature on the stability of the free and immobilized tannase preparations. The immobilized tannase preserved over 60 % of its initial activity while its free counterpart lost half its initial activity after incubation for one hour at 60 °C. It is clear that immobilization provides a more thermally-stable enzyme preparation compared to free tannase. Similar results were observed for tannase from *A. tubingensis* when immobilized onto carboxyl-functionalized super-paramagnetic ferroferric oxide particles,[19] and also tannase from *A. ficuum* immobilized onto pristine MWCNT nanocomposites.[16] The immobilization had put a restriction on the enzyme molecule conformational mobility, thus reducing the likelihoods of thermal-mediated deactivation of the enzyme.[20]

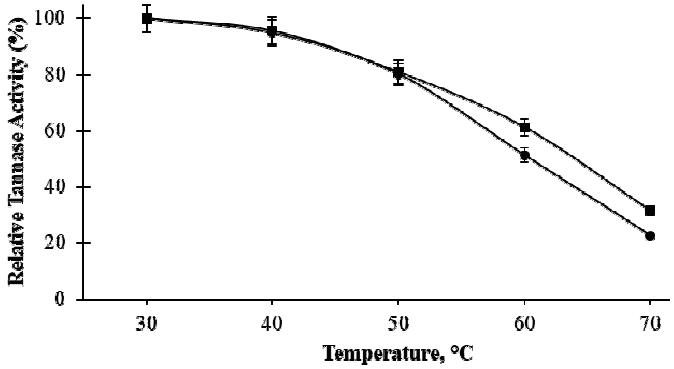

Fig. 5. Thermal stabilities of the free- and immobilized tannase preparations. Square marker refers to immobilized enzyme preparation while circle marker to free tannase.

Reusability of the immobilized tannase

The tannase-immobilized MWCNT–COOH composites retained residual activity above 75 % following ten batches of consecutive reactions (Fig. 6), whereas tannase immobilized onto pristine MWCNT recorded significantly lower residual activity at 34 % after ten cycles.[16] In other study, L-asparaginase-immobilized MWCNT–COOH doped calcium-alginate beads retained only 37 % of its initial activity after ten successive catalytic cycles.[8] From the results, it can be concluded that tannase is far more stable when immobilized onto the MWCNT–

–COOH surface compared to the single use, free enzyme, which opens up a wide possibilities for practical applications of tannase in the future.

Since tannase adsorption onto the MWCNT–COOH is exclusively due to non-specific interactions such as hydrogen bonding and van der Waals, it is highly likely that enzyme leakage, over the combined course of applications and washing steps, is responsible for the observed minor losses of activities during consecutive uses of the immobilized enzyme preparation (Fig. 6). Such occurrence is not uncommon, and almost certain to ensue in the case of physical adsorption of an enzyme to a solid support compared to when an enzyme is covalently coupled to the support. Nonetheless, the observed loss is rather negligible for each cycle relative to its precursor.

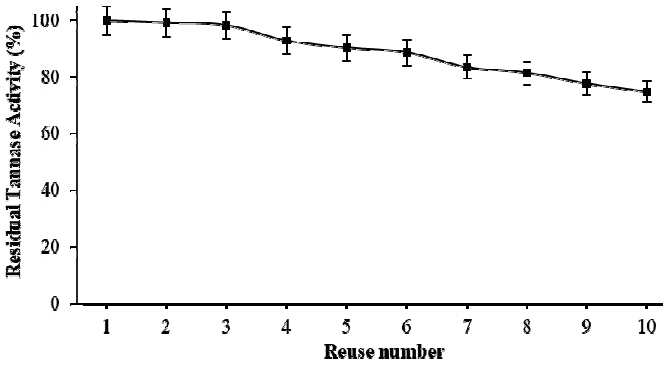

Fig. 6. Reusability of tannase-immobilized MWCNT–COOH preparation.

CONCLUSIONS

This study shows that tannase from *Aspergillus ficuum* was successfully immobilized onto carboxyl-functionalized MWCNT *via* the physical absorption method. The immobilized preparation exhibits identical optimum pH and temperature with its free counterpart with the exception of better thermostability. The facile immobilization also allows for catalytic reusability up to ten consecutive cycles with minor reduction in activity. Potentially wide applications for nano-biocatalyst, with such attributes, are envisaged.

Acknowledgments. This study was carried out in the Bioprocess and Enzyme Technology Laboratory, Institute of Biological Sciences, Universiti Malaya, and supported by the internal research grant of the International University of Malaya-Wales (Ref: RMC/2021-22/03) for which the authors are thankful.

ИЗВОД

АДСОРПЦИЈА ТАНАЗЕ ИЗ *Aspergillus ficuum* НА ВИШЕСЛОЈНЕ УГЉЕНИЧНЕ НАНОЦЕВИ СА КАРБОКСИЛНИМ ГРУПАМА

MATTHEW RAJ ALIAS[1], CHONG-BOON ONG[1] и MOHAMAD SUFFIAN MOHAMAD ANNUAR[2]

[1]*School of Science and Psychology, Faculty of Arts and Sciences, International University of Malaya-Wales, 50480 Kuala Lumpur, Malaysia и* [2]*Institute of Biological Sciences, Faculty of Science, Universiti Malaya, 50603 Kuala Lumpur, Malaysia*

Имобилизација умрежене таназе на мултићелијске угљеничне наноцеви са карбоксилним групама (MWCNT–COOH) је постигнута физичком адсорпцијом. Глутаралдехид је коришћен за умрежавање молекула ензима. Спектроскопска и морфолошка карактеризација композитног материјала ензима и наноцеви је потврдила успешну адсорпцију. Ензимски композит се показао једнаким или бољим од слободне таназе у смислу каталитичке активности и стабилности, под различитим температурним, pH и условима рециклирања. Иако слободна и имобилизована таназа испољавају оптималне каталитичке особине на pH 5,0 и 35 °C, композит таназе и наноцеви има већу термалну стабилности. Имобилизовани препарат задржава 75 % почетне каталитичке активности након десет узастопних примена. У раду је приказан једноставан метод за производњу каталитички ефикасног нанобиокатализатора за биотехнолошку употребу.

(Примљено 21. новембра 2022, ревидирано 3. јануара, прихваћено 1. марта 2023)

REFERENCES

1. A. S. Ristinmaa, T. Coleman, L. Cesar, A. Langborg Weinmann, S. Mazurkewich, G. Brändén, M. Hasani, J. Larsbrink, *J. Biol. Chem.* **298** (2022) (https://dx.doi.org/10.1016/j.jbc.2022.101758)
2. C. S. de Lima, B. T. A. Koelher, E. G. P. da Silva, A. Góes-Neto, R. P. Rezende, A. P. T. Uetanabaro, A. M. da Costa, *Fungal Biology* **126** (2022) 471 (https://dx.doi.org/10.1016/j.funbio.2022.04.001)
3. M. d. R. G. Dias, G. P. C. da Silva, A. de Pauloveloso, N. Krieger, C. Pilissão, *Chirality* **34** (2022) 1008 (https://dx.doi.org/10.1002/chir.23454)
4. M. Markiton, S. Boncel, D. Janas, A. Chrobok, *ACS Sustain. Chem. Eng.* **5** (2017) 1685 (https://dx.doi.org/10.1021/acssuschemeng.6b02433)
5. Z. L. Li, L. Cheng, L. W. Zhang, W. Liu, W. Q. Ma, L. Liu, *Process Saf. Environ. Prot.* **107** (2017) 463 (https://dx.doi.org/10.1016/j.psep.2017.02.021)
6. N. Singh, B. S. Dhanya, M. L. Verma, *Mater. Sci. Energy Technol.* **3** (2020) 808 (https://dx.doi.org/10.1016/j.mset.2020.09.006)
7. Y. Yamada, K. Obuchi, N. Kikuchi, A. A. Almarasy, A. Fujimori, *Langmuir* **38** (2022) 5692 (https://dx.doi.org/10.1021/acs.langmuir.2c00283)
8. A. Ulu, M. Karaman, F. Yapıcı, M. Naz, S. Sayın, E. İ. Saygılı, B. Ateş, *Catal. Lett.* **150** (2020) 1679 (https://dx.doi.org/10.1007/s10562-019-03069-y)
9. S. Zhao, P. Feng, Z. Yu, T. Zhou, T. Gao, M. M. Redina, P. Liu, X. Li, *Chemosphere* **291** (2022) 132934 (https://dx.doi.org/10.1016/j.chemosphere.2021.132934)
10. M. K. Ghide, K. Li, J. Wang, S. A. Abdulmalek, Y. Yan, *Food Chem.* **390** (2022) 133171 (https://dx.doi.org/10.1016/j.foodchem.2022.133171)
11. A. Singh, S. K. Rai, M. Manisha, S. K. Yadav, *Mol. Catal.* **511** (2021) 111723 (https://dx.doi.org/10.1016/j.mcat.2021.111723)

12. L. Y. Jun, N. M. Mubarak, L. S. Yon, C. H. Bing, M. Khalid, P. Jagadish, E. C. Abdullah, *Sci. Rep.* **9** (2019) 2215 (https://dx.doi.org/10.1038/s41598-019-39621-4)
13. R. Ahmad, S. K. Khare, *Bioresour. Technol.* **252** (2018) 72 (https://dx.doi.org/10.1016/j.biortech.2017.12.082)
14. S. Sharma, T. K. Bhat, R. K. Dawra, *Anal. Biochem.* **279** (2000) 85 (https://dx.doi.org/10.1006/abio.1999.4405)
15. M. Mohammadi, M. Ashjari, M. Garmroodi, M. Yousefi, A. A. Karkhane, *RSC Advances* **6** (2016) 72275 (https://dx.doi.org/10.1039/C6RA14142K)
16. C.-B. Ong, M. S. M. Annuar, *Preparative Biochemistry & Biotechnology* **48** (2018) 181 (https://dx.doi.org/10.1080/10826068.2018.1425707)
17. J. S. de Lima, M. P. Cabrera, C. M. de Souza Motta, A. Converti, L. B. Carvalho, Jr., *Food Res. Int.* **107** (2018) 470 (https://dx.doi.org/10.1016/j.foodres.2018.02.066)
18. R. Li, G. Fu, C. Liu, D. J. McClements, Y. Wan, S. Wang, T. Liu, *Int. J. Biol. Macromol.* **114** (2018) 1134 (https://dx.doi.org/j.ijbiomac.2018.03.077)
19. C. Wu, C. Xu, H. Ni, Q. Yang, H. Cai, A. Xiao, *Bioresour. Technol.* **205** (2016) 67 (https://dx.doi.org/10.1016/j.biortech.2016.01.032)
20. A. Xiao, C. Xu, Y. Lin, H. Ni, Y. Zhu, H. Cai, *Electron. J. Biotechnol.* **19** (2016) 1 (https://dx.doi.org/10.1016/j.ejbt.2015.10.001).

Journal of the Serbian Chemical Society
JSCS@tmf.bg.ac.rs • www.shd.org.rs/JSCS
J. Serb. Chem. Soc. *88* (5) 505–520 (2023)
JSCS–5642
Original scientific paper
Published 14 April 2023

Diversifying the chloroquinoline scaffold against SARS-CoV-2 main protease: Virtual screening approach using cross-docking, SiteMap analysis and molecular dynamics simulation

MOHAMED AISSAOUI[1]*, BILLEL BELHANI[1], ABDELMOUMEN BOULEBNANE[2], ABDESLEM BOUZINA[1] and SALAH EDDINE DJILANI[3]

[1]*Laboratory of Applied Organic Chemistry, Synthesis of Biomolecules and Molecular Modelling Group, Department of Chemistry, Sciences Faculty, Badji-Mokhtar-Annaba University, Box 12, 23000 Annaba, Algeria,* [2]*Department of English, University of Algiers 2, Abou El Kacem Saâdallah, Algiers, Algeria and* [3]*Laboratory of Synthesis and Organic Biocatalysis, Department of Chemistry, Badji-Mokhtar-Annaba University, Algeria*

(Received 17 October, revised 3 December 3 2022, accepted 11 January 2023)

Abstract: The absence of designated remedies for coronavirus disease 19 (Covid-19) and the lack of treatment protocols drove scientists to propose new small molecules and to attempt to repurpose existing drugs against various targets of severe acute respiratory syndrome coronavirus 2 (SARS-CoV-2) in order to bring forward efficient solutions. The main protease (M^{pro}) is one of the most promising drug targets due to its crucial role in fighting viral replication. Several antiviral drugs have been used in an attempt to overcome the pandemic, such as hydroxychloroquine (HCQ). Despite its perceived positive outcomes in the beginning of the disease, HCQ was associated with several drawbacks, such as insolubility, toxicity, and cardiac adverse effects. Therefore, in the present study, a structure-based virtual screening approach was performed to identify structurally modified ligands of the chloroquinoline (CQ) scaffold with good solubility, absorption, and permeation aimed at eventually suggesting a more dependable alternative. PDB ID:7BRP M^{pro} was chosen as the most reliable receptor after cross-docking calculation using 30 crystal structures. Then, a SiteMap analysis was performed and a total of 231,456 structurally modified compounds of the CQ scaffold were suggested. After Lipinski criteria filtration, 64,312 molecules were docked and their MM-GBSA free binding energy were calculated. Next, ADME descriptors were calculated, and 12 molecules with ADME properties better than that of HCQ were identified. The resulting molecules were subjected to molecular dynamics (MD) simulation for 100 ns. The results of the study indicate that 3 molecules (CQ_22; CQ_2 and CQ_5) show better interactions and stability with the M^{pro} receptor.

* Corresponding author. E-mail: mohamed.aissaoui@univ-annaba.dz
https://doi.org/10.2298/JSC221017003A

Binding interaction analysis indicates that GLU143, THR26, and HIS41 amino acids are potential binding hot-spot residues for the remaining 3 ligands.

Keywords: COVID19; M^{pro} receptor; structure-based approach; ADME; MM-GBSA.

INTRODUCTION

Since the outbreak of the Covid-19 disease starting from Wuhan city in China, in December 2019, it has been rapidly spreading worldwide and was declared a global health emergency pandemic by the World Health Organization (WHO).[1] Consequently, there was an urgent need for therapeutic strategies to develop antiviral drugs and vaccines that can eradicate this highly contagious virus. This pandemic represents a real threat to global public health and has already infected millions of people leading to a great number of deaths worldwide. The number of casualties is continually increasing at the time of writing this manuscript.[2,3]

Coronaviruses (CoVs) are large-sized enveloped viruses with a spherical shape, holding single-stranded RNA of positive-sense.[4] SARS-CoV2 is a novel strain of coronavirus that shares 79.5 % of genomic sequence similarity to SARS-CoV.[5] The coronavirus has a crown shape that contains four structural proteins.[6] These proteins are the spike (S) surface glycoprotein, the non-glycosylated envelope (E) protein, the membrane (3CLpro, or M^{pro}) protein, and the nucleoprotein (N) protein. The infection triggers when the Spike protein of the SARS-CoV-2 (COVID-19) interacts with the ACE2 (angiotensin-converting enzyme 2) by TMPRSS2 protease.[7–9]

The M^{pro} is considered one of the most interesting therapeutic targets in CoVs, as a result of its crucial function in processing the polyproteins that are translated from the viral RNA.[10] These viral polyproteins are cleaved by a proteolysis process to numerous useful proteins.[11] Since the M^{pro} cleaves at 11 sites to produce smaller proteins for viral replication, and because of its non-similarity to human proteins, makes the M^{pro} a potential target in anti-Covid-19 drug design.[12–14]

Since the Covid-19 outbreak, several antiviral drugs have been considered for the treatment of the disease, but their clinical uses were limited due to quality-related safety issues[15] such as Remdesivir[16] and the antimalarial drug hydroxychloroquine (HCQ)/Chloroquine(CQ), Fig. 1.[17–19]

These drugs were massively used across different countries and were authorised as part of national emergency use programmes and clinical trials by the US Food and Drug Administration (FDA) along with the European Medicines Agency (EMA) for patients affected by SARS-CoV-2 pneumonia.[20]

Despite being less toxic than CQ, HCQ was found to be a potent inhibitor against SARS-CoV-2 *in vitro*.[5] However, this drug was associated with several

downsides such as insolubility, toxicity and instability. Moreover, increasing concerns arose when these drugs were used on patients with Covid-19, whether by administering them alone or in combination with other drugs, as a result of cardiac and neuropsychiatric adverse effects.[21,22] Substantial randomised trials have overpowered features of CQ along with HCQ for Covid-19 effects and there is continued worry about the effects that these treatments may have on patients, whether they have Covid-19 or not.[23–25]

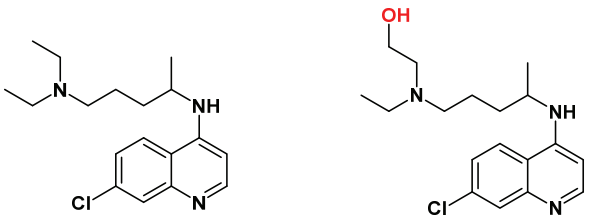

Chloroquine Hydroxychloroquine

Fig. 1. Chemical structures of chloroquine and hydroxychloroquine.

Aiming towards bringing forth a more reliable and safer substitute for HCQ, in the present study a virtual screening (VS) based drug repurposing method was performed to identify structurally modified compounds of the CQ scaffold with good solubility, absorption, permeation, non-toxic and non-carcinogenic characteristics compared to the parent molecule (HCQ). Drug repurposing is a process of exploring new uses for already existing drugs. It can be a cost-saving and quick strategy as new drug discovery can take numerous years.[26,27]

Considering computational studies, molecular docking play a major role in the identification and screening of hit molecules and the pathway involved in their mechanism of action. Several *in silico*-based virtual screening studies were conducted for the identification of potential hit molecules.[28–30]

Accordingly, in this study, Covid-19 M^{pro} crystal complexes available in the PDB were thoroughly explored by cross-docking in order to identify the most reliable PDB structure among them that resulted in PDB ID: 7BRP (Fig. S-1 of the Supplementary material to this paper) as the most appropriate one.[31] Thereafter, SiteMap analysis was undertaken to better explore the active site of M^{pro} followed by VS and then the molecular docking phase. The absorption, distribution, metabolism and excretion (ADME) properties were calculated and the top-scoring compounds were identified as potential M^{pro} inhibitors. Finally, filtered hits with drug-like properties were used for running molecular dynamics (MD) simulations. A systematic approach based on structure-based drug designing was used in this study as described in Scheme 1.

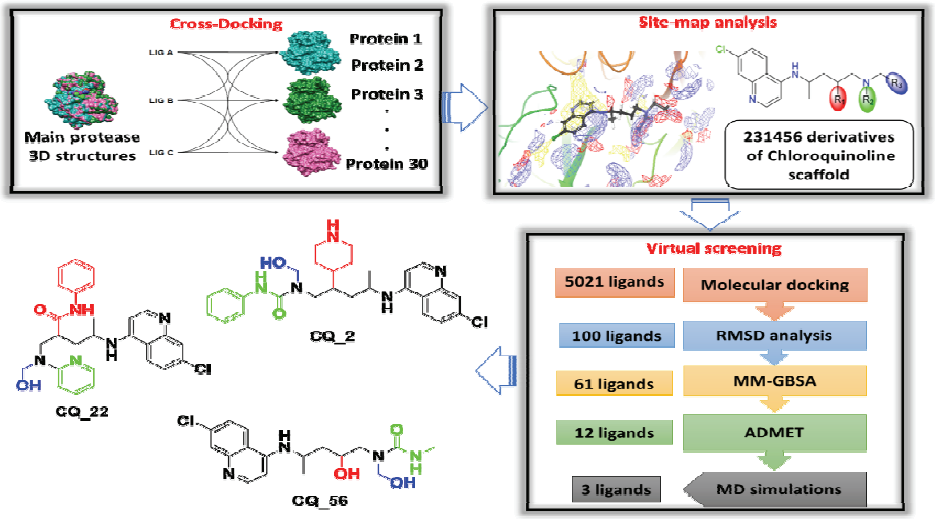

Scheme 1. Schematic representation of the study design illustration.

MATERIAL AND METHODS

Computing system

The VS workflow and analysis were performed on Centos 7.7 x86-64 (Dell Optiplex 7010). The software that were used in this study were Maestro Schrodinger Release 2018-4 (Maestro, Schrödinger, LLC, New York, NY, 2018) and Chimera 1.15.[32]

Cross-docking and protein selection

The three-dimensional structures of 30 M^{pro} targets were retrieved from RCSB PDB.[33] Each protein was prepared using the protein preparation wizard in Maestro.[34] The protein structure was integrity adjusted, and the missing side-chain atoms within the protein residues were predicted by Prime.[35] Hydrogen atoms were added after deleting ions, cofactors and water molecules. The α-carbons of the structures for each target were aligned to each other using a reference structure; then, each ligand was docked into all 30 structures of the target from which the ligand was extracted (Fig. S-2 of the Supplementary material).

Both the docking reliability and protein selection were evaluated by calculating the root--mean-square deviation (*RMSD*) between the crystalized position of the ligand and that predicted by the docking software in the various target structures. The evaluation was performed for both ligands and proteins structures. The XP (extra precision) docking mode included in Glide (grid-based ligand docking with energetics) module of Maestro was selected as the docking protocol in the next steps of virtual screening, with a docking score value of HCQ equal to 22.21 kJ mol^{-1}.

SiteMap analysis

A SiteMap analysis for the docked complex of the M^{pro} HCQ was performed to understand the structure and to exploit the different regions of the active site of the protein in interaction with HCQ. The analysis was performed using the SiteMap module of Schrodinger.[36]

Data set generation and preparation

Using CombGlide,[37] a data set of 231,456 CQ derivatives was generated by creating 3 sites of substitutions on the HCQ structure. The preparation of the ligands was carried out utilizing the LigPrep module of the Schrodinger Suite.[38] The OPLS3 force field was selected for energy minimization.[39] All possible protonation and ionization states including stereochemistry, tautomers and ring conformations were generated. A maximum of 32 stereoisomers per ligand were taken into account when creating stereoisomers. For each ligand, only the conformation with the lowest energy was retained. Through Lipinski Ro5 (rule of five) filtration using QikProp,[40] a module of the Schrödinger software suite, only 64132 CQ derivatives with drug-likeness property were selected for the virtual screening study.

Virtual screening workflow

In order to identify the appropriate compounds that perfectly fit the binding site of the M^{pro}, the above selected derivatives were considered for a virtual screening study. The selected database was initially screened with molecular docking calculations. Only 5021 ligands were selected with an acXP-docking score ≥ 22.21 kJ mol^{-1}. The ones that succeeded were ranked based on the *RMSD* value compared to the HCQ reference structure. Only 100 ligands with a *RMSD* value ≤ 0.2 nm were kept. The Prime MM/GBSA (molecular mechanics/ Poisson–Boltzmann generalized born surface area) was used to rank the best compounds; 71 ligands with MM/GBSA values comparable to or greater than that of the standard ligand (HCQ) were selected. Additionally, a variety of key ADME properties were also calculated with the aid of QuikProp, taking oral absorption as the primary filtering criterion. Therefore, 12 ligands with oral absorption ≥80 % were subjected to molecular dynamics simulations (MD). Finally, to validate the accuracy of the results and the stability of the selected ligands, MD simulations were conducted using Desmond.[41] The simulation started by solvating the complex using the TIP3P water model (transferable intermolecular interaction potential 3) with an orthorhombic box of 1×1×1 nm^3. The system was made electrically neutral by adding appropriate counter ions. OPLS3 force field parameters were utilized for the simulations study. The model systems were relaxed before the simulations. The simulation was then performed using an NPT ensemble system with 300.0 K temperature and 10^5 Pa pressure. The complexes were subjected to molecular dynamics simulation for 100 ns. The *RMSD* of the proteins and ligands was used to assess the stability over time of simulation.

RESULTS AND DISCUSSION

Cross-docking and docking protocol validation

In order to validate both the docking reliability and protein selection in terms of qualitative prediction of the ligand-binding site disposition, 30 M^{pro} targets were considered. Through cross-docking for all complexes, the ligands were extracted from their X-ray complex and subjected to a conformational search. They were then docked in all the structures of the same target using the glide XP docking method and the obtained docking results were compared with the experimentally determined ligand dispositions (co-crystallized ligand) taking into account the average root-mean-square deviation (*RMSD*) as the principal parameter. The main results obtained from the cross-docking studies are summarized in Fig. S-3 of the Supplementary material. The M^{pro} protein with PDB ID:7BRP seemed to be the best performing receptor with an *RMSD* of 0.27 nm. Based on this ana-

lysis, the7BRP receptor was selected in the next stage of this study. The 3D crystal structure of the 7BRP receptor has a resolution of 0.180 nm, a structural weight of 68.81 kDa and amino acid length of 307 and it contains two chains.[42]

SiteMap analysis and dataset creation

The SiteMap analysis was realized using the M^{pro} PDB ID: 7BRP receptor in the complex with HCQ after docking calculation by the Glide-XP method. The SiteMap results are summarized in Table I with a SiteScore of 0.946.

Understanding the interaction of the HCQ in the active site using SiteMap analysis revealed the presence of two principal regions, the first was a hydrophilic region with ligand hydrogen-bond donors and acceptors interactions (Fig. S-4aof the Supplementary material) representing a hydrophilic-score of 0.563, the second was the hydrophobic region occupied by the chloroquinoline moiety that seemed to be suitable for occupancy by this hydrophobic group (Fig. S-4b) with a hydrophobic-score of 0.442.

TABLE I. Summary results of SiteMap analysis using M^{pro}–HCQ complex; SiteScore: the SiteScore is based on a weighted sum of several properties as the number of site points; Dscore: druggability score, uses the same properties as SiteScore but with different coefficients; Phobic: hydrophobic region score; philic: hydrophilic region scores

Site	SiteScore	Size	Dscore	Volume	Contact	Phobic	Philic
Sitemap_site_1	0.946	387	1.044	290.178	0.501	0.442	0.563

The suggested strategies of this study can provide insights into HCQ–M^{pro} interactions to propose an effective modification on the CQ scaffold. After analysis, where modifications on CQ scaffold would be expected to promote the binding mode was revealed. Therefore, 3 substitution sites were suggested (R_1, R_2 and R_3) and a data set of 231,456 molecules based on the CQ scaffold were designed and computationally optimized (Fig. 2).

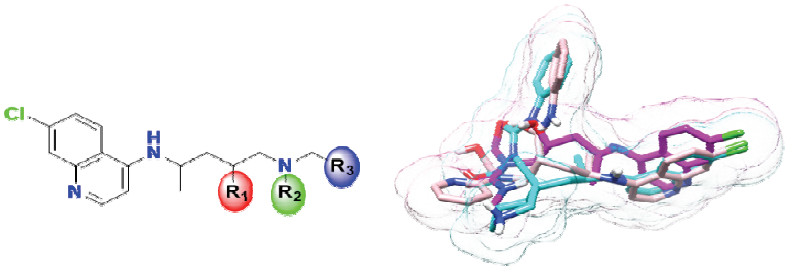

Fig. 2. The proposed chemical structure of the chloroquinoline scaffold.

These molecules were designed by substituting different groups with different characteristics at the positions R1, R2 and R3. The VS methodology using molecular docking, Lipinski Ro5 filtration, as well as MM-GBSA, ADME and

MD simulation were employed to identify the ligands having a better affinity for the M^{pro} protein of SARS-CoV-2.

Virtual screening strategy

Lipinski Ro5 filtration. As the first step of the VS workflow, the 231,456 generated derivatives were subjected to Lipinski's Ro5 filtrations, such as molecular weight, H-bond donor/acceptor and octanol/water partition coefficient (*QPlogPo/w*). Only 64,132 derivatives with drug-likeness property were selected. The docking results of the 64,132 modified CQ scaffold against M^{pro} were examined. As hydroxychloroquine potently inhibits viral infection of SARS coronavirus (SARS-CoV-1),[43] the binding mode of this compound was taken as a reference structure in the next stage of docking calculation. All 64,132 ligands were inspected based on their docking score and the ones showing a docking score ≥ 22,21 kJ mol^{-1} were chosen. Therefore, 5021 ligands were selected. To choose ligands that maintain the same binding mode of HCQ inside the active site, *RMSD* values were calculated between the docked HCQ pose and the remaining 5021 ligands poses using the 'superimpose' module. Finally, 100 ligands having the same binding mode as HCQ with a *RMSD* value of ≤ 0.2 nm were kept.

MM-GBSA study. The stability of the ligand after binding to the active site of the enzyme was confirmed by MM-GBSA analyses computation. All 100 ligands were subjected to calculation of the ligand-receptor binding energy. After MM-GBSA analysis, only 71 ligands with binding energy better than HCQ (Table S-I of the Supplementary material), were submitted to an accurate prediction of their ADME properties

ADME analysis. The ADME properties of the last selected derivatives (71 ligands) were calculated. As the ligands had previously passed through Lipinski Ro5 filtration, it could be predicted that the selected ligands obeyed Lipinski's Ro5 and are likely to be orally active. Hence, these ligands were screened through a variety of key ADME properties based on oral absorption as a primary filtering criterion. Only 13 ligands with oral absorption comparable to or greater than 80 % were selected. The remaining ligands were following the standard parameters and the results are shown in Table II. Finally, ADME property analysis concluded that the final screened ligands show drug-likeness properties.

MD simulation. The simulations were performed to gain more insight into the stability of the ligand–protein complex. The results of the MD simulations were examined based on the *RMSD* of both, the protein backbone (Cα atoms) and the ligand of interest. The protocol was further validated using the crystal structure of M^{pro} (PDB ID:7BRP) complexed with HCQ as the reference structure. MD simulations were processed for 100 ns. The *RMSD* plot for Cα (in blue) complexed with HCQ was observed to be in the range of 0.10–0.20 nm (Fig. 3a),

this result clearly reveals that the presence of HCQ in the active site of protein kept it stable throughout the simulation time.

TABLE II. ADME properties of HCQ and all 13 ligands to determine their "drug-likeness"; *PSA*: van der Waals surface area of polar nitrogen and oxygen atoms (acceptable range : 7.0––200.0); *dHB*: estimated hydrogen bonds that could be donated (acceptable range: 0.0–6.0); *aHB*: estimated hydrogen bonds that could be accepted (acceptable range: 2.0–20.0); *QPlogS*: predicted aqueous solubility (acceptable range: –6.5–0.5); *QPlogPo/w*: predicted octanol/ /water partition coefficient (acceptable range: –2.0–6.5); *QPPCaco*: predicted apparent Caco--2 cell permeability in nm/s (< 25 poor and >500 great); *QPlogBB*: predicted brain/blood partition coefficient (acceptable range: –3.0–1.2); *PHOA*: percent human oral absorption (80 % is high and 25 % is low); *RO5*, number of violations of the Lipinski rule of five (maximum is 4; in all cases found 0)

Title	*MW* g mol^{-1}	*PSA* nm^2	*dHB*	*aHB*	*QPlogS* mol dm^{-3}	*QPlogPo/w*	*QPPCaco*	*QPlogBB*	*PHOA* %
H_CQ	335.876	0.48946	2	5.7	–3.385	3.265	383.503	–0.322	90.308
CQ_7	442.947	0.80245	1	9.4	–4.761	3.807	836.988	–1.262	100.000
CQ_10	499.008	1.07465	3	9.4	–4.724	3.745	513.809	–1.291	100.000
CQ_22	490.003	0.85299	3	7.7	–5.635	4.409	1409.075	–0.921	100.000
CQ_56	366.847	1.00931	3	6.4	–3.517	2.303	222.546	–1.303	100.000
CQ_2	496.051	0.91490	3	6.2	–5.455	4.604	97.758	–0.890	100.000
CQ_15	427.933	0.89329	3	8.7	–4.518	2.976	793.489	–0.947	96.267
CQ_49	470.013	0.81156	3	9.4	–4.321	3.611	248.735	–0.647	90.968
CQ_52	385.895	0.79992	4	7.2	–4.444	3.299	206.815	–0.759	87.706
CQ_64	425.911	1.02547	3	9.6	–4.077	3.412	138.152	–1.394	85.229
CQ_42	401.895	1.11224	2	8.5	–3.974	2.329	295.147	–1.351	84.791
CQ_43	401.895	1.11224	2	8.5	–3.974	2.329	295.147	–1.351	84.791
CQ_53	441.962	0.96928	3	8.7	–3.560	3.121	100.413	–1.150	81.049
CQ_14	480.054	0.81486	2	9.0	–3.909	4.021	49.230	–0.615	80.777

The Ligand–*RMSD* plot for HCQ (in red) was found in the range of 0.05 to 0.48 nm with a little fluctuation during initial time of simulation. However, it gradually attained stability towards the end of the simulation with an *RMSD* of 0.18 nm. The graph of Ligand–*RMSD* specifies that the M^{pro}–HCQ complex is stable during the MD simulation time and the HCQ ligand constantly maintained its interactions with the receptor during the whole simulation.

The 13 compounds selected through the VS study were subjected to the same MD simulations protocol described above. The *RMSD* of their disposition during the simulation compared to their initial docking pose was calculated and the stability of the interactions predicted by docking calculations were analysed. Only compounds showing an average *RMSD* < 0.3 nm and maintained at least one H-bond with the receptor for more than 70 % of the whole MD simulation were then retrieved.

Applying this restriction, 10 compounds were rejected and the remaining 3 compounds, CQ_22, CQ_2 and CQ_56 (Fig. 4) were considered for 3D inter-

action analysis due to their stability during MD simulations (Fig. 3b, c and d). A summary of structure-based VS strategy is provided in Table III.

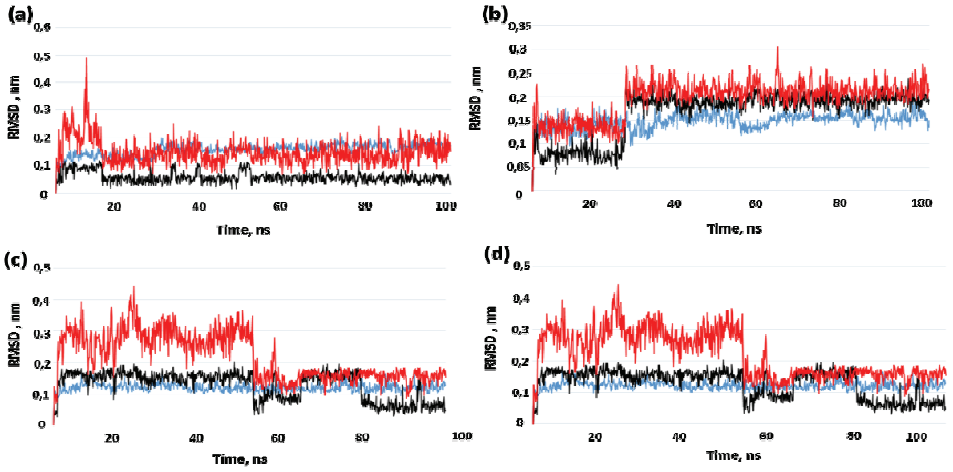

Fig. 3. The *RMSD* graphs obtained after MD analysis of: a) HCQ; b) CQ_22; c) CQ_2; d) CQ_56.

TABLE III. Mpro residue interactions, docking score and energy of HCQ and the 3 hits

Title	Docking score, kJ mol^{-1}	Glide energy kJ mol^{-1}	Glide model, kJ mol^{-1}	Residual interactions		
				H-bond	π–π stacking	Hydrophobic
H_CQ	–22.24	–170.47	–196.09	CYS145, SER144	HIS41	MET165, MET49
CQ_22	–23.89	–261.30	–363.50	THR26, GLY143	HIS41	VAL186, MET49
CQ_2	–22.30	–244.09	–300.19	THR26, CYS145, GLY143	HIS41	MET165, PHE140, VAL186,
CQ_56	–27.16	–215.89	–281.72	HIS164, ASN142, GLY143, THR26	HIS41	MET165, MET49

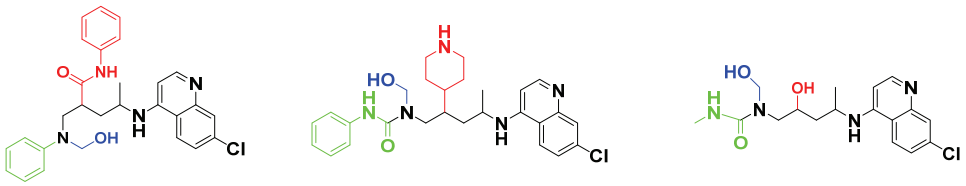

Fig. 4. 2D Structure of the 3 selected hits.

The root mean square fluctuation (*RMSF*) value of macromolecular residues for the 3 complexes was determined to be well within the allowed range of 0.3 nm. A few residues changed slightly, with an *RMSF* values of 0.2–0.3 nm. However, the bulk of residues exhibited smaller variations, with an average value of less than 0.1 nm as shown in Fig. S-5 of the Supplementary material. The observed *RMSF* of the 3 ligands complex within the M^{pro} binding site was found to be within the range. The observed *RMSF* of the 3 ligands (CQ_22, CQ_2 and CQ_56) complex within the active binding site of the M^{pro} enzyme was found to be within the range of 0.09–0.25 nm throughout the 100 ns simulation time as shown in Fig. S-6 of the Supplementary material. This clearly indicates that the ligands were stabilized within the active site with minor functional fluctuations that are required for interacting with the target macromolecule.

The interactions made by ligands CQ_22, CQ_2 and CQ_56 with M^{pro} enzyme are given in Fig. S-7 of the Supplementary material in which the interaction types with their percentages during 100 ns MD simulation run are represented. Histograms represent the interaction fraction of these ligands. Hydrogen bonds, hydrophobic interactions such as π cation, π–π stacking, water bridges and ionic interactions made by ligand with amino acids of proteins during 100 ns MD simulation are represented in Fig. S-7. For all the histograms in Fig. S-7, the stacked bar histograms are normalised over the course of the trajectory; for example, a value of 0.8 suggests that 80 % of the simulation time of the specific interaction is maintained. Values over 1.0 are possible as some protein residue may make multiple contacts of the same subtype with the ligand. All the histogram bars suggest that all the ligands (CQ_22, CQ_2 and CQ_56) form strong interactions with several amino acids of M^{pro}. In several instances, the interaction fraction shoots above the value of 0.7, which shows strong interaction of ligands with that amino acid.

Binding interactions analysis of Mpro_HCQ complex

In this investigation, the function of amino acids within the M^{pro} active site evaluated. Therefore, a molecular interaction study was performed and HCQ binding mode interaction was taken as reference. As shown in Fig. S-8 of the Supplementary material, the binding mode analysis of HCQ with M^{pro} showed the presence of hydrogen bond interactions as well as hydrophobic interactions. The terminal hydroxyl group of the HCQ made two H-bonds as an acceptor with SER144 and CYS145. The quinoline ring of HCQ displayed π–π stacking interactions with HIS41, and hydrophobic interactions with MET165; MET49 and VAL186.[44]

Binding interactions analysis of the Mpro_CQ22, CQ_2 and CQ_56 complexes

Docking results showed that the CQ_22 molecule was mainly combined with M^{pro} through three H-bonds. The first as a donor through the hydroxyl

group with THR26, the second exhibited by the pyrimidine nitrogen as an acceptor with the same residue, and the last as an acceptor with GLY143 through the carbonyl group. Moreover, favourable conventional interaction was displayed by the quinoline ring as π–π stacking interaction with HIS41. Hydrophobic interactions with VAL186, and MET49 were also present, as shown in Fig. 5a.

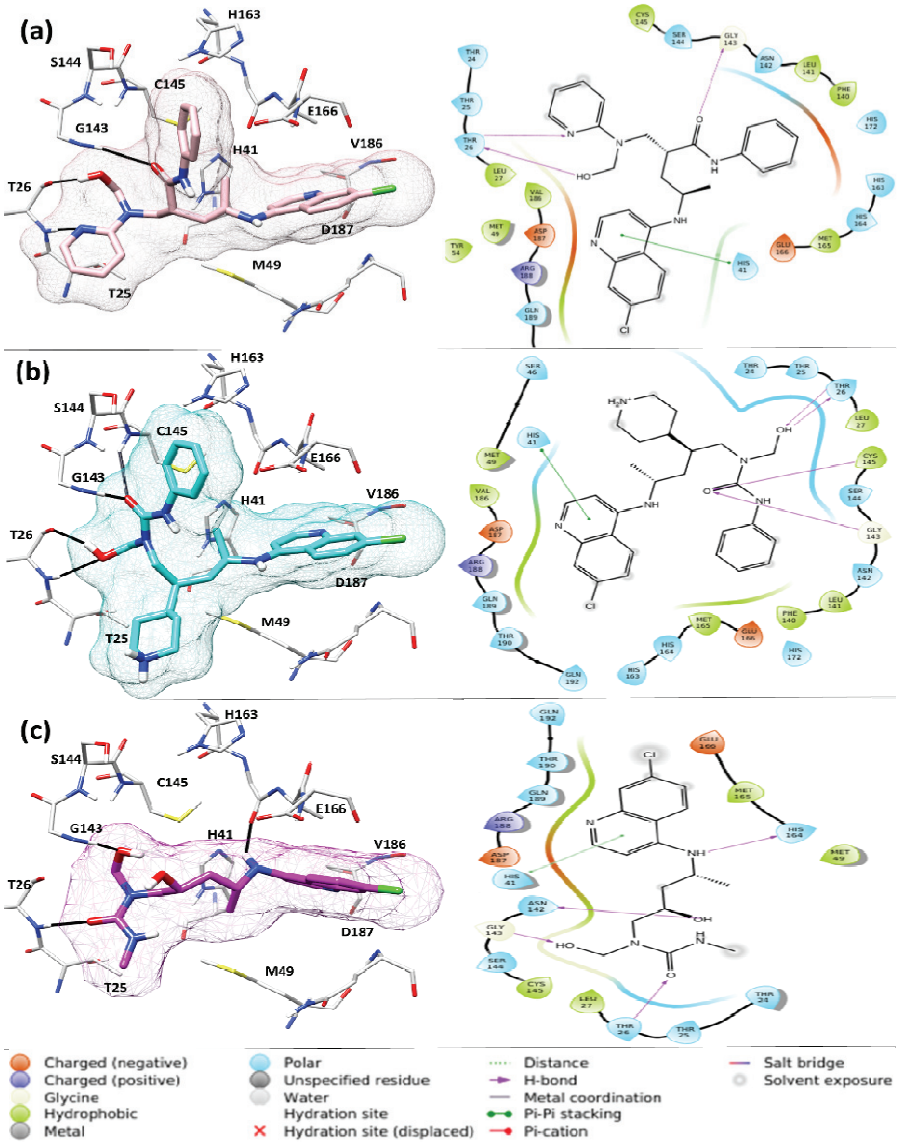

Fig. 5. Binding disposition of selected ligands after docking calculations in the active site of M^{pro}: a) CQ_22 in pink sticks; b) CQ_2 in cyan sticks; c) CQ_56 in magnate sticks. H-bonds are shown as black lines.

Considering CQ_2, four H-bonds were formed; one among them was similar to the HCQ with CYS145 as an acceptor through the carbonyl group. The same carbonyl group formed a hydrogen bond with GLY143. The two-remaining H-bonds were exhibited by hydroxyl group with THR26 as acceptor and donor simultaneously. The presence of π–π stacking conventional interaction through quinoline ring with HIS41was noted (Fig. 5b).

Compound CQ_56 showed four H-bonds; the first through the amino group, located at the fourth position with HIS164 as a donor group. The second as a donor with ASN142 through the hydroxyl, located at the second position. The last two H-bonds as acceptor with GLY143 and THR26 through hydroxyl and carbonyl groups, respectively. Likewise, π–π stacking conventional interaction through the quinoline ring with HIS4 was present (Fig. 5c). The ligand–amino acid interaction of residue HIS41 always took place in all the 3 stable ligands through π–π stacking interactions with the quinoline ring.

In addition, common H-bound interactions were detected with GLY143 and THR26 residues, when these compounds have substituent with acceptor and donor character in that region (hydrophilic region, Fig. S-4), which is not the case in the HCQ molecule. This suggests that the presence of a hydrogen bond interaction with both GLY143 and THR26 may improve the stability within the M^{pro} active site. Therefore, the docking results indicate that GLY143, THR26 and HIS41 amino acids in the binding pocket are potential binding hot-spot residues for our ligands. Additionally, the presence of substituents with acceptor and donor characters in the hydrophilic region improves the stability and the interaction mode of the molecules.

CONCLUSIONS

The Covid-19 pandemic caused a global health crisis worldwide leading to many casualties. The constant mutations of the virus jeopardized the effectiveness of vaccines as a distinct solution. This emphasized the need for therapeutic drugs that target and inhibit the replication of the virus. Drug repurposing is considered as an important strategy in fighting the pandemic considering the urgency of the health situation given that the traditional process of developing targeted drug can take a long time. HCQ was considered by research organizations as a potential drug against the coronavirus during the early days of the pandemic. However, the lack of sufficient evidence of its usefulness along with some adverse effects lead the WHO to eventually revoke the drug. Thus, the present study attempts to conduct a structure-based VS approach to discover a new modified CQ scaffolds able to affect the Sars-CoV2 M^{pro} that may be more effective and reliable alternatives. The results of the study show that CQ_22, CQ_2 and CQ_56 molecules demonstrate better docking scores (–5.712, –5.332 and –6.493, respectively) as well as better ADME properties in comparison to HCQ. Analysis

of the binding interactions of the selected ligands shows that within the active substrate binding pocket of M^{pro}, HIS41, THR26 and GLY143 are the specific amino acid residues involved in interaction with target molecules. This emphasizes their significance as key residues capable of facilitating substrate-ligand complex formation and modulating the M^{pro} enzyme function as potential inhibitors. The presented data may provide some insights into the development of novel potent M^{pro} inhibitors and hold promise for new potential SARS-CoV-2 drugs.

SUPPLEMENTARY MATERIAL

Additional data and information are available electronically at the pages of journal website: https://www.shd-pub.org.rs/index.php/JSCS/article/view/12105, or from the corresponding author on request.

Acknowledgments. The authors would like to thank The General Directorate for Scientific Research and Technological Development (DG-RSDT), the Algerian Ministry of Scientific Research, Applied Organic Chemistry Laboratory (FNR 2000).

ИЗВОД

ДИВЕРЗИФИКАЦИЈА СКЕЛЕТА ХЛОРОХИНОЛИНА ЗА БЛОКИРАЊЕ ГЛАВНЕ ПРОТЕАЗЕ SARS-CoV-2: ПРИСТУП ВИРТУАЛНИМ СКЕНИРАЊЕМ КОРИСТЕЋИ CROSS-DOCKING, SITEMAP АНАЛИЗУ И СИМУЛАЦИЈУ МОЛЕКУЛСКОМ ДИНАМИКОМ

MOHAMED AISSAOUI[1], BILLEL BELHANI[1], ABDELMOUMEN BOULEBNANE[2], ABDESLEM BOUZINA[1] и SALAH EDDINE DJILANI[3]

[1]*Laboratory of Applied Organic Chemistry, Synthesis of Biomolecules and Molecular Modelling Group, Department of Chemistry, Sciences Faculty, Badji-Mokhtar-Annaba University, Box 12, 23000 Annaba, Algeria,* [2]*Department of English, University of Algiers 2, Abou El Kacem Saâdallah, Algiers, Algeria and* [3]*Laboratory of Synthesis and Organic Biocatalysis, Department of Chemistry, Badji-Mokhtar-Annaba University, Algeria*

Одсуство одређених лекова за болест корона вируса 19 (Covid-19) и немање протокола за третирање, навело је научнике да предложе нове мале молекуле и да покушају постојеће лекове да пренамене против различних циљаних тешких респираторних синдрома коронавируса 2 (SARS-CoV-2) и дођу до ефикасних решења. Главна протеаза (M^{pro}) је једна од највише обећавајућих мета лекова због своје кључне улоге у борби против репликације вируса. Неколико антивирусних лекова је коришћено у покушају да се превазиђе пандемија, попут хидроксихлорокина (HCQ). Упркос опаженим позитивним исходима у почетку болести, HCQ је повезан са неколико недостатака попут нерастворљивости, токсичности и нежељених ефеката на срце. Зато, у овој студији, урадили смо на-структури-заснован виртуални скрининг да би идентификовали структурно модификоване лиганде хлорохинолинског (CQ) скелета који имају добру растворљивост, апсорпцију и прожимање у циљу евентуалног сугерисања поузданије алтернативе. PDB ID:7BRP M^{pro} је изабран као најпоузданији рецептор након cross-docking израчунавања користећи 30 кристалних структура. Онда је урађена SiteMap анализа и предложено је укупно 231456 структурно модификопваних једињења са CQ скелетом. Након филтрирања са критеријума Липинског, 64312 молекула је доковано и израчунате су њихове MM-GBSA слободне енергије везивања. Затим су израчунати њихови ADME дескриптори, и идентификовано је 12 молекула са ADME својствима бољим од HCQ. Ти молекули су подвргнути симулацији молекулском динамиком (MD) за 100 ns. Резултати сту-

дије показују да три молекула (CQ_22; CQ_2 и CQ_56) показују бољу интеракцију и стабилност са M^{pro} рецептором. Везивне интеракције указују да су GLU143, THR26 и HIS41 амино киселине потенцијалне вруће тачке за преостала 3 лиганда.

(Примљено 17. октобра, ревидирано 3. децембра 2022, прихваћено 11. јануара 2023)

REFERENCES

1. S. Ludwig,A. Zarbock, *Anesth. Analg.* **131** (1) (2020) 93 (https://doi.org/10.1213/ane.0000000000004845)
2. K. Dhama, S. K. Patel, K. Sharun, M. Pathak, R. Tiwari, M. I. Yatoo, Y. S. Malik, R. Sah, A. A. Rabaan,P.K. Panwar, *Travel. Med. Infect. Dis.* **37** (2020) 101830 (https://doi.org/10.1016/j.tmaid.2020.101830)
3. K. Yuki, M. Fujiogi,S. Koutsogiannaki, *Clin. Immunol.* **215** (2020) 108427 (https://doi.org/10.1016/j.clim.2020.108427)
4. I. M. Artika, A. K. Dewantari, A. Wiyatno, *Heliyon.* **6** (2020) e04743 (https://doi.org/10.1016/j.heliyon.2020.e04743)
5. Y. Zhou, Y. Hou, J. Shen, Y. Huang, W. Martin, F. Cheng, *Cell Discov.* **6** (2020) 14 (https://doi.org/10.1038/s41421-020-0153-3).
6. C. Wu, Y. Liu, Y. Yang, P. Zhang, W. Zhong, Y. Wang, Q. Wang, Y. Xu, M. Li, X. Li, M. Zheng, L. Chen,H. Li, *Acta Pharm. Sin. B.* **10** (2020) 766 (https://doi.org/10.1016/j.apsb.2020.02.008)
7. J. Shang, Y. Wan, C. Luo, G. Ye, Q. Geng, A. Auerbach,F. Li, *Proc. Natl. Acad. Sci. U.S.A.* **117** (2020) 11727 (https://doi.org/10.1073/pnas.2003138117).
8. L. Mousavizadeh,S. Ghasemi, *J. Microbiol. Immunol. Infect.* **54** (2021) 159 (https://doi.org/10.1016/j.jmii.2020.03.022)
9. J. Yang, S. J. L. Petitjean, M. Koehler, Q. Zhang, A. C. Dumitru, W. Chen, S. Derclaye, S. P. Vincent, P. Soumillion, D. Alsteens, *Nat. Commun.* **11** (2020) 4541 (https://doi.org/10.1038/s41467-020-18319-6)
10. X. Xue, H. Yu, H. Yang, F. Xue, Z. Wu, W. Shen, J. Li, Z. Zhou, Y. Ding, Q. Zhao, X.C. Zhang, M. Liao, M. Bartlam, Z. Rao, *J. Virol.* **82** (2008) 2515 (https://doi.org/10.1128/JVI.02114-07)
11. C. Liu, Q. Zhou, Y. Li, L.V. Garner, S.P. Watkins, L .J. Carter, J. Smoot, A. C. Gregg, A. D. Daniels, S. Jervey, D. Albaiu, *ACS Cent. Sci.* **6** (2020) 315 (https://doi.org/10.1021/acscentsci.0c00272)
12. M. T. ul Qamar, S. M. Alqahtani, M. A. Alamri,L.-L. Chen, *J. Pharm. Anal.* **10** (2020) 313 (https://doi.org/10.1016/j.jpha.2020.03.009)
13. Z. Jin, X. Du, Y. Xu, Y. Deng, M. Liu, Y. Zhao, B. Zhang, X. Li, L. Zhang, C. Peng, Y. Duan, J. Yu, L. Wang, K. Yang, F. Liu, R. Jiang, X. Yang, T. You, X. Liu, X. Yang, F. Bai, H. Liu, X. Liu, L.W. Guddat, W. Xu, G. Xiao, C. Qin, Z. Shi, H. Jiang, Z. Rao, H. Yang, *Nature.* **582** (2020) 289 (https://doi.org/10.1038/s41586-020-2223-y)
14. M. Bzówka, K. Mitusińska, A. Raczyńska, A. Samol, J. A. Tuszyński,A. Góra, *Int. J. Mol. Sci.* **21** (2020) 3099 (https://doi.org/10.3390/ijms21093099)
15. R. K. Harwansh, S. Bahadur, *Curr. Pharm. Biotechnol.* **23** (2022) 235 (https://doi.org/10.2174/1389201022666210322124348)
16. C. Scavone, S. Brusco, M. Bertini, L. Sportiello, C. Rafaniello, A. Zoccoli, L. Berrino, G. Racagni, F. Rossi, A. Capuano, *Br. J. Pharmacol.* **177** (2020) 4813 (https://doi.org/10.1111/bph.15072)
17. M. Nimgampalle, V. Devanathan, A. Saxena, *J. Biomol. Struct. Dyn.* **39** (2021) 4949 (https://doi.org/10.1080/07391102.2020.1782265)

18. P. Gautret, J. C. Lagier, P. Parola, V. T. Hoang, L. Meddeb, M. Mailhe, B. Doudier, J. Courjon, V. Giordanengo, V. E. Vieira, H. Tissot Dupont, S. Honoré, P. Colson, E. Chabrière, B. La Scola, J. M. Rolain, P. Brouqui, D. Raoult, *Int. J. Antimicrob. Agents* **56** (2020) 105949 (https://doi.org/10.1016/j.ijantimicag.2020.105949)
19. M. Wang, R. Cao, L. Zhang, X. Yang, J. Liu, M. Xu, Z. Shi, Z. Hu, W. Zhong, G. Xiao, *Cell Res.* **30** (2020) 269 (https://doi.org/10.1038/s41422-020-0282-0)
20. European Medicine Agency, *COVID-19: Chloroquine and hydroxychloroquine only to be used in clinical trials or emergency use programmes*, 2020 (https://www.ema.europa.eu/en/news/covid-19-chloroquine-hydroxychloroquine-only-be-used-clinical-trials-emergency-use-programmes)
21. K. Sato, T. Mano, A. Iwata,T. Toda, *Biosci. Trends* **14** (2020) 139 (https://doi.org/10.5582/bst.2020.03082)
22. C. Chatre, F. Roubille, H. Vernhet, C. Jorgensen,Y.-M. Pers, *Drug. Saf.* **41** (2018) 919 (https://doi.org/10.1007/s40264-018-0689-4)
23. Z. Kashour, M. Riaz, M. A. Garbati, O. Al Dosary, H. Tlayjeh, D. Gerberi, M. H. Murad, M. R. Sohail, T. Kashour, I. M. Tleyjeh, *J. Antimicrob. Chemother.* **76** (2021) 30 (https://doi.org/10.1093/jac/dkaa403)
24. X. Cui, J. Sun, S.J. Minkove, Y. Li, D. Cooper, Z. Couse, P. Q. Eichacker, P. Torabi-Parizi, *Rev. Med. Virol.* **31** (2021) e2228 (https://doi.org/10.1002/rmv.2228)
25. T. Fiolet, A. Guihur, M. E. Rebeaud, M. Mulot, N. Peiffer-Smadja,Y. Mahamat-Saleh, *Clin. Microbiol. Infect.* **27** (2021) 19 (https://doi.org/10.1016/j.cmi.2020.08.022)
26. T. U. Singh, S. Parida, M. C. Lingaraju, M. Kesavan, D. Kumar, R. K. Singh, *Pharmacol. Reports* **72** (2020) 1479 (https://doi.org/10.1007/s43440-020-00155-6)
27. A. Khataniar, U. Pathak, S. Rajkhowa, A. N. Jha, *Covid* **2** (2022) 148 (https://doi.org/10.3390/covid2020011)
28. D. M. Teli, M. B. Shah, M. T. Chhabria, *Front. Mol. Biosci.* **7** (2021) 599079 (https://doi.org/10.3389/fmolb.2020.599079)
29. M. G. Santibáñez-Morán, E. López-López, F. D. Prieto-Martínez, N. Sánchez-Cruz, J. L. Medina-Franco, *RSC Adv.* **10** (2020) 25089 (https://doi.org/10.1039/D0RA04922K)
30. R. K. Gupta, E. L. Nwachuku, B. E. Zusman, R. M. Jha, A. M. Puccio, *PLoS ONE.* **16** (2021) e0257784 (https://doi.org/10.1371/journal.pone.0257784)
31. L. Fu, F. Ye, Y. Feng, F. Yu, Q. Wang, Y. Wu, C. Zhao, H. Sun, B. Huang, P. Niu, H. Song, Y. Shi, X. Li, W. Tan, J. Qi, G. F. Gao, *Nat. Commun.* **11** (2020) 4417 (https://doi.org/10.1038/s41467-020-18233-x)
32. E. F. Pettersen, T. D. Goddard, C. C. Huang, G. S. Couch, D. M. Greenblatt, E. C. Meng,T. E. Ferrin, *J. Comput. Chem.* **25** (2004) 1605 (https://doi.org/10.1002/jcc.20084)
33. H. M. Berman, J. Westbrook, Z. Feng, G. Gilliland, T. N. Bhat, H. Weissig, I. N. Shindyalov, P. E. Bourne, *Nucleic Acids Res.* **28** (2000) 235 (https://doi.org/10.1093/nar/28.1.235)
34. J. C. Shelley, A. Cholleti, L. L. Frye, J. R. Greenwood, M. R. Timlin, M. Uchimaya, *J. Comput. Aided Mol. Des.* **21** (2007) 681 (https://doi.org/10.1007/s10822-007-9133-z)
35. M. P. Jacobson, R. A. Friesner, Z. Xiang, B. Honig, *J. Mol. Biol.* **320** (2002) 597 (https://doi.org/10.1016/S0022-2836(02)00470-9)
36. T. A. Halgren, *J. Chem. Inf. Model.* **49** (2009) 377 (https://doi.org/10.1021/ci800324m)
37. T. A. Halgren, R. B. Murphy, R. A. Friesner, H. S. Beard, L. L. Frye, W. T. Pollard, J. L. Banks, *J. Med. Chem.* **47** (2004) 1750 (https://doi.org/10.1021/jm030644s).
38. M. F. Al Ajmi, M. T. Rehman, A. Hussain,G. M. Rather, *Inter. J. Bio. Macromol.* **116** (2018) 173 (https://doi.org/10.1016/j.ijbiomac.2018.05.023)

39. E. Harder, W. Damm, J. Maple, C. Wu, M. Reboul, J. Y. Xiang, L. Wang, D. Lupyan, M. K. Dahlgren, J. L. Knight, J. W. Kaus, D. S. Cerutti, G. Krilov, W. L. Jorgensen, R. Abel, R. A. Friesner, *J. Chem. Theory Comput.* **12** (2016) 281 (https://doi.org/10.1021/acs.jctc.5b00864)
40. A. O. Fadaka, R. T. Aruleba, N. R. S. Sibuyi, A. Klein, A. M. Madiehe, M. Meyer, *J. Biomol. Struct. Dyn.* **40** (2022) 3416 (https://doi.org/10.1080/07391102.2020.1847197)
41. K. J. Bowers, D. E. Chow, H. Xu, R. O. Dror, M. P. Eastwood, B. A. Gregersen, J. L. Klepeis, I. Kolossvary, M. A. Moraes, F. D. Sacerdoti, J. K. Salmon, Y. Shan, D. E. Shaw, in *SC '06: Proceedings of the 2006 ACM/IEEE Conference on Supercomputing*, Tampa, FL, 11–
–17 Nov. 2006, p. 43 (https://doi.org/10.1109/SC.2006.54).
42. L. Fu, F. Ye, Y. Feng, F. Yu, Q. Wang, Y. Wu, C. Zhao, H. Sun, B. Huang,P. Niu, *Nat. Commun.* **11** (2020) 1 (https://doi.org/10.1038/s41467-020-18233-x)
43. X. Yao, F. Ye, M. Zhang, C. Cui, B. Huang, P. Niu, X. Liu, L. Zhao, E. Dong, C. Song, S. Zhan, R. Lu, H. Li, W. Tan,D. Liu, *Clin. Infect. Dis.* **71** (2020) 732 (https://doi.org/10.1093/cid/ciaa237)
44. H. Rai, A. Barik, Y. P. Singh, A. Suresh, L. Singh, G. Singh, U. Y. Nayak, V. K. Dubey, G. Modi, *Mol Divers.* **25** (2021) 1905 (https://doi.org/10.1007/s11030-021-10188-5).

Journal of the Serbian Chemical Society
JSCS@tmf.bg.ac.rs • www.shd.org.rs/JSCS
J. Serb. Chem. Soc. 88 (5) S139–S144 (2023) *Supplementary material*

SUPPLEMENTARY MATERIAL TO

Diversifying the chloroquinoline scaffold against SARS-CoV-2 main protease: Virtual screening approach using cross-docking, SiteMap analysis and molecular dynamics simulation

MOHAMED AISSAOUI[1]*, BILLEL BELHANI[1], ABDELMOUMEN BOULEBNANE[2], ABDESLEM BOUZINA[1] and SALAH EDDINE DJILANI[3]

[1]*Laboratory of Applied Organic Chemistry, Synthesis of Biomolecules and Molecular Modelling Group, Department of Chemistry, Sciences Faculty, Badji-Mokhtar-Annaba University, Box 12, 23000 Annaba, Algeria,* [2]*Department of English, University of Algiers 2, Abou El Kacem Saâdallah, Algiers, Algeria and* [3]*Laboratory of Synthesis and Organic Biocatalysis, Department of Chemistry, Badji-Mokhtar-Annaba University, Algeria*

J. Serb. Chem. Soc. 88 (5) (2023) 505–520

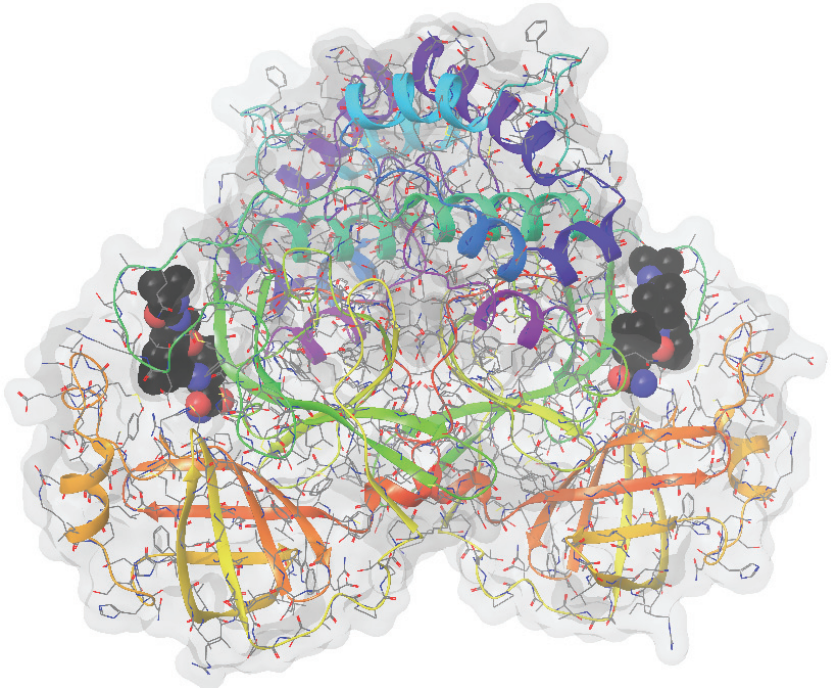

Fig. S-1. Crystal structure of [SARS-CoV-2/M^{pro}] complex (PDB ID: 7BRP).

* Corresponding author. E-mail: mohamed.aissaoui@univ-annaba.dz

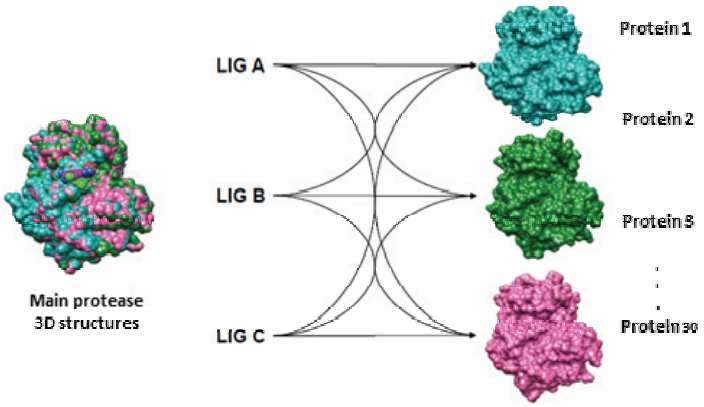

Fig. S-2. Cross-docking schematic approach.

	6LZE	6WCO	6WTK	6XBG	6XHM	7BQY	7BRP	7BUY	7K40	6M2N	6XA4	6XR3	6LU7	6M0K	6W63	6W79	6WNP	6WTJ	6WTT	6XBH	6XBI	6XFN	6Y2F	6Y2G	6ZRU	7C8R	7C8T	7COM	7D3I	7JYC
6LZE	**2.30**	4.59	2.30	3.82	3.06	4.22	2.54	10.51	3.71	5.20	8.25	5.50	5.73	4.99	5.16	6.94	4.76	7.29	9.93	9.02	4.97	6.50	4.03	4.09	3.59	3.54	9.79	7.61	4.18	4.35
6WCO	5.64	**5.58**	5.89	5.87	5.72	2.04	2.23	4.91	3.66	4.66	8.37	5.66	4.23	8.17	6.94	9.08	4.53	4.59	4.12	4.73	5.79	13.35	4.73	3.10	4.15	4.11	4.64	5.55	3.86	10.51
6WTK	6.78	5.39	**5.08**	4.52	4.51	4.98	2.26	4.64	5.15	2.68	8.16	5.37	3.31	6.50	10.58	6.88	4.26	6.13	4.00	5.62	5.78	8.15	4.52	6.41	4.31	3.47	3.83	8.82	5.43	5.27
6XBG	4.77	6.06	4.70	**4.38**	9.27	4.80	4.82	4.77	4.28	4.26	8.37	5.67	4.07	6.94	1.27	8.60	4.93	9.37	5.45	5.78	8.03	7.36	5.71	5.26	8.33	5.08	4.53	8.88	4.79	8.05
6XHM	6.88	8.51	3.73	4.08	**3.50**	4.26	2.13	5.70	4.11	5.18	8.30	5.55	5.00	7.41	1.43	8.59	10.69	7.53	5.71	5.50	5.83	4.93	5.70	7.66	3.63	5.22	4.55	5.45	4.07	7.17
7BQY	6.54	8.42	8.76	5.04	8.13	**5.42**	1.79	7.15	5.26	6.76	6.68	9.61	8.20	3.48	5.27	8.26	4.05	6.23	5.80	5.79	4.25	9.67	3.60	4.40	5.14	4.92	5.66	2.40	4.47	5.63
7BRP	5.98	8.22	5.80	5.21	8.66	6.71	**1.65**	7.45	3.53	7.28	7.03	5.17	8.15	5.09	5.01	5.86	5.33	5.62	2.44	5.66	1.36	6.35	2.31	3.58	3.68	5.22	5.39	2.58	10.27	10.99
7BUY	7.51	7.14	3.13	6.59	3.81	5.37	1.42	**5.86**	8.76	4.93	7.39	5.68	8.19	5.85	5.25	8.31	6.61	5.76	8.09	6.31	8.31	5.34	8.32	5.76	2.86	5.13	5.40	10.75	5.59	5.63
7K40	6.14	8.24	5.75	5.32	8.63	6.82	1.65	5.14	**2.35**	5.85	4.25	4.94	8.14	8.13	6.80	7.63	4.15	2.25	8.16	6.34	8.27	5.05	5.39	5.48	3.03	5.16	2.82	4.49	5.17	1.78
6M2N	5.89	2.91	6.68	5.63	5.99	4.83	1.70	6.99	2.26	**6.80**	3.68	5.52	8.24	5.58	6.93	1.12	2.49	4.63	3.73	4.71	3.94	5.18	9.82	3.53	2.91	4.07	6.61	5.67	3.74	1.51
6XA4	5.55	7.05	2.49	6.02	6.06	2.29	3.53	4.06	2.52	5.58	**3.64**	6.05	5.31	5.40	5.13	7.56	6.68	1.53	5.27	5.21	5.78	5.12	5.22	4.93	3.00	3.85	7.64	4.50	5.03	1.99
6XR3	5.25	8.91	5.10	5.45	5.10	5.42	4.48	5.99	2.27	7.34	11.67	**4.68**	3.64	2.44	2.86	1.08	7.02	9.95	6.04	7.21	6.51	6.66	5.13	5.77	2.97	5.16	3.22	3.92	3.20	1.57
6LU7	7.16	7.09	8.73	9.99	8.50	9.99	2.98	8.38	2.32	7.57	10.52	3.94	**4.95**	2.36	5.48	1.14	8.58	3.40	4.30	0.97	7.46	4.94	6.18	3.23	5.45	4.78	3.52	3.75	4.82	1.59
6M0K	2.99	5.46	7.57	1.60	3.88	4.28	3.07	6.06	7.75	7.22	6.87	9.30	5.82	**6.53**	1.03	5.44	8.66	3.57	3.99	11.58	7.31	8.54	4.53	3.54	6.97	6.45	3.16	5.31	8.52	5.10
6W63	1.59	6.14	6.02	7.06	5.91	6.06	1.67	9.97	9.15	7.59	4.56	9.19	5.91	6.31	**2.33**	8.64	8.56	3.43	5.38	6.87	6.22	2.86	5.29	3.16	5.13	9.15	3.49	4.02	8.47	4.11
6W79	1.37	6.02	5.94	7.01	5.84	5.97	2.59	9.26	9.29	7.49	5.27	4.41	5.16	6.86	8.38	**3.39**	8.66	3.56	5.57	4.44	1.54	3.36	4.69	3.52	3.17	4.53	3.40	5.41	2.74	8.58
6WNP	5.61	7.82	6.00	5.05	8.63	6.33	2.00	6.04	5.03	8.93	5.26	4.81	6.15	8.42	9.99	4.73	**1.66**	3.43	5.20	6.94	9.90	7.57	9.12	3.40	10.29	9.91	8.41	9.78	2.90	3.67
6WTJ	7.07	7.97	4.39	6.53	4.18	5.23	3.50	4.99	9.98	5.44	3.29	4.86	5.27	2.19	6.80	7.48	9.98	**3.47**	5.59	7.18	5.20	5.95	6.30	4.27	5.57	6.60	4.30	4.54	2.80	3.91
6WTT	7.10	8.64	4.11	6.19	4.05	3.96	3.63	4.44	4.31	6.02	3.12	4.41	5.46	8.63	7.07	5.09	6.09	4.18	**5.43**	7.56	5.22	4.72	8.61	4.00	6.52	3.25	3.95	5.79	2.95	5.15
6XBH	8.18	5.71	4.89	4.56	7.43	7.26	3.02	4.38	9.85	6.02	5.13	5.40	1.34	8.60	3.68	8.51	5.51	4.63	7.78	**1.43**	5.19	7.23	8.57	4.22	2.78	6.60	4.77	3.29	2.79	5.52
6XBI	9.40	4.70	4.31	7.59	5.99	4.30	4.10	5.89	6.60	8.69	5.41	3.06	6.21	8.75	4.07	4.05	6.44	2.97	5.59	5.87	**5.20**	6.15	8.67	3.12	4.56	4.31	3.10	3.50	3.78	5.46
6XFN	7.93	7.80	7.75	6.34	7.23	8.09	4.86	5.97	6.01	8.76	5.33	5.78	8.26	8.57	3.48	4.41	3.02	5.20	10.22	5.97	5.21	**8.69**	4.69	5.53	2.84	8.93	3.01	3.24	6.58	5.57
6Y2F	3.13	8.30	9.03	9.45	9.07	8.99	1.66	5.42	5.98	5.78	5.72	5.87	2.08	8.61	4.07	3.82	4.87	8.04	2.63	6.12	5.59	8.85	**5.39**	5.45	2.74	8.87	3.40	3.44	10.39	6.21
6Y2G	3.19	8.26	9.10	9.58	9.18	9.02	1.79	7.65	5.85	3.64	5.92	5.91	5.95	7.45	3.86	4.39	8.07	8.11	2.01	5.89	5.33	8.53	5.48	**5.55**	6.45	8.02	6.00	3.44	8.47	8.71
6ZRU	6.12	8.26	5.79	5.30	8.61	6.79	1.57	7.88	6.20	5.97	8.97	7.20	9.26	5.53	3.54	4.21	5.59	5.70	7.80	6.30	5.77	8.89	9.18	8.01	**6.46**	9.94	6.12	6.35	6.59	4.49
7C8R	8.89	9.53	10.23	6.59	7.44	6.10	2.23	4.09	4.50	7.28	5.58	10.81	4.81	4.45	9.44	7.46	5.73	5.80	4.79	7.43	5.85	8.79	9.05	4.56	8.67	**5.08**	4.62	6.42	6.63	7.76
7C8T	6.29	8.53	5.97	4.94	6.16	3.42	4.09	4.29	3.62	7.38	4.65	4.69	6.23	5.47	7.03	3.98	5.06	9.87	1.76	7.32	3.82	7.14	9.27	4.49	4.30	5.04	**5.65**	4.50	10.12	8.46
7COM	5.88	7.98	5.85	5.19	8.65	6.62	1.82	4.01	5.93	11.21	6.50	8.01	3.98	5.54	7.77	4.94	5.17	7.75	8.43	4.43	7.89	7.23	9.02	7.55	3.27	6.41	5.11	**7.09**	2.78	8.07
7D3I	6.74	7.73	4.51	7.46	7.20	6.60	2.91	4.23	8.34	5.41	4.35	5.74	7.41	7.73	8.85	7.43	5.17	4.50	6.25	4.54	5.20	7.06	9.11	4.46	9.26	4.95	5.75	6.24	**2.64**	4.05
7JYC	10.38	9.33	5.97	6.99	10.79	6.58	3.38	4.24	5.21	7.53	6.81	4.29	7.68	6.06	7.43	7.93	8.20	6.23	4.77	6.49	4.66	2.51	7.54	7.30	5.47	6.33	5.02	9.02	1.77	**4.04**
RMSD avrge	**5.94**	**7.21**	**5.85**	**5.98**	**6.71**	**5.76**	**2.70**	**6.01**	**5.46**	**6.48**	**6.30**	**5.90**	**5.80**	**6.27**	**5.56**	**5.90**	**6.02**	**5.49**	**5.54**	**5.97**	**5.71**	**6.76**	**6.51**	**4.84**	**4.92**	**5.80**	**4.90**	**5.53**	**5.18**	**5.50**

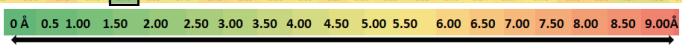

Fig. S-3. RMSD summary results of the cross-docking calculation.

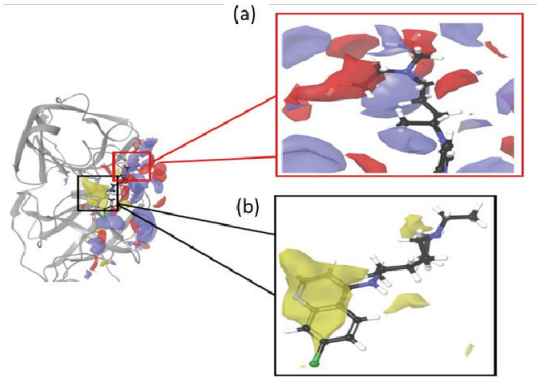

Fig. S-4. Focus on the SiteMap analysis of the M^{pro}-HCQ complex: a) hydrophilic region and b) hydrophobic region.

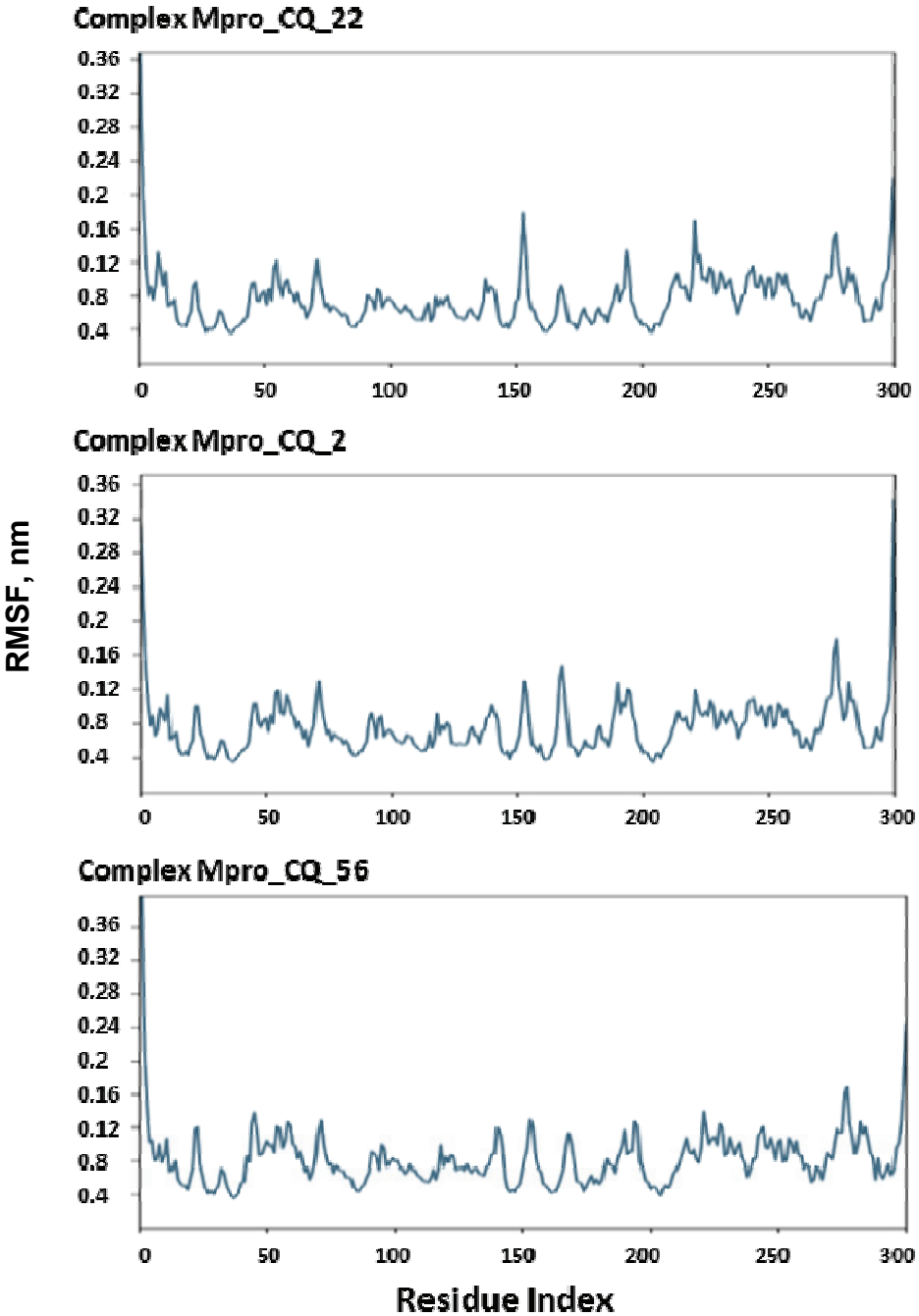

Fig. S-5. RMSF of the M^{pro} enzyme in complex with CQ_22, CQ_2 and CQ_56 during the 100 ns period of the MD simulation.

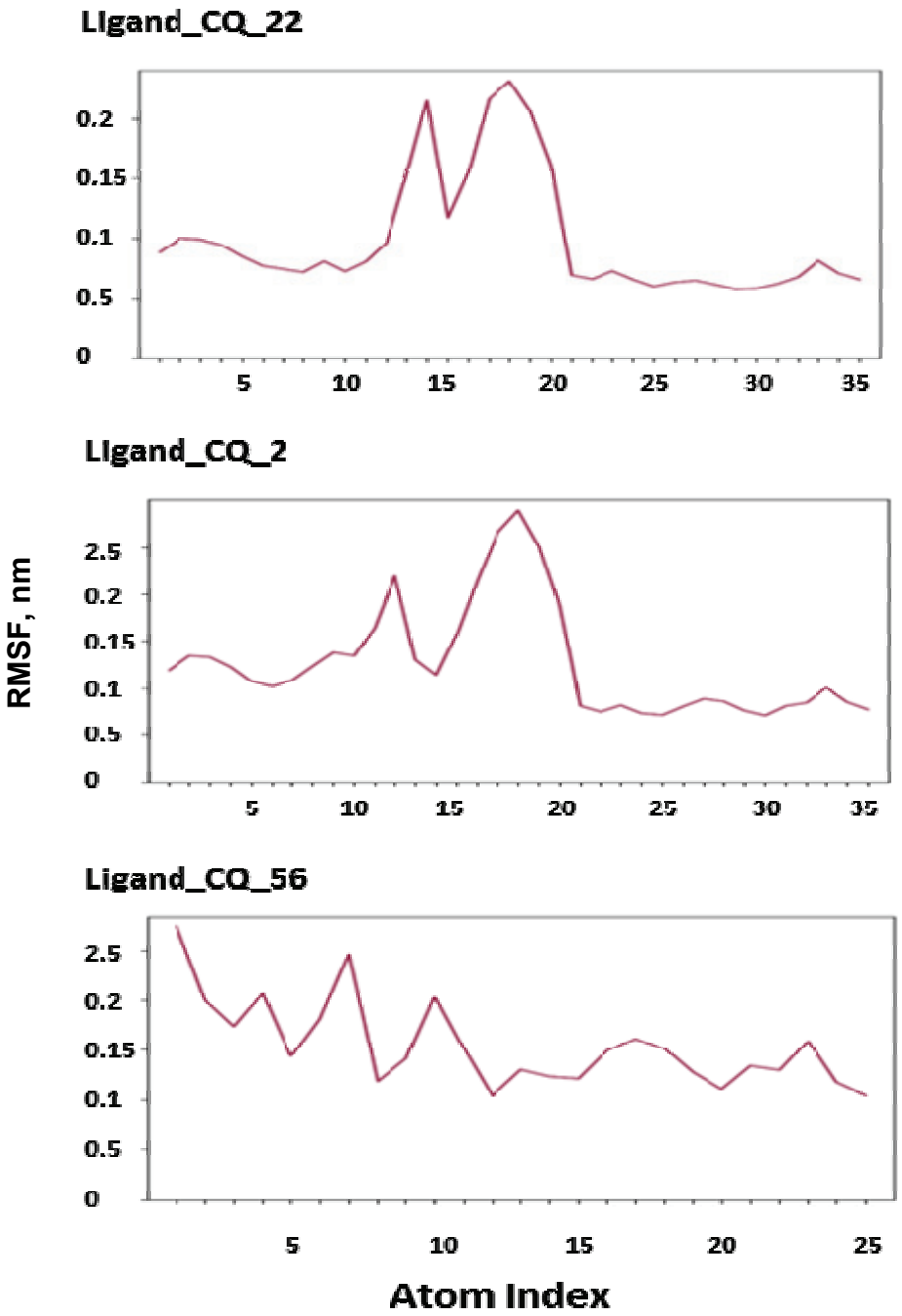

Fig. S-6. Root mean square fluctuation: During the 100 ns timeframe of the MD simulation, the RMSF of the complexed ligands CQ_22, CQ_2 and CQ_56.

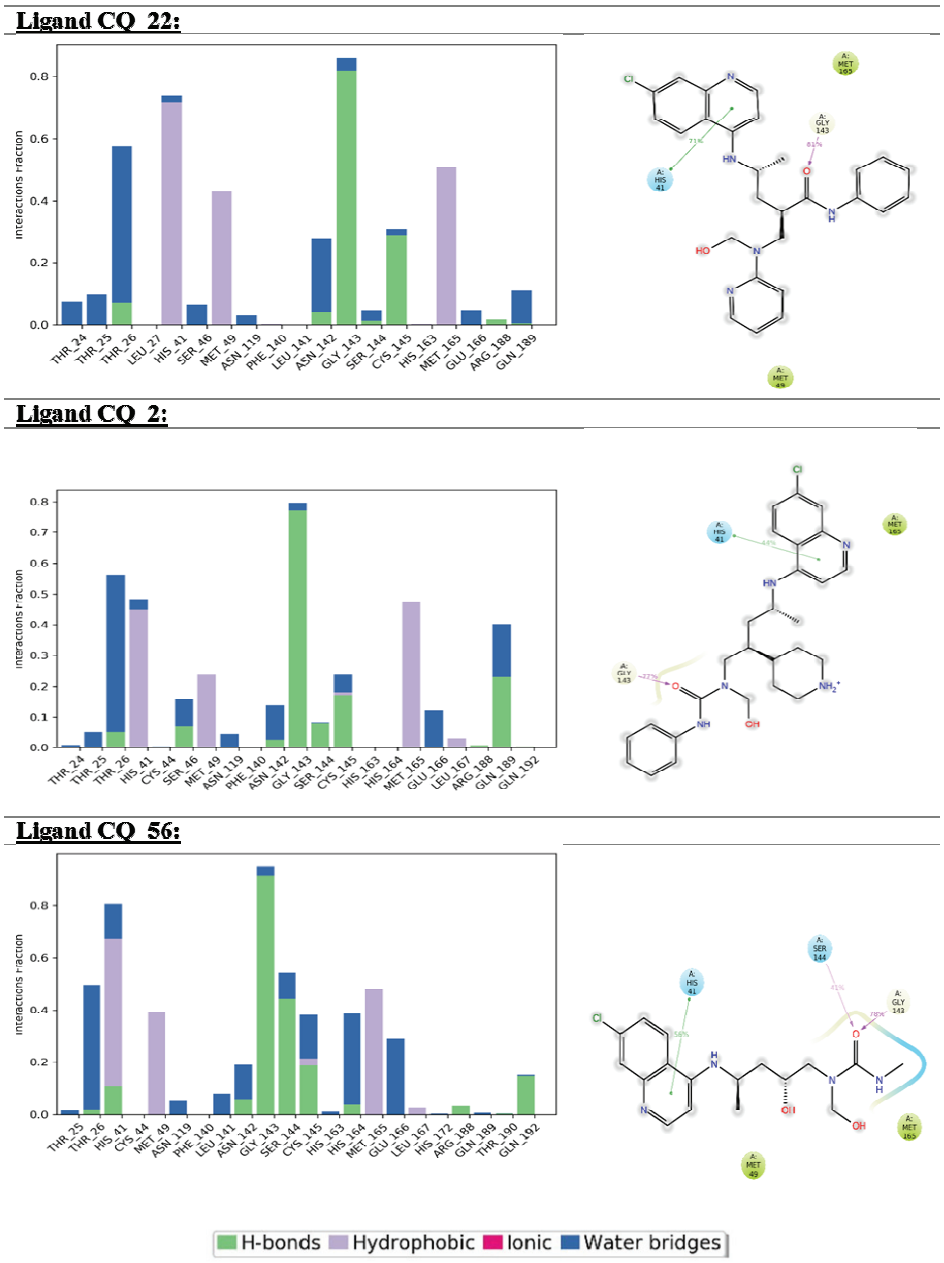

Fig. S-7. Protein–ligand contact during 100 ns MD simulation timescale.

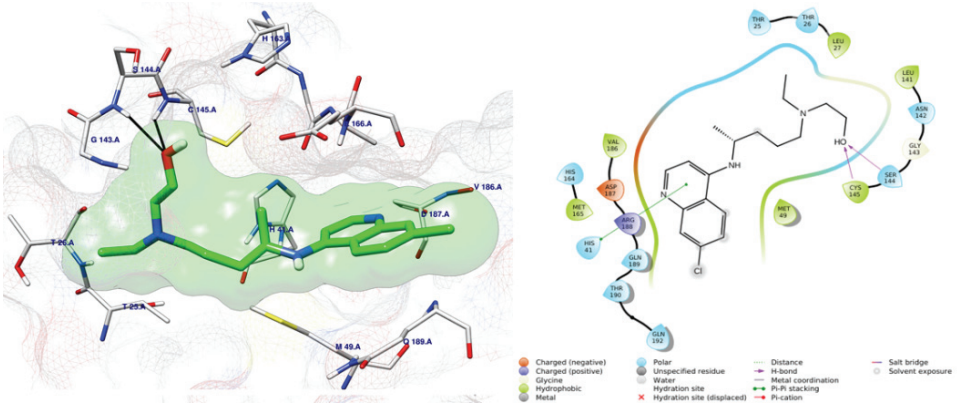

Fig. S-8. Binding disposition of HCQ after docking calculations in the active site of M^{pro}; HCQ in green sticks. H-bonds are shown as black lines. The 2D interaction diagram is shown i in the lower panel.

Journal of the Serbian Chemical Society
JSCS-info@shd.org.rs • www.shd.org.rs/JSCS
J. Serb. Chem. Soc. *88* (5) 521–536 (2023)
JSCS–5643
Original scientific paper
Published 21 May 2023

Designing an electrochemical biosensor based on tyrosinase for highly sensitive and rapid detection of bisphenol A and its derivatives

ONUR CAN BODUR[1], MERVE KESKIN[2]*, BAŞAK ARSLAN AVAN[3] and HALIT ARSLAN[1]

[1]*Department of Chemistry, Faculty of Science, Gazi University, Ankara, Republic of Türkiye,* [2]*Vocational School of Health Services, Bilecik Seyh Edebali University, Bilecik, Republic of Türkiye and* [3]*Department of Orthodontics, Faculty of Dentistry, Gazi University, Ankara, Republic of Türkiye*

(Received 22 November 2022, revised 13 February, accepted 21 March 2023)

Abstract: Bisphenol A (BPA) is a monomer commonly used in the production of epoxy resins, plastic bottles and dental filling materials. Due to its chemical structure, BPA and its derivates show activity similar to the endocrine hormones. It can bind to estrogen receptors and cause neurological disturbances, even at low doses. Therefore, it is important to determine BPA and its derivatives quickly and sensitively at low concentrations. In this study, a single amperometric tyrosinase enzyme biosensor was designed for the determination of the amount of BPA, bisphenol F (BPF) and bisphenol S (BPS) monomers. Tyrosinase was immobilized onto a modified carbon paste electrode by cross-linking with glutaraldehyde. The amount of BPA (BPS and BPF) was determined directly on the reduction of quinone compound released as a result of the enzymatic reaction at –0.15V. $K_{m(app)}$ value of the designed biosensor for BPA was found 0.00067 μM, the linear operating range was 0.001–0.005 μM (a) and 0.03–0.1 μM (b) and the lower detection limit was found 1 nM for each monomer. It is clear that designed biosensor enable the fast, efficient and precise determination of BPA and its derivatives released from materials used in dental materials.

Keywords: BPA; BPF; BPS; tyrosinase enzyme; biosensor; estrogen.

INTRODUCTION

Bisphenol A (2,2-bis(4-hydroxyphenyl) propane, 4,4′-isopropylidenediphenol, BPA) is an important industrial chemical used as a basic component in the production of epoxy resins and polycarbonate plastics, which have wide applications in industry. It is frequently used in plastic products in our daily lives such

* Corresponding author. E-mail: merveozdemirkeskin@gmail.com
https://doi.org/10.2298/JSC221122013B

as large returnable, refillable water bottles, food service products, feeding bottles, jugs, glasses, household food containers. In addition, BPA is an important component of bisphenol A glycidylmethacrylate (Bis-GMA), a molecule known to be the basis of composite resins used in dentistry.[1,2] In the international dentistry literature, it is stated that BPA and/or its derivatives can be released into the oral cavity from composite fillings and fissure sealants at doses that can produce active substance.

BPA shows activity similar to endocrine hormones due to its chemical structure. In other words, the emphasis that estradiol and diethylstilbestrol, due to the presence of phenol groups in their structures, BPA and its derivatives have similar effects by binding to estrogen receptors, and that they can cause neurological disorders even at low doses worries researchers.[3] For this reason, it is important to determine BPA and its derivatives (bisphenol S, BPS, bisphenol F, BPF, *etc.*) quickly and sensitively at low concentrations.

Due to the negative effects of BPA and its derivatives on human health, a number of methods have been developed to determine its amount in the liquids which comes into contact with BPA containing products.[4] The BPA derivates BPF (4,4′-dihydroxydiphenylmethane) and BPS (4,4′-sulfonyldiphenol) also have estrogenic, progesteronic and anti-androgenic effects and are used in production of daily life products such as food cans, plastic bottles, *etc*.

However, most of methods to determine BPA and its derivates are based on spectrophotometry and/or chromatography, requiring time-consuming sample preparation and pre-analysis processes. In addition, these methods depend on large capital investment causing high operating costs. Moreover, the analysis with these methods require qualified person and interpretation of analysis results is time-consuming.[5,6] For this reason, many research groups are working on developing fast, sensitive, innovative and relatively cheaper methods for the analysis of BPA and its derivatives. Biosensor could be one of the innovative methods used in BPA determination. Biosensor is defined as a device combined with a biological agent and a physicochemical converter.

In this study, a new biosensor modified with Fe_3O_4 nanoparticle was designed to determine the released amounts of BPA and its derivatives contained in some orthodontic materials. For this purpose, carbon paste electrode was modified by using commercial Fe_3O_4 nanoparticle. Tyrosinase enzyme was immobilized onto modified electrode by cross-linking with bovine serum albumin (BSA) and glutaraldehyde. Optimum operating conditions of the biosensor as temperature, pH, glutaraldehyde amount and substrate concentration were studied. Linear operating range and detection limit were defined. Released BPA concentration from different dental filling materials as real sample was determined under determined optimum operating conditions of the biosensor. Although there are biosensor studies for BPA determination in the literature, it was seen that there are

almost no biosensor studies for the determination of BPA derivate such as BPS and BPF. In this study, a fast, high sensitivity and sensitivity low detection limit as well as low cost new biosensor has been developed for the determination of both BPA and BPS and BPF.

EXPERIMENTAL

Tyrosinase enzyme (purified from fungus and as 2500 units) was purchased from Sigma-Aldrich. BPA, BPS, BPF, mineral oil, glutaraldehyde, carbon powder, disodium hydrogen phosphate and monosodium hydrogen phosphate were obtained from Merck.

All electrochemical experiments were performed using a computer-connected CHI1230A model electrochemical analyzer of CHI Company (CH Instrument, BASi, Kent Avenue, West Lafayette, IN, USA). Amperometric measurements were performed in a three-electrode cell system. A carbon paste electrode with a surface area of 0.6 cm^2 was used as the working electrode, Ag/AgCI (BAS RE-5B) was used as the reference electrode and platinum wire (MW--1032) was used as the counter electrode. After each electrochemical study, the working electrode was stored at 4 °C in distilled water or in the buffer solution.

Modification of carbon paste electrode

A known amount of graphite powder (0.0650 g) was weighed precisely, 30 µl of nujol and 40 mg of Fe_3O_4 nanoparticles were added to it and mixed homogeneously. The resulting mixture was filled into the electrode chamber so that there was no space left. Finally, the surface was cleaned and polished.[7]

Enzyme electrode preparation and amperometric measurements

2.0 mg BSA (bovine serum albumin), 50.0 µL phosphate buffer solution, 100.0 µL tyrosinase (50.0 units/mL) and 40.0 µL glutaraldehyde (2.5%) was mixed homogeneously. This mixture (190 µL totally) was dropped onto the surface of modified carbon paste electrode (MCPE) and dried at room temperature. The prepared enzyme electrode was washed first with distilled water and then with buffer solution. It was stored in the buffer solution at 4 °C when not in use (Fig. 1 a).[8]

BPA, BPF and BPS were used as different substrates of tyrosinase separately. Determination of the amount of BPA is based on the reduction of quinone compound released as a result of the enzymatic reaction (Fig. 1b). For this purpose, 0.1 M supporting electrolyte (NaCl) was added to the measurement medium (pH 7.0 phosphate buffer). The electrode was equilibrated at varying potentials (*versus* Ag/AgCl electrode (3.0 M KCl)) until a constant current value was obtained. BPA solution was added to the cell after equilibrium current (i_a) was recorded, and the system was stirred. At the end of the reaction, the final current (i_b) was recorded. The BPA concentration was plotted against the obtained current difference.[9]

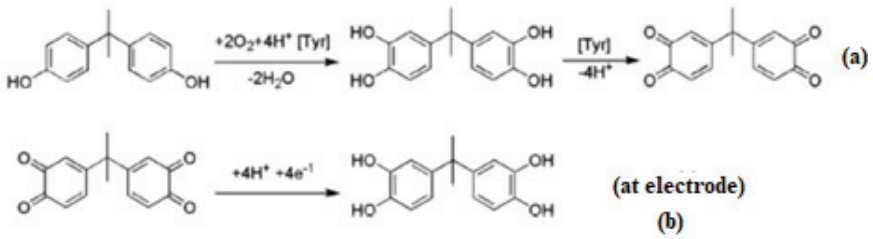

Fig. 1. Possible oxidation mechanism of BPA by tyrosinase.[4]

After determining the working potential, the optimum conditions (substrate concentration, pH, temperature) and the factors affecting its performance (operational stability, storage stabilization, interference effects) of the designed biosensor were determined. Finally, the amounts of BPA released from different dental filling materials were determined.

RESULTS AND DISCUSSION

BPA, a monomer of resins and plastics in the structure of many products used in daily life, released over time, increases the amount of intake into the human body and creates a toxic effect. Released BPA should be below the tolerable daily intake level (0.05 mg per kg of body mass).[6] Due to its chemical structure, BPA can imitate estrogen and exhibit similar activity. It is stated in studies that BPA has negative effects on human health, especially on the endocrine system.[3,11] For this reason, it is important to determine BPA quickly and with high sensitivity.[11]

Electrochemical characterization and determination of the response and working potential of CPE and MCPE electrodes to BPA

The electrochemical performance of the CPE and MCPE were studied using cyclic voltammetry and $K_3Fe(CN)_6$ as a redox probe.[12] The cyclic voltammograms of the electrodes are presented in Fig. 2. 0.05 mM $K_3Fe(CN)_6$ solution in 0.10 M H_2SO_4 supporting electrolyte with a scan rate of 100 mV s^{-1} were documented. It was clear that the reduction and oxidation peaks of 0.05 mM $K_3Fe(CN)_6$ are seen quite clearly in the alternating voltammograms of the bare carbon paste electrode, while the 0.05 mM $K_3Fe(CN)_6$ obtained in the modified carbon paste electrode under the same conditions.

The voltammograms of CPE was shown in Fig. 2a (2). The reduction peak at 0.22 V and the oxidation peak at 0.34 V were obtained. When 0.05 mM $K_3Fe(CN)_6$ solution was added in cell (voltammogram 3), the reduction peaks at 0.22 V and oxidation peaks at 0.34 V increased. This increasing of the peaks were related with increased amount of $K_3Fe(CN)_6$. The same process was performed with the MCPE under the same conditions (Fig. 2b). As examined from the voltammograms 2 and 3 in Fig. 2b, no visible reduction or oxidation peak was observed with the addition of $K_3Fe(CN)_6$. According to this results it could be concluded that the surface of the carbon paste electrode has changed by modification of Fe_3O_4 nanoparticles. The decrease in the peaks indicated the modification of the carbon paste electrode (Fig. 2).

To determine the response of carbon paste electrode (CPE) and MCPE to BPA, the electrodes established equilibrium at –0.20 V potential separately.[13,14] Then, tyrosinase enzyme was added into the cell and was kept for a while until equilibrium was reached, and the equilibrium current recorded. The current differences (Δi) were recorded by adding bisphenol A solution at increasing cell concentrations between 1–500 μM. The current differences against increasing

bisphenol A concentrations were plotted (Fig. 3a). As seen in Fig. 3a, the bisphenol A response of the prepared modified carbon paste electrode is approximately two times higher than that of the carbon paste electrode.

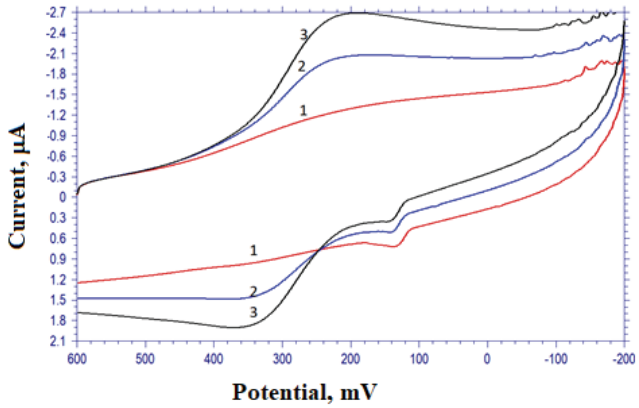

(a)

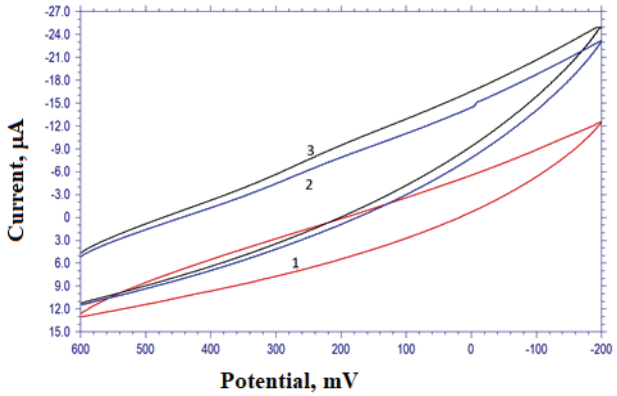

(b)

Fig. 2. Cyclic voltammograms of $K_3Fe(CN)_6$ in 0.10 M H_2SO_4 supporting electrolyte (scan rate of 100 mV s^{-1}); a) bare CPE; b) MCPE. 1. 10.0 mL 0.10 M supporting electrolyte; 2. 1 + 0.05 mM $K_3Fe(CN)_6$; 3. 2 + 0.05 mM $K_3Fe(CN)_6$.

The working potential of the MCPE was determined after the working electrode reached the equilibrium at potentials ranging from –0.1 to –0.25V. BPA solution was added into the cell at increasing concentrations (1–500 µM) and the current values obtained at the end of the reaction were recorded. Current differences *versus* bisphenol A concentration were plotted (Fig. 3b). With the data obtained, the best reduction potential of the quinone compound formed at the end of the reaction was determined as –0.15 V.

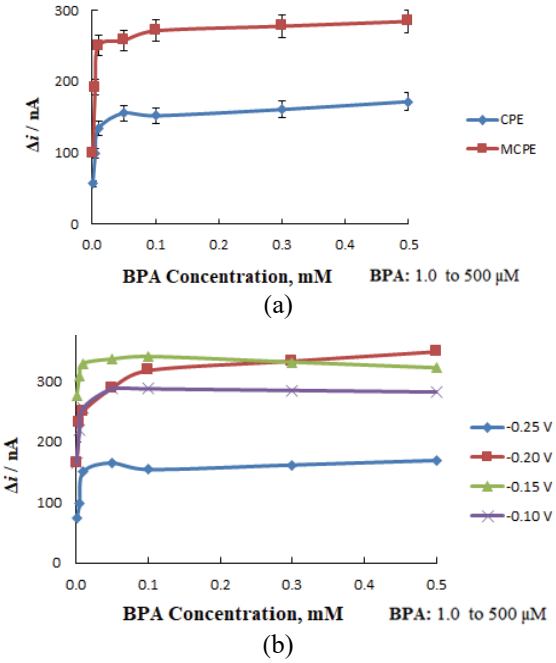

Fig. 3. a) Amperometric responses of CPE and MCPE to different concentrations of BPA; b) effect of working potential on BPA response of MCPE (at 25 °C, in 0.1 M, pH 7.0, phosphate buffer).

Effects of Fe_3O_4 nanoparticles amount on amperometric response of BPA effect of the amount of glutaraldehyde

In order to find out the optimum quantity of Fe_3O_4 nanoparticles in MCPE on response of quinone compound, working electrodes were prepared by adding 35.0, 40.0 and 45.0 mg Fe_3O_4 separately. The reduction currents of quinone compound were measured with each electrode at –0.15 V. The BPA concentration was plotted against Δi results and 40.0 mg Fe_3O_4 showed the best linearity and the highest response current (Fig. 4a).

In many studies, glutaraldehyde ($CHO–CH_2CH_2CH_2–CHO$) is preferred as a cross linker.[7,15] Since glutaraldehyde is a small molecule, it can interact with amine groups both on the enzyme surface and interior and as a result the active site of the enzyme may be blocked by excessive cross-linking. The three-dimensional structure of the enzyme may change and activity losses may occur.[16] The amount of glutaraldehyde used should be investigated, for being sure that the active site of the enzyme is not affected, to avoid loss of activity. Best glutaraldehyde amount was defined by using prepared electrodes with the addition of 20, 30, 40 and 50 μL (2.5 %) glutaraldehyde solution separately for the determination of bisphenol A. Equilibrium current was recorded and current differences

were plotted. An increase in currents was observed when the amount of glutaraldehyde was increased from 20 to 30 μL and from 30 to 40 μL. There was a loss in activity detected by decreased currents with the electrode prepared by the addition of 50 μL glutaraldehyde. It was clearly seen from the graph that the highest currents recorded with the electrode designed by using 40 μL glutaraldehyde (Fig. 5b). The findings could be explained as 30 μL glutaraldehyde was insufficient to immobilize the enzyme and had difficulty in holding the structure together, and 50 μL glutaraldehyde caused loss of activity in the enzyme due to excessive binding.

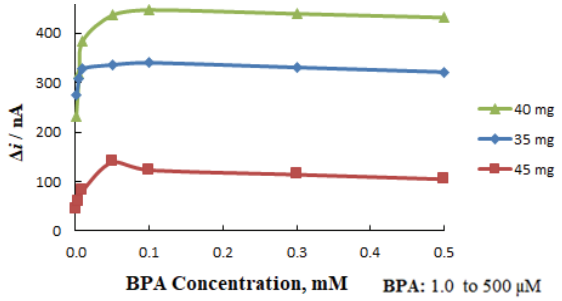

(a)

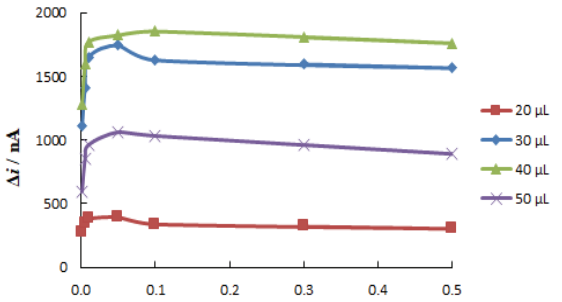

(b)

Fig. 4. Effect of Fe_3O_4 (a) and glutaraldehyde (b) amount on BPA response of MCPE (at 25 °C, in 0.1 M, pH 7.0, phosphate buffer).

Effects of pH and temperature

One of the most important factors for enzymes, to show their activities with maximum velocity and low K_m value, is pH. Since there could be different ionizations on the active site or side groups of the enzyme at different pH values, the optimum pH value at which the enzyme shows the best activity should be determined. For this purpose, different buffer solutions ranged between 4.0 and 9.0 were used to determine the effect of pH on amperometric response of designed electrode. An acetate (acetic acid/sodium acetate) buffer solutions of pH 4.0 and

5.0, phosphate (Na_2HPO_4/NaH_2PO_4) buffer solutions of pH 6.0, 7.0 and 8.0 and glycine/sodium hydroxide buffer of pH 9.0 were used. When the Δi response current values at increasing concentrations (1–500 μM) were plotted against pH, the highest response current values were at pH 5.0 representing the optimum pH of the designed biosensor (Fig. 5a).

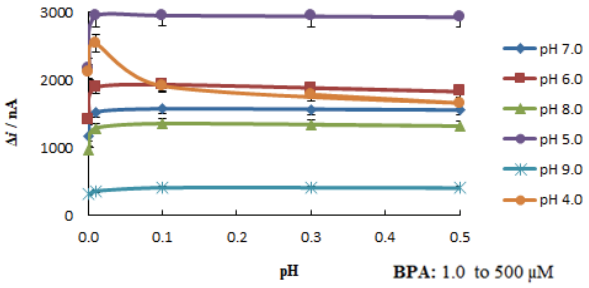

(a)

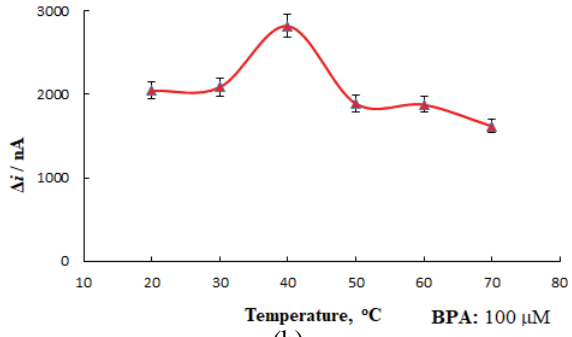

(b)

Fig. 5. Effect of pH (a) and temperature (b) on BPA response of MCPE.

In literature, it was stated that BPA biosensors prepared with different materials had optimum operating performance at different pH values varied between 3.0 and 7.0.[11,17–19] The reasons for this difference in pH values could be explained by the different modification materials and immobilization process.

Temperature is an important parameter for enzyme activity. Enzymes degrade at high temperature. To examine the effect of temperature on the current response of enzyme electrode, the temperature of the solution in the thermostatic cell was adjusted to 20 °C using a thermostatic circulating water bath. Then, BPA solution was added with an intracellular concentration of 1.0×10^{-4} M, and at the end of the reaction Δi value for 20 °C was calculated. The same process was carried out for the temperatures between 30 and 70 °C with 10 °C step. These amperometric response currents were measured at different temperatures in triplicate and plotted (Fig 5b). It is clear that the enzyme electrode showed the best

activity at 40 °C. Nevertheless, in terms of the practicality of the biosensor, all studies were carried out at room temperature.[7,11,15]

Substrate concentration and calibration curves BPA and its derivates

In order to examine the effect of the substrate concentration on the prepared biosensor, the amperometric currents of the increasing bisphenol A concentration (1–500 nM) at –0.15 V were recorded. Δ*i* current obtained by increasing bisphenol A concentration results were used for preparing Michaelis–Menten curve. It was observed that the current differences increased linearly as the bisphenol A concentration increased, then deviated from linearity and increased hyperbolically at increasing concentrations. The same process was also carried out separately for BPS and BPF substrates. Lineweaver–Burk curve was prepared to calculate the K_m constant by plotting the data as (1/([BPA]–1) Δi^{-1}. The observed value of $K_{m(app)}$ provides important information about the catalytic activity and affinity between enzyme and substrates. A low $K_{m(app)}$ value indicates a high affinity and kinetic activity between enzyme and substrate. Increasing concentrations of bisphenol A, BPS and BPF separately resulted in a quite small current differences after a certain concentration.

When the data of Fig. 6a in linear regions were plotted, it was seen that there were two calibration charts that could be used for the determination of bisphenol A. When the calibration graphs were examined, it was determined that there were linear operating ranges between the concentrations 1–5 nM and 30–100 nM. This situation allows to determine BPA and its derivatives in wide range. The limit of detection (*LOD*), was calculated according to *S*/*N* = 3 criterion and calculated as 1 nM.

The $K_{m(app)}$ value as 0.00067 μM and the $I_{max(app)}$ value as 3.34 μA was clearly seen in Fig. 6a. Different $K_{m(app)}$ values as 0.00815 M;[20] 3.26 μM;[21] 12 μM;[22] 0.34 mM[23] were reported earlier. It is obvious that the $K_{m(app)}$ value of designed biosensor, in the present study, is quite lower than the $K_{m(app)}$ values reported in literature. One of the biggest advantages of the designed biosensor is its ability to measure even at very low concentrations.

When the data of Fig. 6b in linear regions were plotted, two calibration charts were seen that could be used for the bisfenol S determination. When the calibration graphs were examined, it was observed that there were linear operating ranges between 1–5 nM and 10–100 nM concentrations and the lower detection limit was 1 nM. It is seen that the $K_{m(app)}$ value is 0.00075 μM and the $I_{max(app)}$ value is 2.50 μA (Fig. 6b).

When the data of Fig. 7 in linear regions were plotted, it was noticed that there were two calibration charts that could be used for the determination of bisphenol F. When the calibration graphs were examined, it was determined that there were linear operating ranges between 3–10 nM and 10–50 nM concentrate-

ions and the lower detection limit was 1 nM. It is seen that the $K_{m(app)}$ value is 0.00075 μM and the $I_{max(app)}$ value is 2.50 μA (Fig. 7).

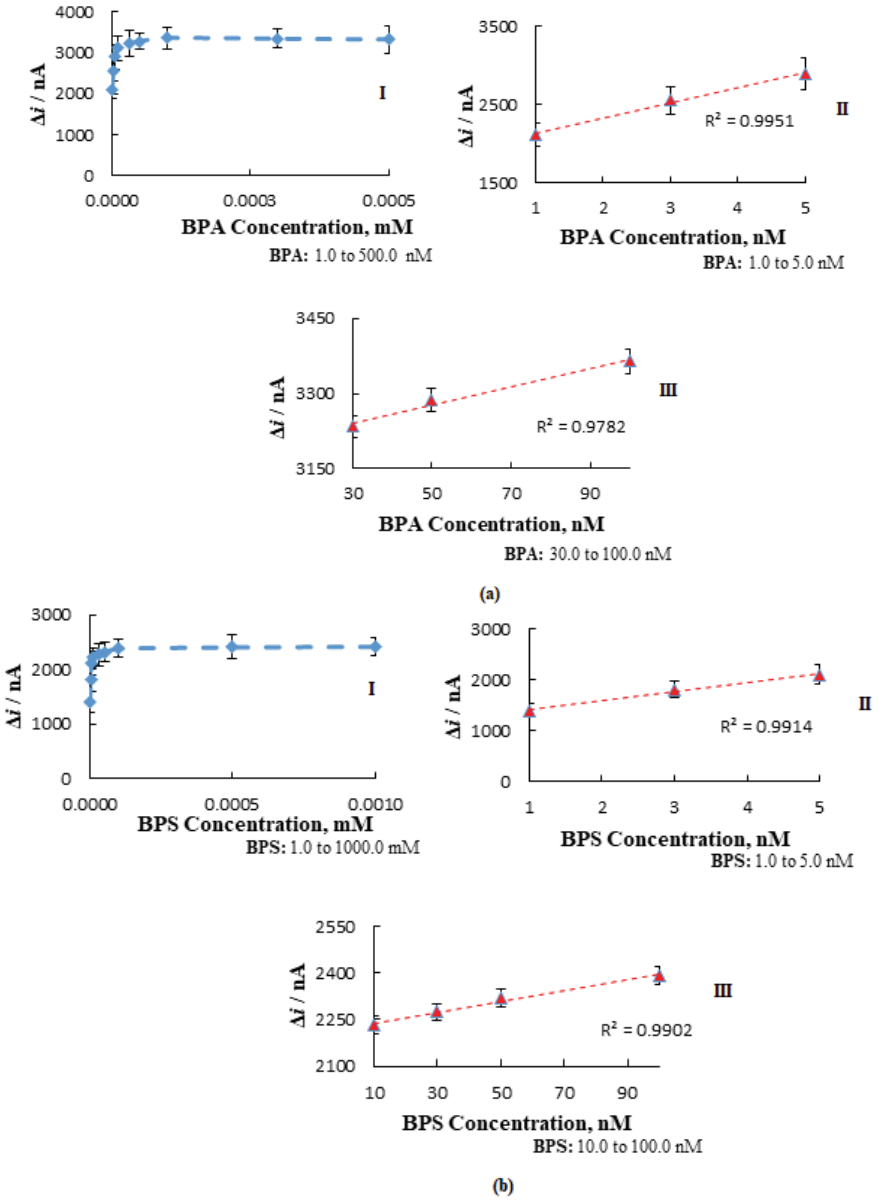

Fig. 6. Effect of: a) bisphenol-A (BPA) and b) bisphenol-S (BPS) concentration on the response of biosensor; I) Michael–Menten curve, II) calibration curve 1 and III) calibration curve 2 (–0.15 V operating potential, at 25 °C, in 0.1 M, pH 5.0, acetate buffer).

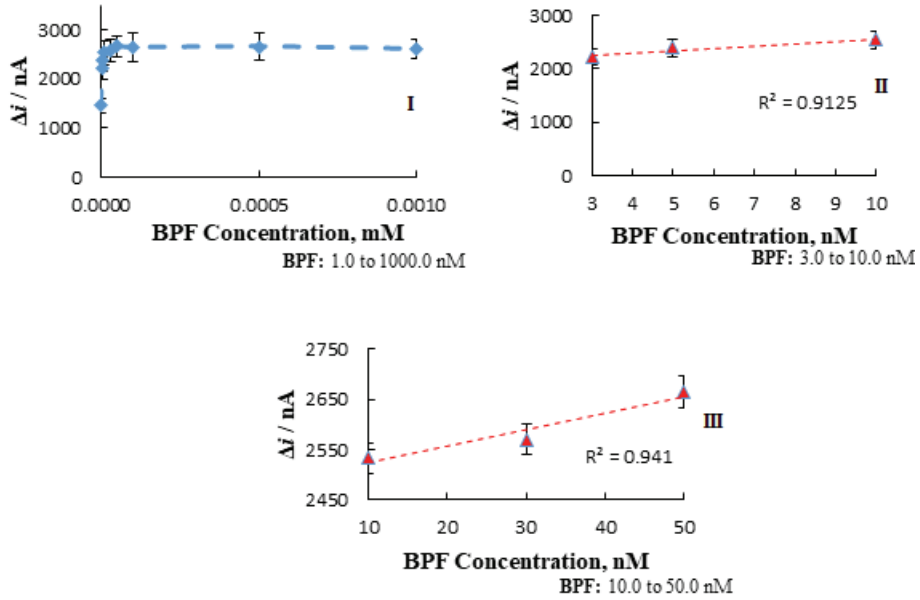

Fig. 7. Effect of bisphenol F (BPF) concentration on the response of biosensor; I) Michael–Menten curve, II) calibration curve 1 and III) calibration curve 2 (–0.15 V operating potential, at 25 °C, in 0.1 M, pH 5.0, acetate buffer).

It is clear that the designed biosensor has low $K_{m(app)}$, *LOD* and *LOQ* values for all three substrates. This shows that the tyrosinase enzyme has a high affinity for all three substrates (BPA, BPF and BPS) individually.

In Table I, characteristic analytical parameters of the different BPA biosensors were compared. It is clear that the designed biosensor has a low detection limit and wide calibration range for each substrate, and that BPA and its derivatives can be determined with high sensitivity in complex analysis environments.

TABLE I. Comparison of analytical characteristics of the different BPA biosensors

Immobilization matrix	Working *E* / V	Linearity of biosensor μmol L^{-1}	*LOD* nmol L^{-1}	K_m μM	Optimum pH	*RSD* %	Long-term stability	Ref.
Tyr/Au@PDA-rGO-CS/GCE	–0.20	0.012–3.68	0.01	nr	7.0	1.69	After 30 days, the modified electrode remained 92 % of its initial response	14
CYP2C9-PAM/GCE	–0.36	1.25–10.0	0.58	3.90	7.0	nr	The amperometric response after 10 days is 92 %	24

TABLE I. Continued

Immobilization matrix	Working E / V	Linearity of bio-sensor μmol L^{-1}	*LOD* nmol L^{-1}	K_m μM	Optimum pH	*RSD* %	Long-term stability	Ref.
Tyr/SWCNT-PolyLys/GCE	–0.10	4.00–11.5	0.97	nr	6.0	2.1 (n = 5)	The amperometric response after 30 days is 94.2 %	25
Tyr/TiO_2-MWCNT-PDDA-Nafion/GCE	–0.50	0.28–45.05	0.066	nr	6.0	5.1 (n = 5)	The response on the 14th day was 25 % of the initial value	26
Au-rGO paste based 3D-printed platform	–	100 nM L^{-1} to 10 mM L^{-1}	3.52	–	7.4	5.60 (n = 5)	–	27
MD/Graphene	–	10 nM L^{-1} to 0.10 mM L^{-1}	3.05	–	–	–	–	28
Try/Fe_3O_4 NPs modified carbon paste electrode	–0.15	0.001–0.005 and 0.03–0.1	1.0	0.00067	5.0	4.91 (n = 18)	The amperometric response after 20 days is 57.11 %	This study

Operational stability of BPA biosensor and storage stabilization of the enzyme electrode

To investigate the reusability of the electrode, the current changes were determined after successive measurements at a constant substrate concentration of 10 nM. The Δi values were plotted against the number of measurements (Fig. 8a). The relative standard deviation (*RSD*) calculated from the current changes obtained as a result of 18 measurements was found 4.91 % and it was observed that the electrode lost 5.43 % of its initial activity. The reusability of the electrode prepared in this study was found to be quite good.

In order to determine the storage stabilization of the electrode, amperometric response current was measured using 10 nM BPA concentration at certain intervals (1–3–10–15–20. days) for 20 days by resting the enzyme electrode in the buffer solution (pH 5.0) at 4 °C. At the end of the 20th day, the electrode retained 57 % of its initial activity (Fig. 8b).

Interference effects

Acetonitrile, ethyl acetate, hexane, phenol, nitrophenol, urea and potassium nitrate were chosen as interfering agents. The effect of interfering agents on bisphenol A determination was examined at concentration of 10 nM both for substrate and interfering agents. Minimizing or eliminating the interferences that may occur is important for the detection and accuracy of real sample analysis. It

was determined that none of these interfering agents caused an interference in bisphenol A determination.

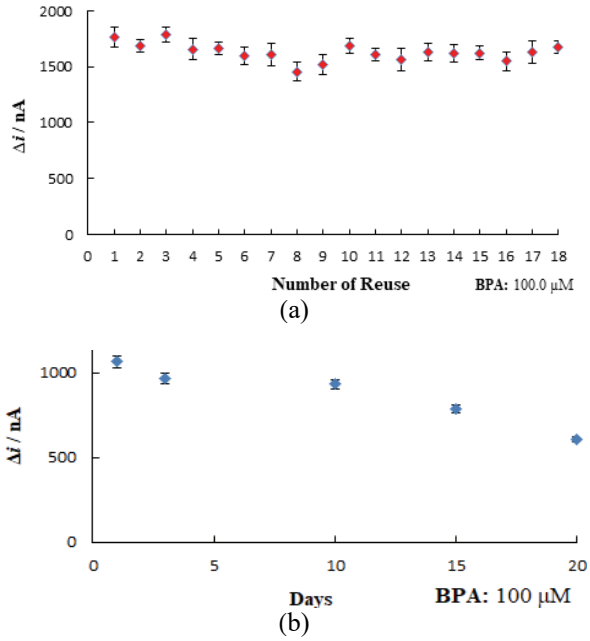

Fig. 8. a) Operational stability of the biosensor; b) storage stability of the biosensor.

BPA determination in different dental materials

Three different orthodontic materials were examined to determine the effectiveness of the biosensor on real samples. In the first sample, the orthodontic adhesive (Transbond XT, 3M Unitek, CA, USA) used to bond the brackets to the tooth surface was prepared in a metal mold with a height of 2 mm and a diameter of 4 mm, and the LED light source (VALO LED, Ultradent, South Jordan, UT, USA) It was polymerized by applying it for 3 s on both the front and back sides. The obtained sample was placed in a glass tube containing 5 mL of distilled water.[9]

In the second sample, a 1 mm thick 1 cm×1 cm piece of thermoplastic plaques (Simona Ag, Kirn, Germany) used in the reinforcing treatment was placed in a glass tube containing 5 mL of distilled water in order to preserve the new position of the teeth after orthodontic treatment.

In the third sample, during the fixed orthodontic treatment, the braces remain in the slots on the brackets without moving, thus transmitting force towards the tooth; 10 pieces of elastic ligature (Dentsply GAC, Islandia, NY, USA) were placed in a glass tube containing 5 ml of distilled water, considering that they

would be placed on the brackets of the incisors, canines and premolars on a single jaw.

Measurements were made after the samples were kept in glass tubes for 1 h. Care was taken not to use plastic materials during the preparation and experimentation of the samples. 100 μL of the obtained sample was added to the measurement medium, and after 20 min of mixing, the measurement was taken in 200 s. These studies were repeated three times and averaged, Δi mean value was calculated and plotted against bisphenol A concentration. The average of the current difference (Δi) for 3 different samples was calculated to determine the amount of BPA of the samples. It was determined that $(0.0002196\pm8.18)\times10^{-7}$, $(0.0000909\pm1.02)\times10^{-6}$ and $(0.000275\pm4.08)\times10^{-6}$ mg/kg BPA from 1 mg of composite to 1 mL of water was released for samples I, II and III, respectively.

CONCLUSION

In this study, a new tyrosinase enzyme-based biosensor was designed by modifying the carbon paste electrode using Fe_3O_4 nanoparticles. The designed biosensor has a response time of 200 s, two linear detection intervals and a very low detection limit (1 nM) for each substrate (BPA, BPS and BPF). Released BPA should be below the tolerable daily intake level (0.05 mg per kg of body mass).[6] With this designed biosensor, measurements can be made at concentrations lower than 0.05 mg/kg.

With this newly designed biosensor, it is possible to detect three different species (BPA, BPS and BPF) separately with a single biosensor, at low concentrations, with high sensitivity, and with a wide detection range. Considering the reproducibility, shelf life and interference effects on the biosensor, the designed biosensor is capable of providing fast, high-sensitivity and economical BPA and its derivatives determination.

Acknowledgement. This study was supported by Gazi University with project number 05/2020-11.

ИЗВОД

ДИЗАЈНИРАЊЕ ЕЛЕКТРОХЕМИЈСКОГ БИОСЕНЗОРА БАЗИРАНОГ НА ТИРОЗИНАЗИ ЗА ВИСОКО ОСЕТЉИВУ И БРЗУ ДЕТЕКЦИЈУ БИСФЕНОЛА А И ЊЕГОВИХ ДЕРИВАТА

ONUR CAN BODUR[1], MERVE KESKIN[2], BAŞAK ARSLAN AVAN[3] и HALIT ARSLAN[1]

[1]Department of Chemistry, Faculty of Science, Gazi University, Ankara, Republic of Türkiye, [2]Vocational School of Health Services, Bilecik Seyh Edebali University, Bilecik, Republic of Türkiye и [3]Department of Orthodontics, Faculty of Dentistry, Gazi University, Ankara, Republic of Türkiye

Бисфенол А (BPA) је мономер који се обично користи у производњи епокси смола, пластичних боца и материјала за зубне пломбе. Због своје хемијске структуре, BPA и његови деривати показују активност сличну ендокриним хормонима. Он се може везати за естрогенске рецепторе и изазвати неуролошке поремећаје, чак и у малим дозама. Стога је важна брза и осетљива детекција BPA и његових деривата у малим концентра-

цијама. У овом истраживању је дизајниран амперометријски биосензор на бази ензима тирозиназе за квантитативно одређивање мономера BPA, бисфенол F (BPF) и бисфенол S (BPS). Тирозиназа је имобилисана на електроди од угљеничне пасте модификованој умрежавањем са глутаралдехидом. Количина BPA (BPS и BPF) је одређена директно редукцијом хинонског једињења које је ослобођено у ензимској реакцији на –0,15 V. Одређено је да је вредност $K_{m(app)}$ дизајнираног биосензора за BPA $6{,}7\times10^{-4}$ μM, линеарни радни опсег је 0,001–0,005 μM и 0,03–0,1 μM и да доња граница детекције износи 1 nM за сваки од мономера. Јасно је показано да дизајнирани биосензор омогућава брзо, ефикасно и прецизно одређивање BPA и његових деривата ослобођених из денталних материјала.

(Примљено 22. новембра 2022, ревидирано 13. фебруара, прихваћено 21. марта 2023)

REFERENCES

1. F. Fleisch, P. E. Sheffield, C. Chinn, B. L. Edelstein, P. J. Landrigan, *Pediatrics* **126** (2010) 760 (https://doi.org/10.1542/peds.2009-2693)
2. L. A. D. Gugoasa, *J. Electrochem. Soc.* **167** (2020) 037506 (https://doi.org/10.1149/2.0062003JES)
3. K. V. Ragavan, N. K. Rastogi, M. S. Thakur, *TrAC - Trends Anal. Chem.* **52** (2013) 248 (http://doi.org/10.1016/j.trac.2013.09.006)
4. EFSA, *EFSA J.* **428** (2006) (https://doi.org/10.2903/j.efsa.2004.86)
5. X. Lu, X. Wang, L. Wu, L. Wu, L. Fu, Y. Gao, J. Chen*, ACS Appl. Mater. Interf.* **8** (2016) 16533 (https://doi.org/10.1021/acsami.6b05008)
6. H. Yin, L. Cui, Q. Chen, W. Shi, S. Ai, L. Zhu, L. Lu, *Food Chem.* **125** (2011) 1097 (https://doi.org/10.1016/j.foodchem.2010.09.098)
7. O. C. Bodur, S. Dinç, M. Özmen, F. Arslan, *Biotechnol. Appl. Biochem*. **68** (2021) 20 (https://doi.org/10.1002/bab.1886)
8. S. Donmez, F. Arslan, N. Sarı, E. Hasanoğlu Özkan, H. Arslan, *Biotechnol. Appl. Biochem.* **64** (2017) 745 (https://doi.org/10.1002/bab.1533)
9. F. Arslan, *Sensors* **8** (2008) 5492 (https://doi.org/10.3390/s8095492)
10. P. C. Pwavodi, V. H. Ozyurt, S. Asir, M. Ozsoz, *Micromachines* **12** (2021) 312 (https://doi.org/10.3390/mi12030312)
11. P. Deng, Z. Xu, Y. Kuang, *Food Chem.* **157** (2014) 490 (https://doi.org/10.1016/j.foodchem.2014.02.074)
12. S. S., Shankar, R. M., Shereema, V., Ramachandran, T. V., Sruthi, V. S., Kumar, R. B. Rakhi, *ACS Omega* **4** (2019) 7903 (https://doi.org/10.1021/acsomega.9b00230)
13. S. Wang, Y. Tan, D. Zhao, G. Liu, *Biosens. Bioelectron.* **23** (2008) 1781 (https://doi.org/10.1016/j.bios.2008.02.014)
14. X. Xu, Q. Zheng, G. Bai, L. Song, Y. Yao, X. Cao, C. Yao, *Electrochim. Acta* **242** (2017) 56 (https://doi.org/10.1016/j.electacta.2017.05.007)
15. E. Aynacı, A. Yaşar, F. Arslan, *Sensors Actuators, B* **202** (2014) 1028 (https://doi.org/10.1016/j.snb.2014.06.049)
16. Q. Xin, R. M. Wightman, *Brain Res.* **776** (1997) 126 (https://doi.org/10.1016/S0006-8993(97)00996-7)
17. L. Wu, X. Lu, K. Niu, Dhanjai, J. Chen, *Biosens. Bioelectron*. **165** (2020) 112407 (https://doi.org/10.1016/j.bios.2020.112407)

18. M. Sýs, M. Obluková, V. Kolivoška, R. Sokolová, L. Korecká, T. Mikysek, *J. Electroanal. Chem.* **864** (2020) 114066 (https://doi.org/10.1016/j.jelechem.2020.114066)
19. Erkmen, S. Kurbanoglu, B. Uslu, *Sensors Actuators, B* **316** (2020) 128121 (https://doi.org/10.1016/j.snb.2020.128121)
20. M. Najib, M. E. Ghicad, C. Dridia, B. M. Alia, M. A. Christopher, *Talanta* **184** (2018) 388 (https://doi.org/10.1016/j.talanta.2018.03.031)
21. F. A. A. Manan, W. W. Hong, J. Abdullah, N. A. Yusof, I. Ahmad, *Mater. Sci. Eng., C* **99** (2019) 37 (https://doi.org/10.1016/j.msec.2019.01.082)
22. Wong, A. Santos, O. Fatibello Filho, M. Sotomayor, *Electroanalysis* **33** (2020) 431 (https://doi.org/10.1002/elan.202060084)
23. L. A. Mercante, L. E. Iwaki, V. P. Scagion, O. N. Oliveira, L. H. Mattoso, D. S. Correa, *Electrochem*. **2** (2021) 41 (https://doi.org/10.3390/electrochem2010004)
24. P. Sun, Y. Wu, *Sensors Actuators, B* **178** (2013) 113 (https://doi.org/10.1016/j.snb.2012.12.055)
25. M. Han, Y. Qu, S. Chen, Y. Wang, Z. Zhang, M. Ma, Z. Wang, G. Zhan, C. Li, *Microchim. Acta* **180** (2013) 989 (https://doi.org/10.1007/s00604-013-1018-3)
26. J. Kochana, K. Wapiennik, J. Kozak, P. Knihnicki, A. Pollap, M. Woźniakiewicz, P. Kościelniak, *Talanta* **144** (2015) 163 (https://doi.org/10.1016/j.talanta.2015.05.078)
27. L.A. Gugoasa, R.I. Stefan-van Staden, J.F. van Staden, M. Coroş, S. Pruneanu, *Anal. Lett.* **52** (2019) 2583 (https://doi.org/10.1080/00032719.2019.1620262)
28. R.I. Stefan-van Staden, L.A. Gugoaşă, B. Calenic, J.F. van Staden, J. Legler, *Anal. Chem. Res.* **1** (2014) 1 (https://doi.org/10.1016/j.ancr.2014.06.001)
29. B. Arslan, E. Yıldırım, C. O. Bodur, B. B. Tuncer, Ç. M. Ulusoy, C. Tuncer, *Turk. J. Orthod.* **35** (2022) 27 (https://doi.org/10.5152/TurkJOrthod.2021.21176).

Journal of the Serbian Chemical Society
JSCS-info@shd.org.rs • www.shd.org.rs/JSCS
J. Serb. Chem. Soc. *88* (5) 537–550 (2023)
JSCS–5644
Original scientific paper
Published 20 May 2023

Biosynthesis of silver-based nanoparticles on polypropylene non-woven material for efficient antimicrobial activity

ANA G. KRKOBABIĆ[1], JOVANA D. STOJIČIĆ[1], MAJA M. RADETIĆ[1#] and DARKA D. MARKOVIĆ[2*#]

[1]*University of Belgrade, Faculty of Technology and Metallurgy, Karnegijeva 4, 11120 Belgrade, Serbia and* [2]*University of Belgrade, Innovation Centre of the Faculty of Technology and Metallurgy, Karnegijeva 4, 11120 Belgrade, Serbia*

(Received 13 January, revised 23 February, accepted 9 April 2023)

Abstract: The outbreak of the COVID 19 pandemic confirmed the importance of personal protective equipment including the respiratory face masks as barriers to pathogens. Taking into account that face masks are mainly composed of polypropylene (PP) non-woven materials this study explores the possibility of *in situ* biosynthesis of silver-based nanoparticles as an antimicrobial agent on PP material. A pomegranate peel extract was used as a "green" agent for synthesis and stabilization of nanoparticles. Hydrophobicity of PP fibers was overcome by modification with corona discharge at atmospheric pressure. In order to improve the binding of silver ions, corona modified PP material was impregnated with biopolymer chitosan in the presence of crosslinker 1,2,3,4-butanetetracarboxylic acid. SEM analysis revealed the presence of spherical Ag-based nanoparticles on the fiber surface with an average size of approximately 69 nm. The higher the concentration of the precursor salt, the higher the silver content after the reduction. Larger amounts of Ag-based nanoparticles provided stronger antimicrobial activity against bacteria *Escherichia coli* and *Staphylococcus aureus*, and yeast *Candida albicans*.

Keywords: pomegranate peel; chitosan; Ag nanoparticles; corona discharge.

INTRODUCTION

Until the outbreak of the COVID 19 pandemic, protective personal equipment including respiratory face masks has been mainly reserved for medical professionals but the years of living with SARS-CoV-2 virus stressed the importance of protective masks in everyday life.[1] Commonly used respiratory protective masks such as N95 and KN95 are composed of multiple layers of polypropylene (PP) non-woven material. In general, PP non-woven materials are widely used in

* Corresponding author. E-mail: darka@tmf.bg.ac.rs
# Serbian Chemical Society member.
https://doi.org/10.2298/JSC230113020K

medical textiles as a part of personal protective equipment like facemasks, disposable surgical gowns, drapes, shoe covers, head covers, *etc*.[2] Keeping in mind that PP fibers do not provide any antimicrobial activity, protective masks can only act as a physical barrier to pathogens transmission but they are not able to inactivate pathogens.[1] Furthermore, the probability of pathogen penetration through the mask increases with wearing time.[1,3] To overcome the possible contamination of users, frequent change of mask is recommended, but this is not economically and environmentally acceptable. Moreover, properties of PP fibers and fabrication method of face masks do not allow the efficient sterilization for re-use by standard methods in disinfect solutions.[1,3,4] These shortcomings of personal protective equipment are particularly common in hospital environment where transmission of pathogens from patients to personnel and *vice versa* induces additional spreading of hospital infections.[5]

A variety of antimicrobial agents have been tested for possible application to PP non-woven materials.[6–12] Extraordinary antimicrobial activity against *E. coli*, *S. aureus* and *C. albicans* is obtained by impregnation of PP non-woven material with thymol using supercritical CO_2.[6] During the pandemic of fly influence A H1N1, Borkov *et al.* discovered that respiratory protective face masks impregnated with copper oxide showed influenza biocidal properties without change of physical barrier properties.[7] Excellent antimicrobial activity is also obtained by *in situ* synthesis of copper oxide nanoparticles on PP non-woven material using ascorbic acid as a reducing agent.[8] Coating of protective mask with a thin layer of copper film results in the reduction of virus SARS-CoV-2 by more than 75 %.[9] Kumar *et al*. reported that face masks coated with copper nanoparticles could provide significant protection from SARS-CoV-2 transmission.[10] Promising method for imparting biocide activity to N95 facemasks proposes simultaneous polymerization and grafting of C12-quaternized benzophenone using a UV irradiation.[1] Nanostructured silver films successively deposited on the surface of PP non-wovens by magnetron sputter coating provides satisfactory antibacterial activity.[11] Good antimicrobial activity is also achieved by *in situ* synthesis of silver nanoparticles on PP material with glucose as a reducing agent.[12]

Modification of PP non-woven material is a big challenge for scientists because of chemical inertness and hydrophobicity of PP fibers. To overcome this problem, many authors proposed the deposition of active agents like copper oxide or silver onto PP surface using magnetron sputter coating systems.[9,11] Kumar and co-workers designed special microfluidic 3D spray device for depositing the nanocomposite layer onto a non-woven mask.[10] The deposition of quaternary ammonium salts by dissolving them in acetone and then exposing to 254 nm UV light to initiate benzophenone cross-linking is also proposed.[1] The activation of PP surface by corona discharge at atmospheric pressure before further processing is another efficient approach.[8] Namely, plasma oxidation

results in introduction of polar groups on the fiber surface improving the hydrophilicity and reactivity, and facilitating the further coating with biopolymer alginate and copper oxide nanoparticles.[8]

In the current study, corona discharge is applied for the activation of PP non-woven material prior to coating with biopolymer chitosan in the presence of crosslinker 1,2,3,4-butanetetracarboxylic acid. Chitosan, which is non-toxic, biocompatible, biodegradable, was selected due to its affinity to heavy metal ions, and thus to Ag-ions.[13] To keep in line with environmental friendless and follow the trends in the synthesis of metal-based nanoparticles (NPs), a waste pomegranate peel (*Punica granatum*) was used as a green agent for the synthesis of Ag-based NPs. Pomegranate peel is reach in various polyphenolic compounds, which act as stabilizing agent. The influence of the concentration of silver nitrate as a precursor salt on antimicrobial activity of textile nanocomposite against Gram-negative bacteria *E. coli*, Gram-positive bacteria *S. aureus* and yeast *C. albicans* was explored. To the best of our knowledge there are no literatures data dealing with biosynthesis of Ag-based NPs using pomegranate peels extract onto PP nonwoven material modified with cross-linked chitosan.

EXPERIMENTAL

Modification of PP non-woven material

PP non-woven material cleaned with ethanol (Zorka Pharma) was treated with corona discharge at atmospheric pressure using a commercial device Vetaphone CP-Lab MK II. The sample was placed on the electrode roll covered with silicon coating, rotating at the minimum speed of 4 m/min. The power was set to 700 W, the number of passages was 30 and the distance between the electrodes was 2.2 mm. This sample is denoted CPP.

CPP fabric was further treated with biopolymer chitosan (CH, ChitoClear®, source: *Pandalous borealis*, Primex, deacetylation degree of 90 % and viscosity of 847 mPa·s,) with or without 1,2,3,4-butanetetracarboxylic acid (BTCA, Acros Organics). A CH solution was prepared by dissolving 1.00 g of CH in 100 mL of 1 vol. % acetic acid (Zorka Pharma), which was stirred at room temperature for 24 h. In order to eliminate the gas bubbles formed during the agitation, the solution was left to settle for 30 min.

CPP sample of 0.50 g was immersed in 75 mL of freshly prepared CH solution and left for 1 h at the room temperature. After padding (1 kg cm^{-3}), the sample was dried at 80 ºC for 8 min, rinsed with distilled water and left to dry at room temperature. This sample is denoted CPP_CH.

The coating in the presence of BTCA was performed using the following procedure: 2 % of BTCA and 1.2 % of sodium hypophosphite (SHP, Acros Organics) as a catalyst were added to 75 mL of prepared CH solution. After being immersed in 75 mL of freshly prepared solution for 1 h, the sample was padded, dried at 80 °C for 5 min and cured at 120 °C for 3 min. Dry sample was then rinsed with distilled water and left to dry at room temperature. This sample is denoted CPP_CHB.

CPP sample (0.50 g) was also treated with 75 mL of 2 % BTCA solution in the presence of 1.2 % of SHP. This sample is denoted CPP_B.

Extraction of reducing agent and in situ *biosynthesis of Ag-based NPs*

Pomegranate peel was collected and further grinded in the Institute for Medical Plant Research "Dr Josif Pančić" (Serbia). 5 % water extract was prepared at 80 °C within 1 h. Extract was subsequently filtered and used for the synthesis of Ag nanoparticles.

CPP_B, CPP_CH and CPP_CHB (0.50 g) were immersed in 30 mL of 10 and 20 mM solution of $AgNO_3$ for 2 h and then rinsed with distilled water. The synthesis of Ag-based NPs was conducted in 30 mL of pomegranate peel extract at 60 °C for 1 h. The samples were thoroughly rinsed with distilled water and dried at room temperature. The samples obtained from 10 mM $AgNO_3$ solution are denoted CPP_B_Ag10, CPP_CH_Ag10 and CPP_CHB_Ag10. In the same manner the samples synthetized form 20 mM $AgNO_3$ solution are denoted CPP_B_Ag20, CPP_CH_Ag20 and CPP_CHB_Ag20. CPP_CHB sample treated only with pomegranate peel extract is denoted CPP_CHB_P. The whole procedure is illustrated in Fig. 1.

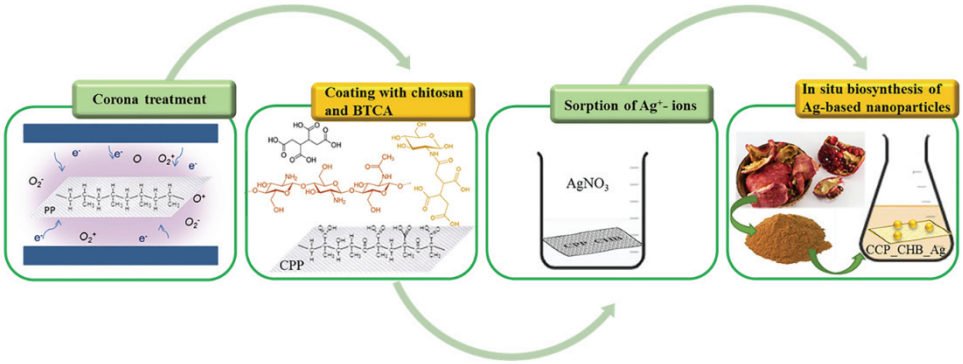

Fig. 1. Schematic illustration of proposed procedure.

Characterization of synthetized materials

The morphology of the samples along with the qualitative analysis of chemical composition and distribution of silver over the surface was investigated by field emission scanning electron microscopy equipped with an energy dispersive X-ray spectrometer (FESEM-EDS, FEI SCIOS 2 Dual Beam). The samples were recorded under high vacuum with an acceleration voltage of 7 keV, while the EDS mapping acquisition time was 30 min. The size and size distribution of NPs were analyzed using the open-access imaging software tool ImageJ.

The Ag^+ uptake on CPP_CHB_Ag10 and CPP_CHB_Ag20 from $AgNO_3$ solution was calculated on the basis of the concentration of residual Ag^+ in the solution which was measured using a Spectra AA 55 B (Varian) atomic absorption spectrometer (AAS). The Ag^+ uptake (q) was calculated as:

$$q = \frac{V(C_{Ag_0} - C_{Ag})}{m} \quad (1)$$

where C_{Ag0} is the initial concentration of Ag^+ in the solution (mol L^{-1}), C_{Ag} is the concentration of Ag^+ in the solution after 2 h long adsorption (mol L^{-1}), V is the volume of the $AgNO_3$ solution (L) and m is the weight of the fabric (g).

AAS was also applied for measuring the total Ag content in the materials after reduction. The samples were solved in 1:1 HNO_3 solution. The experiments were done in triplicate.

Color coordinates (CIE L^*, a^*, b^*) of the fabrics were determined by spectrophotometer (Datacolor SF300, USA) under illuminant D65 using the 10° standard observer. On the basis of measured CIE color coordinates, the color difference (ΔE^*) between the fabrics before and after the synthesis of Ag NPs was determined as:

$$\Delta E^* = \sqrt{\left(\Delta a^*\right)^2 + (\Delta b^*)^2 + (\Delta L^*)^2} \quad (2)$$

where: ΔL^* – the lightness difference; Δa^* – red/green difference; Δb^* – yellow/blue difference.

Fourier transform infrared (FTIR) spectra of control and synthetized samples were recorded in the ATR mode using a Nicolet iS5 FTIR spectrometer (Thermo Scientific) at 2 cm^{-1} resolution, in the wavenumber range 500–4000 cm^{-1}.

The wettability of the samples was studied using a thin-layer wicking test of wettability (TLW) which was carried out in the horizontal direction according to Chibowski and Gonzales-Caballero.[14] The samples were cut into strips (1 cm×10 cm) and dried for 30 min at 100 °C. Each dry sample was inserted between two glass plates with a ruler and carefully put into touch with deionized water in a Petri dish. Starting from the moment when the water began to penetrate into the fabric sample, the time at which the water penetrated a certain distance in the fabric was measured. For each fabric sample, at least 10 measurements were made, and the average value was presented as a result.

The antimicrobial activity of PP samples modified with Ag-based nanoparticles was tested against Gram-negative bacteria *E. coli* ATCC 25922, Gram-positive bacteria *S. aureus* ATCC 25923 and fungi *C. albicans* ATCC 24433, using a standard test method for determination of the antimicrobial activity of immobilized antimicrobial agents under dynamic contact conditions ASTM E 2149-01 (2001). Microorganisms were cultivated in 3 mL of tryptone soy broth (supplemented with 0.6 % of yeast extracts) at 37 °C in thermostat for 18 h (late exponential stage of growth). 50 mL of sterile physiological saline solution was subsequently inoculated with 0.5 mL of microbial inoculum. One gram of each sample, control and impregnated with particles, was sterilized in autoclave (30 min) and placed into a flask (with sterile physiological saline solution and inoculum) that was shaken at 37 °C for 2 h. 1 mL aliquots from the flask were taken for viable cell determination and put (1 mL) in a Petri dish on the tryptone soy agar (with 0.6 % yeast extracts). The Petri dishes were incubated at 37 °C for 24 h. After 24 h of incubation at 37 °C, zero-time (inoculum) and two-hour counts of viable microorganisms were made. The percentage of microbial reduction (R, %) was calculated in accordance with the following equation:

$$R = 100\frac{C_0 - C}{C_0} \quad (3)$$

where C_0 (CFU – colony forming units) is the number of microorganism colonies on the control fabric and C (CFU) is the number of microorganism colonies on the fabric impregnated with Ag particles. Number of microorganism's colonies was expressed as colony forming units in 0.1 mL aliquots. The experiments were done in triplicate.

In an attempt to evaluate the leaching of Ag^+ from the samples, impregnated fabrics were dipped into physiological saline solution (9 g L^{-1} NaCl) and left to rest at temperature of 37 °C for 1, 3, 6 and 24 h. The concentration of released Ag^+ was measured after 1, 3, 6 and 24 h by AAS. The experiments were done in triplicate.

RESULTS AND DISCUSSION

Taking into account that corona treatment leads to activation of PP fibers surface, *i.e.*, creation of polar groups in the polymer chain, the first step in the current study was to examine if newly formed polar groups only altered the fiber surface hydrophilicity or they could be potential sites for binding of Ag^+. The preliminary results confirmed that corona activation of PP non-woven material brought about significantly improved hydrophilicity. Biosynthesis of Ag-based NPs is commonly followed by color change (yellow shades) of textile substrates. The lack of color change of CPP samples after the synthesis of Ag-based NPs pointed out that the synthesis of NPs did not occur. In other words, corona activation did not provide adequate active groups for binding of Ag^+. The next step was to select an environmentally benign agent that can provide desirable active groups for the sorption of Ag^+. The ability of biopolymer chitosan to form the complexes with heavy metal ions was utilized for modification of CPP non-woven material. Amino groups of chitosan enhanced the binding of Ag^+ and consequently the substrates changed the color to yellow shades after the NPs synthesis step with bio-extract. A distinct color unevenness of obtained sample indicated insufficiently efficient coating of CPP sample with chitosan. In order to improve the coating of CPP samples, chitosan was eventually applied in the presence of BTCA as a crosslinking agent. Fig. 2a shows that such modification produces uniform color of the samples suggesting that BTCA enhances the binding of chitosan to fibers. Fig. 2a also illustrates three successive synthesis steps through the color change. Namely, after the adsorption of Ag^+, as expected, the samples retained white. After the synthesis step in the presence of pomegranate peel extract, the color was changed to ocher and finally, after drying the samples, became brownish. Evident color changes confirm the formation of Ag-based NPs.[15–17]

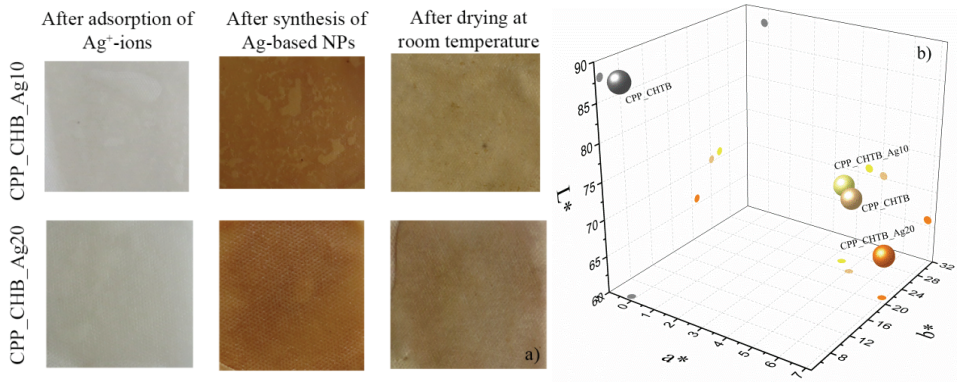

Fig. 2. Color change of the samples during the synthesis of nanoparticles: a) photographs of the samples after each step of *in situ* biosynthesis and b) CIE L^*, a^*, b^* coordinates.

The results of objective quantification of color change are presented in Fig. 2b and Table I. Compared to control sample, the samples impregnated with Ag--based NPs are significantly darker. This is particularly pronounced in the sample where 20 mM $AgNO_3$ solution was applied. A large color difference ($\Delta E^* = 7.46$) between CPP_SHB_Ag10 and CPP_CHB_Ag20 indicates that the concentration of precursor salt strongly affects the amount of synthesized Ag-based NPs and consequently, the color of the samples. Evident color changes are in line with AAS analysis (Table II), which shows that higher concentration of $AgNO_3$ solution causes larger Ag^+ uptake and higher total content of silver in the samples. The difference between the values of initial uptake and the total content of silver (Table II) is suggested to be due to the reduction processes ran at higher temperature. Such trend is already described in literature.[17]

TABLE I. CIE L^*, a^*, b^* differences between the samples

Control	Sample	ΔE^*	ΔL^*	Δa^*	Δb^*	Descriptions
CPP	CPP_CHB_P	26.6	–17.6	5.23	19.26	Darker, less green, yellow
	CPP_CHB_Ag10	27.4	–17.0	4.63	30.0	Darker, less green, yellow
	CPP_CHB_Ag20	28.3	–22.1	7.01	16.1	Darker, less green, yellow
CPP_CHB_Ag10	CPP_CHB_Ag20	7.46	–5.09	2.45	–4.87	Darker redder less yellow

TABLE II. Ag^+ uptake and total content of silver in the samples

Sample	Ag^+ uptake, μmol g^{-1}	Total content of silver after reduction, μmol g^{-1}
CPP_CHB_Ag10	10.44±0.84	4.10±0.10
CPP_CHB_Ag20	35.24±0.13	7.69±0.13

Chemical changes induced by corona and chitosan treatment are evaluated by FTIR spectroscopy. FTIR spectra of PP, CPP and CPP_CHB samples are shown in Fig. 3. The spectrum of PP non-woven fabric reveals all characteristic bands for PP: CH_3 and CH_2 asymmetric and symmetric stretching vibrations (2950–2830 cm^{-1}), CH_3 asymmetric deformation vibrations or CH_2 scissor vibrations and CH_3 symmetric deformation vibrations (1457–1356 cm^{-1}) and vibrations associated with C–C bonding (1200–800 cm^{-1}).[18,19] Corona treatment results in creation of two new bands at 1720 and 1636 cm^{-1}. The absorption band at 1720 cm^{-1} is ascribed to carbonyl groups in aldehydes and ketones, respectively. The band at 1636 cm^{-1} is likely due to COO^- asymmetric stretching vibrations.[18,19] Coating with chitosan led to decrease in intensity of the band at 1720 cm^{-1} along with significant decrease in the intensity of band at 1636 cm^{-1}. Additionally, a new band at 1555 cm^{-1} attributed to vibration in secondary amide appeared.[20,21] The appearance of this band implies that amide groups are formed between the amino groups of chitosan and carboxyl group of BTCA. A broad

band between 3225-3350 cm^{-1}, that is pronounced in CPP_CHB spectra, is ascribed to asymmetric stretching vibrations of $–NH_2$ or –OH groups.[21]

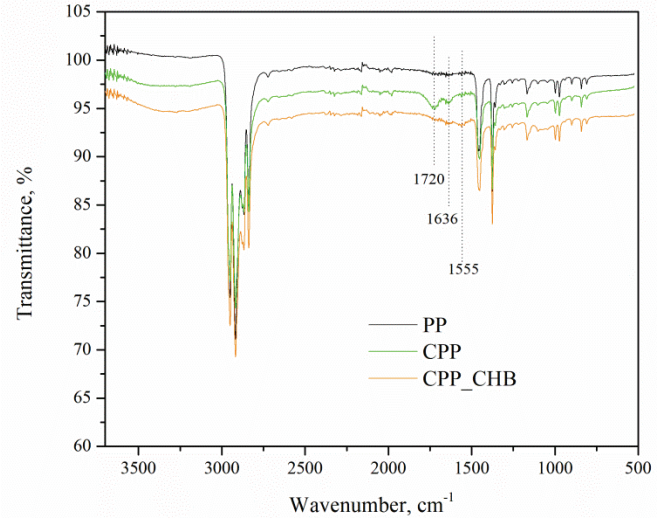

Fig. 3. FTIR spectra of the samples after modification with corona and chitosan.

In addition to chemical changes, corona treatment causes morphological changes on the PP fibers surface. FESEM micrograph shows that corona discharge creates the holes (Fig. 4b) on the flat surface of PP fibers (Fig. 4a). This is in line with our previous observation.[8] Fig. 4c reveals that spherical Ag-based NPs with an average size of 69±17 nm are synthetized on the surface of CPP_CHB_Ag20 sample pointing out that waste pomegranate peels could be successfully exploited for the synthesis of NPs. It is reported that pomegranate peel extract consists on punicalagin and punicalin components, that belong to the group of ellagatannins containing 16 and 10 phenolic hydroxyls per molecule, respectively.[16] Polyphenols can act as reducing and stabilizing agents to some metal ions.[22] XPS analysis revealed that use of pomegranate peels for *in situ* biosynthesis of Ag--based NPs results in the formation of AgCl NPs.[16] Other researchers also suggested that that AgCl is the most typical compound found in final product of plant-mediated synthesis of Ag NPs.[23,24] Fig. 4c shows EDX element distribution mapping of CPP_CHB_Ag20 surface. Different colors were used to visually distinguish the presence of carbon (red), nitrogen (green), oxygen (cyan), chlorine (violet) and silver (yellow). Besides carbon and oxygen, the obtained maps indicate that nitrogen along with chlorine and silver uniformly covered the fiber surface. The regions with a larger silver content were found to approximately coincide with those covered with chlorine indicating that NPs might be synthesized in the form of AgCl, which is in line with literature.[15,16,23,24] Namely,

AgCl is the most typical compound detected in the final product of plant-mediated synthesis of Ag NPs.[23,24] A size distribution of NPs (Fig. 4d) demonstrates that significant number of particles, synthetized on the CPP_CHB_Ag20 surface, are in the range between 30 and 90 nm.

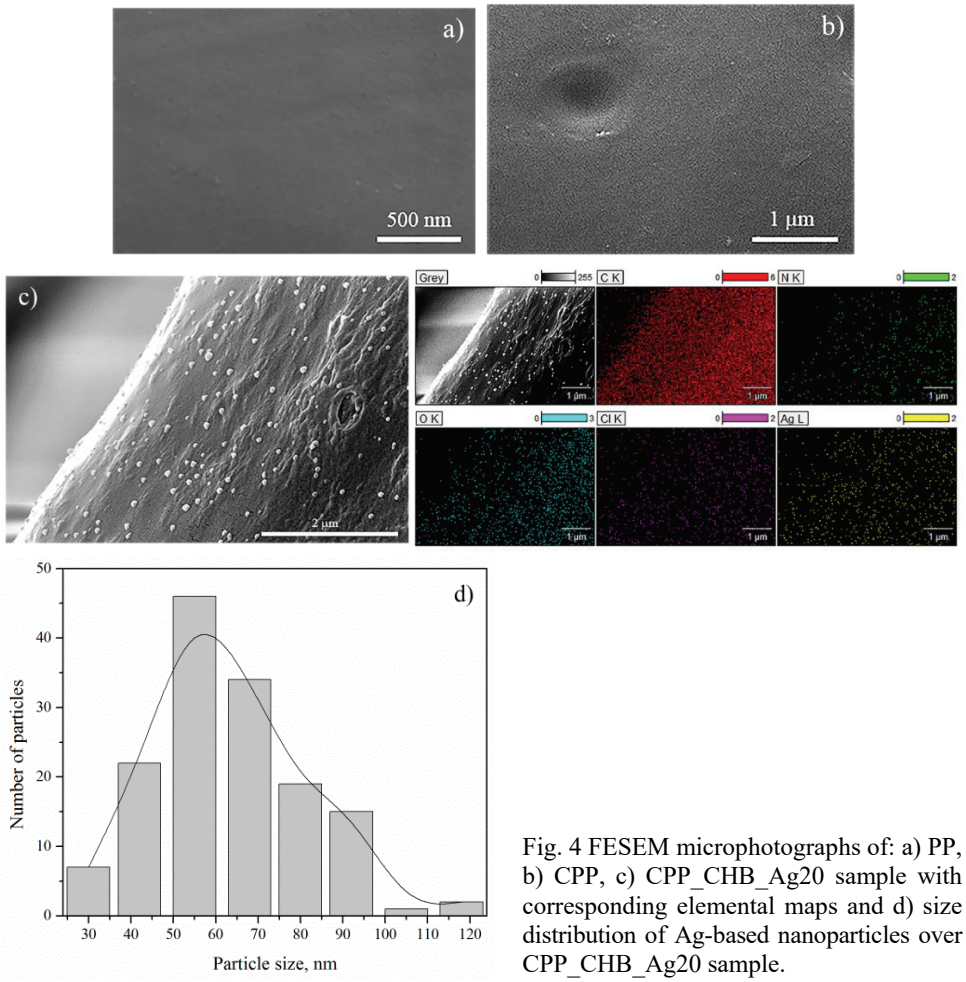

Fig. 4 FESEM microphotographs of: a) PP, b) CPP, c) CPP_CHB_Ag20 sample with corresponding elemental maps and d) size distribution of Ag-based nanoparticles over CPP_CHB_Ag20 sample.

As already mentioned, corona treatment was performed to improve the hydrophilicity of PP fibers. Thin-layer wicking test cannot be applied for evaluation of the control PP material as it is highly hydrophobic. Simple drop test showed that PP non-woven fabric became immediately wet after corona treatment. Coating with biopolymer chitosan diminished the effect obtained with corona (Fig. 5), but the material can be still considered as hydrophilic because the wetting time measured by drop test was less than 2 min. It is interesting to note that the coat-

ing of CPP fibers with biopolymer alginate also has a negative influence on the fiber surface hydrophilicity.[8] Synthesis of Ag-based NPs positively affected the material hydrophilicity compared to CPP_CHB sample. The difference between CPP_CHB_Ag10 and CPP_CHTB_Ag20 samples as a consequence of the total content of Ag was observed once again. CPP_CHB_Ag10 sample demonstrated better hydrophilicity than CPP_CHB_Ag20 sample.

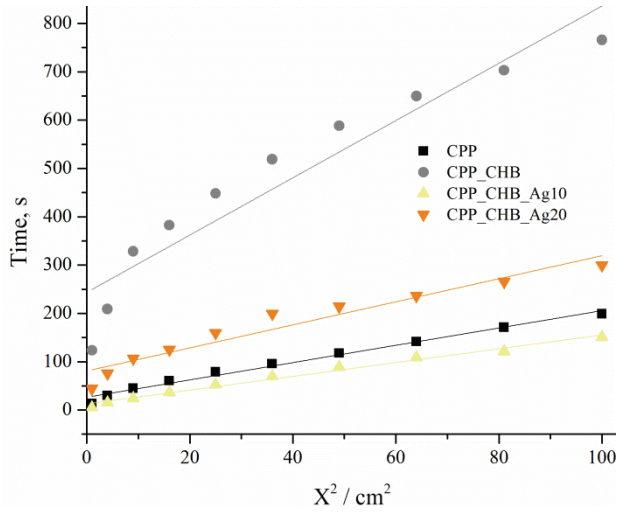

Fig. 5. Rate (X^2/time) of thin-layer wicking of water into investigated samples.

Finally, the main reason for the synthesis of Ag-based NPs was to impart antimicrobial activity to PP non-woven material. The three most frequently tested pathogens were selected for investigation of antimicrobial activity of synthesized samples. The results, summarized in Table III, reveal that both samples provided excellent antimicrobial activity against Gram-positive bacteria *S. aureus* and yeast *C. albicans*. In the case of Gram-negative bacteria *E. coli* moderate antibacterial activity was obtained. The larger the amount of silver in the samples, the better the antimicrobial activity. It should be emphasized that CPP, CPP_CHB and CPP_CHB_P samples did not provide any antimicrobial activity against tested strains. Although the antimicrobial action of Ag NPs has been widely investigated for a long-time, the exact mechanism of their antimicrobial action has not been completely resolved yet. It is supposed that the combination of various processes such as attack of cell membrane by Ag^+ released from Ag NPs, metal–microorganism contact, generation of ROS, *etc*., leads to cells death.[24,25]

The possible release of silver was assessed in the physiological saline solution. Physiological saline solution was selected to simulate the body fluids. Fig. 6 presents the dependence of released amount of Ag^+ on time. A similar amounts of Ag^+ were released from the sample independently of time. Again, the higher

the total silver content, the larger the amount of released Ag^+. Taking into account the results from Table II, it is clear that after the release study approximately 87 and 92 % of silver retained in the CPP_CHB_Ag10 and CPP_CHB_Ag20 samples, respectively. Since the released amount of Ag^+ did not change significantly over time, it could be assumed that stable nanocomposite was obtained.

TABLE III. Antimicrobial activity of samples with Ag-based NPs

Sample	Microorganism					
	E. coli		*S. aureus*		*C. albicans*	
	CFU	*R* / %	CFU	*R* / %	CFU	*R* / %
Inoculum	8.5×10^5	–	9.2×10^4	–	1.3×10^5	–
PP	6.6×10^5	–	4.0×10^4	–	8×10^4	–
CPP_CHB_Ag10	7.0×10^4	89.3	185	99.5	1.2×10^3	98.5
CPP_CHB_Ag20	2.8×10^4	95.8	20	99.9	800	99.0

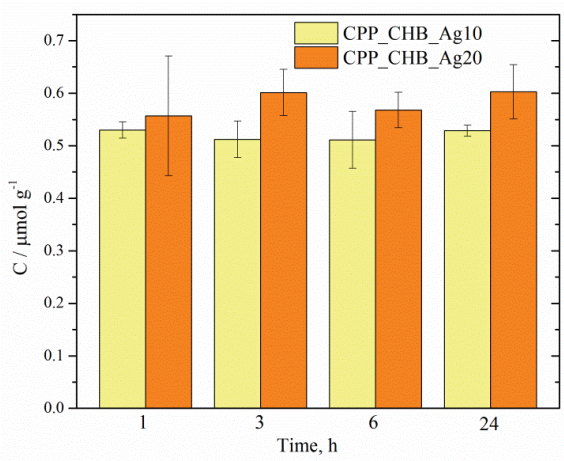

Fig. 6. Release study of Ag^+ from sample in physiological saline solution.

Moreover, the amount of released Ag^+ is very important from the cytotoxicity point of view since cytotoxicity of metal-based NPs have been thoroughly investigated over the last decade. Results from Fig. 6 implied that maximum amount of released Ag^+ was about 0.7 μmol g^{-1} within 24 h. According to our previous studies and literature data, detected amount of released Ag^+ could be considered as safe for human skin cells.[15,26,27]

CONCLUSION

Antimicrobial PP non-woven materials can be efficiently produced by proposed green synthesis procedure, which includes: *i*) activation of PP fibers by corona discharge at atmospheric pressure, *ii*) coating with biopolymer chitosan in the presence of BTCA and *iii*) *in situ* biosynthesis of Ag-based nanoparticles

using pomegranate peel extract as stabilizing agent. Each synthesis step induces change in color, hydrophilicity and surface chemistry of fibers. FESEM micrograph revealed that surface of PP fibers was covered with spherical nanoparticles implying that applied extract can be successfully used as a green agent for synthesis of Ag-based nanoparticles. Larger amounts of silver were synthesized with higher concentrations of precursor salt. Developed nanocomposite material provides a good antimicrobial protection against *S. aureus* and *C. albicans* with small quantity of released ions into physiological saline solution.

Acknowledgement. This work was financially supported by the Ministry of Science and Technological Development and Innovation of the Republic of Serbia (Contracts No. 451-03--47/2023-01/200135 and 451-03-47/2023-01/200287).

ИЗВОД

БИОСИНТЕЗА НАНОЧЕСТИЦА НА БАЗИ СРЕБРА НА НЕТКАНОМ ПОЛИПРОПИЛЕНСКОМ МАТЕРИЈАЛУ ЗА ЕФИКАСНУ АНТИМИКРОБНУ АКТИВНОСТ

АНА Г. КРКОБАБИЋ[1], ЈОВАНА Д. СТОЈИЧИЋ[1], МАЈА М. РАДЕТИЋ[1] и ДАРКА Д. МАРКОВИЋ[2]

[1]Универзитет у Београду, Технолошко–металуршки факултет, Карнегијева 4, 11120 Београд и [2]Универзитет у Београду, Иновациони центар Технолошко–металуршког факултета, Карнегијева 4, 11120 Београд

Појавом COVID 19 пандемије је потврђена важност употребе личне заштитне опреме као што су респираторне маске које пружају физичку заштиту од патогених сојева микроорганизама. Имајући у виду да се заштитне маске углавном производе од нетканог материјала од полипропиленских влакана, у овом раду је испитана могућност *in situ* биосинтезе наночестица на бази сребра као антимикробног средства на полипропиленском материјалу. Екстракт од коре нара је употребљен као „зелено“ средство за синтезу наночестица. Хидрофобност полипропиленских влакана је превазиђена њиховом модификацијом корона пражњењем на атмосферском притиску. У циљу побољшања везивања јона сребра, полипропиленски материјал модификован короном је импрегниран биополимером хитозаном у присуству умреживача 1,2,3,4-бутантетракарбоксилне киселине. ФЕСЕМ анализом је потврђено присуство сферних наночестица на површини влакана, просечних димензија око 69 nm. Већа концентрација раствора соли прекурсора доприноси већем садржају сребра након редукције. Веће количине честица на бази сребра обезбедиле су снажнију антимикробну активност према бактеријама *Escherichia coli* и *Staphylococcus aureus* и квасцу *Candida albicans*.

(Примљено 12. јануара, ревидирано 23. фебруара, прихваћено 9. априла 2023)

REFERENCES

1. M. Sorci, T. D. Fink, V. Sharma, S. Singh, R. Chen, B. L. Arduini, K. Dovidenko, C. L. Heldt, E. F. Palermo, R. H. Zha, *ACS Appl. Mater. Interfaces* **14** (2022) 25135 (https://doi.org/10.1021/acsami.2c04165)
2. D. Markovic, S. Milovanovic, M. Radetic, B. Jokic, I. Zizovic, *J. Supercrit. Fluids* **101** (2015) 215 (https://doi.org/10.1016/j.supflu.2015.03.022)
3. L. Liao, W. Xiao, M. Zhao, X. Yu, H. Wang, Q. Wang, S. Chu, Yi Cui, *ACS Nano* **14** (2020) 6348 (https://dx.doi.org/10.1021/acsnano.0c03597)

4. J. S. Smith, H. Hanseler, J. Welle, R. Rattray, M. Campbell, T. Brotherton, T. Moudgil, T. F. Pack, K. Wegmann, S. Jensen, J. Jin, C. B. Bifulco, S. A. Prahl, B. A. Fox, N. L. Stucky, *J. Clin. Translat. Sci.* **5** (2020) 1 (https://dx.doi.org/10.1017/cts.2020.494)
5. A. Kramer, I. Schwebke, G. Kampf, *BMC Infectious Diseases* **6** (2006) 130
6. Y. Gao, R. Cranston, *Text. Res. J.* **78** (2008) 60
7. G. Borkow, S. Zhou, T. Page, J. Gabbay, *PLoS One* **5** (2010) e11295 (https://doi.org/10.1371/journal.pone.0011295)
8. D. Marković, H. H. Tseng, T. Nunney, M. Radoičić, T. I. Tomic, M. Radetić, *Appl. Surf. Sci*. **527** (2020) 146829 (https://doi.org/10.1016/j.apsusc.2020.146829)
9. S. Jung, J. Y. Yang, E. Y. Byeon, D. G. Kim, D. G. Lee, S. Ryoo, S. Lee, C. W. Shin, H. W. Jang, H. J. Kim, S. Lee, *Polymer* **13** (2021) 1367 (https://doi.org/10.3390/polym13091367)
10. S. Kumar, M. Karmacharya, S. R. Joshi, O. Gulenko, J. Park, G. H. Kim, Y. K. Cho, *Nano Lett.* **21** (2021) 337 (https://doi.org/10.1021/acs.nanolett.0c03725)
11. H. Wang, J. Wang, J. Hong, Q. Wei, W. Gao, Z. Zhu, *J. Coat. Technol. Res.* **4** (2007) 101 (https://doi.org/10.1007/s11998-007-9001-8)
12. S. M. Gawish, S. Mosleh, *Fiber. Polym.* **21** (2020) 19 (https://dx.doi.org/10.1007/s12221-020-9519-2)
13. P. Wei, H. Lou, X. Xu, W. Xu, H. Yang, W. Zhang, Y. Zhang, *Appl. Surf. Sci*. **539** (2021) 148195 (https://doi.org/10.1016/j.apsusc.2020.148195)
14. E. Chibowski, F. Gonzales-Caballero, *Langmuir* **9** (1993) 330 (https://doi.org/10.1021/la00025a062)
15. N. Shreyash, S. Bajpai, M. A. Khan, Y. Vijay, S. K. Tiwary, M. Sonker, *ACS Appl. Nano Mater.* **4** (2021) 11428 (https://doi.org/10.1021/acsanm.1c02946)
16. A. Krkobabić, M. Radetić, H.H. Tseng, T. S. Nunney, V. Tadić, T. Ilic-Tomic, D. Marković, *Appl. Surf. Sci*. **611** (2023) 155612 (https://doi.org/10.1016/j.apsusc.2022.155612)
17. A. Krkobabić, D. Marković, A. Kovačević, V. Tadić, M. Radoičić, T. Barudžija, T. Ilic-Tomic, M. Radetić, *Fiber. Polym.* **22** (2022) 954 (https://doi.org/10.1007/s12221-022-4639-5)
18. R. Morent, N. de Geyter, C. Leys, L. Gengembre, E. Payen, *Text. Res. J.* **77** (2007) 471 (https://doi.org/10.1177/0040517507080616)
19. K.G. Kostov, T.M.C. Nishime, L.R.O. Hein, A. Toth, *Surf. Coat. Technol*. **234** (2013) 60 (https://doi.org/10.1016/j.surfcoat.2012.09.041)
20. R. Molina, P. Jovancic, S. Vilchez, T. Tzanov, C. Solans, *Carbohydr. Polym.* **103** (2014) 472 (https://doi.org/10.1016/j.carbpol.2013.12.084)
21. S. Rashid, C. Shen, X. Chen, S. Li, Y. Chen,Y. Wen, J. Liu, *RSC Adv.* **5 (**2015) 90731(https://doi.org/10.1039/c5ra14711e)
22. S. Eslami, M. A. Ebrahimzadeh, P. Biparva, *RSC Adv*. **8** (2018) 26144 (https://doi.org/10.1039/c8ra04451a)
23. N. Durán, G. Nakazato, A.B. Seabra, *Appl. Microbiol. Biotechnol*. **100** (2016) 6555 (https://doi.org/10.1007/s00253-016-7657-7)
24. V.Ravichandran, S.Vasanthi, S.Shalini, S.A.A. Shah, M.Tripathy, N. Paliwal, *Results Phys*. **15** (2019) 102565 (https://doi.org/10.1016/j.rinp.2019.102565)
25. J.P Ruparelia, A.K. Chatterjee, S.P. Duttagupta, S. Mukherji, *Acta Biomater*. **4** (2008) 707 (https://doi:10.1016/j.actbio.2007.11.006)

26. Q. Xu, R. Li, L. Shen, W. Xu, J. Wang, Q. Jiang, L. Zhang, F. Fu, Y. Fu, X. Liu, *App. Surf. Sci*. **497** (2019) 143673 (https://doi.org/10.1016/j.apsusc.2019.143673)
27. A. I. Ribeiro, V. Shvalya, U. Cvelbar, R. Silva, R. M. Oliveira, F. Remião, H.P. Felgueiras, J. Padrão, A. Zille, *Polymers* **14** (2022) 1138 (https://doi.org/10.3390/polym14061138).

Journal of the Serbian Chemical Society
JSCS@tmf.bg.ac.rs • www.shd.org.rs/JSCS
J. Serb. Chem. Soc. *88* (5) 551–562 (2023)
JSCS–5645
Original scientific paper
Published 14 April 2023

The influence of geological setting and land use on the physical and chemical properties of the soil at the Fruška Gora Mountain

MILICA KAŠANIN-GRUBIN, GORICA VESELINOVIĆ, NEVENA ANTIĆ*, GORDANA GAJICA, SANJA STOJADINOVIĆ, ALEKSANDRA ŠAJNOVIĆ and SNEŽANA ŠTRBAC

Institute of Chemistry, Technology and Metallurgy, University of Belgrade, Njegoševa 12, 11000 Belgrade, Serbia

(Received 21 December 2022, revised 1 March, accepted 3 March 2023)

Abstract: Soil erosion is a problem that affects the landscape at different scales and represents a serious challenge for land management and soil conservation in both natural forests and meadows. The aim of this study was to determine how the parent material and land use affect the physical and chemical properties of the soil in the area of the Fruška Gora Mountain. The soils were separated into five bedrock types: serpentinite, marl, trachyte, shale, loess and two land use types: forest and meadow. Twenty-three forest soil and 24 meadow soil from a depth of 0–20 cm were sampled from the Fruška Gora Mt. The following properties were determined: pH, electrical conductivity, oxidation-reduction potential, content of organic carbon, sodium adsorption ratio, aggregate size and stability. There is no statistically significant difference in pH values, redox potential (*Eh*), electrical conductivity (*EC*) and sodium adsorption ratio (*SAR*) values between the analysed forest and meadow soils, but there is a statistically significant difference in the content of organic carbon (C_{org}). It can be concluded that both the parent material, and to a slightly less extent, land use have a great influence on physico-chemical properties of the soil.

Keywords: soil characteristics; bedrock; forest; meadow; environmental change.

INTRODUCTION

Physical and chemical properties of soils are important for those in charge to choose the best land use practise on the local level.[1] This is especially important when soil protection is in question. Applying forest management strategies that maintain forests with a closed canopy can help prevent soils erosion processes. However, the resistance to erosion of forest soils can dramatically change in the conditions of climate changes, with increasing occurrences of outbreaks of pests and pathogens, forestfires, *etc*.[2]

* Corresponding author. E-mail: nevena.antic@ihtm.bg.ac.rs
https://doi.org/10.2298/JSC221221012G

Similar to forests, meadow soils are also subjected to climate change impacts, such as increased temperatures and changing precipitation patterns. Dryer and hotter conditions may result in loss of valuable habitat, but also in the encroachment of new species, and a greater risk of wildfire. Increased drought frequency could also cause major changes in vegetation cover. Vegetation shifts can impact ecosystems and species, and changes in species composition and plant productivity may also impact the human communities that rely on agricultural production in these regions. Losses of vegetative cover coupled with increases in precipitation intensity and climate-induced reductions in soil aggregate stability will dramatically increase potential erosion rates.[3]

Forest soils, especially those under native forests, differ from soils of other land use systems in terms of their infrequent (but sometimes major) disturbance, and high organic matter content which may increase the capacity to buffer the effects of climate change. Some of the effect of climate change on soils in such forests may be slow but cumulative, and would require special and sensitive parameters to detect any change in terms of soil health. Any alteration to either the quantity or the quality of soil organic matter under climate change is probably the most important factor affecting soil health under forests. This is because organic matter exerts strong controls on the physical,chemical and biological properties affecting soil "fertility".[3] Mountain soils are generally shallow and their fertility is often concentrated in the uppermost layers. Therefore, soil erosion is a key problem that affects the landscape at different scales and represents a serious challenge for land management and soil conservation.[4]

Soil structure is important for soil stability and land degradation and depends on geological settings and land use practices. Physical and chemical features determine soil erodibility, but less is known how their interactions alter erodibility.[5] Soil texture, the content of organic carbon, pH value, electrical conductivity, and total water-soluble cations clearly differentiate forest soils by the type of bedrock and were proven to be explanatory variables.[6]

Physicochemical characteristics can be directly or indirectly influenced by the soil aggregate stability which can be used as a soil degradation indicator.[7] Aggregate stability is the ability of aggregates to resist stresses causing their disintegration such as tillage, swelling and shrinking of clay minerals, raindrop impact, *etc*. Land use has a significant impact on aggregate stability, and forest soils generally have better structure than meadow soils.[8]

Forest soils contain more carbon per unit area than meadow or arable land.[9] The increased organic carbon content in forest soils is associated with the type of vegetation.

Besides land use, bedrock is essential for soil quality; however, its impact on soil degradation is not sufficiently understood. Soil degradation in changed environmental conditions depends largely on the bedrock, which was until rec-

ently considered of subordinate significance compared to climate and pedological characteristics. Bedrock has a significant role in vegetation growth through the regulation of soil physico-chemical properties, and it can alter the response of vegetation to climate properties.[11]

Considering the heterogeneous nature of soils, more information is needed for a better understanding of the effect of both land use and geological settings. The aim of this study is to determine how the parent material and land use affect the physical and chemical properties of the soil in the area of the Fruška Gora Mt.

EXPERIMENTAL

Details related to sampling sites and procedure are given in the Supplementary material to this paper.

Determination of soil aggregate size and aggregate stability, content of organic carbon (C_{org}), pH value, redox potential (*Eh*), determination of electrical conductivity (*EC*) and available ions concentration (Na^+, K^+, Ca^{2+}, Mg^{2+}) were conducted. Sodium adsorption ratio (*SAR*), as an index of soil disperisvity, was calculated from the concentration of available ions.

Aggregate size analysis was done according to a standard sieving procedure using a set of sieve sizes ranging from 16 to 1 mm (16, 8, 4, 2 and 1 mm).

Stability of soil agregates was determined by sieving previously air-dried soil through a sieve of 4 and 2 mm pore size to obtain fraction of 2–4 mm size aggregates. 5 g of these agregates were weighed and gently placed into a 250 cm^3 beaker containing 50 cm^3 of distilled water. At the moment of descent, the stopwatch was turned on. After 10 min, the water was sucked out with a pipette, and the soil was dried. The dried soil was sieved on a 2 mm sieve. The content of stable aggregates was obtained from the differences between the initial weight of the soil aggrregates and the portion that remained on the sieve.

Elemental analysis was performed in order to determine the content of organic carbon (C_{org}) in the tested samples. Measurements were performed on a Vario EL III instrument, CHNOS elemental analyzer, Elementar Analysen Systeme GmbH.

Determination of the pH value of the soil was obtained using a pH meter AD 1000 pH / mV & temperature meter (Adwa), which was previously calibrated with buffer solutions from the set of instruments, pH values 4, 7, 9. The redox potential was determined potentiometrically, using a Pt electrode, and a calomel electrode as a reference, on the HI 9321 Microprocessor pH meter (Hanna Instruments) and soil electrical conductivity was determined using a Cond-330i conductivity meter (WTW). For all three measurments the soil was prepared in the same way. 5 g of representative sample was added to 25 cm^3 of distilled water, and the suspension was placed on a shaker for 30 min, after which the sample was centrifuged.

Determination of available Na^+, K^+, Ca^{2+} and Mg^{2+} in soil was done by inductively coupled plasma optical emission spectrometry (ICP-OES) method, analytical method used for the qualitative and quantitative determination of elements. The ICP-OES instrument used for this analysis was the Thermo Scientific iCAP 6500 Duo ICP (Thermo Fisher Scientific, Cambridge, UK). The parameters of the source at which the measurements were performed were: RF generator power: 1150 W, axial gas flow rate: 0.5 L/min, nebulizer gas flow rate: 0.5 L/min, cooling gas flow rate: 12 L/min.

The dispersivity index/sodium adsorption ratio (*SAR*), where all concentrations are in milliequivalents per L, was calculated using the equation:[12]

$$SAR = \frac{\sqrt{2}\left[\mathrm{Na}^{+}\right]}{\sqrt{\left[\mathrm{Ca}^{2+}\right]+\left[\mathrm{Mg}^{2+}\right]}} \quad (1)$$

Statistical *t*-test was used to analyze the existence of possible differences in soil properties according to the land use. The least significant difference (*LSD*) one-way analysis of variance (ANOVA) test was used in the context of the analysis of variance between bedrock types with the *F*-ratio suggesting rejection of the null hypothesis, when the difference between the population means is significant. For interpretation of parameter results, the principal component analysis (PCA) and correlation coefficients were calculated using the SPSS Statistics 20 package.

RESULTS AND DISCUSSION

Soil samples of five types of bedrock and two types of land use from the Fruška Gora Mt. were analyzed with the aim to determine the possible differences in their physicochemical properties.

The soil aggregate size analysis was conducted with the purpose of determining the most represented aggregate size class. On average, meadow soils have a larger portion of soil aggregates in the class < 2 mm, with a total of 38.77 % compared to 23.87 % of forest soils, and vice versa, the content of 16–8 mm and 8–4 mm aggregates are higher in the forest soils. The dominant aggregate size for most soils is 8–4 mm, except for loess meadow and trachyte forest with the 4–2 mm aggregate size being dominant (Table I). The highest content of 16–8 mm and 8–4 mm aggregates is found in marl forest soils, followed by the shale forest. Highest portion of smallest aggregates have loess meadow and serpentinite meadow soils.

TABLE I. Distribution of soil aggregate size, %; LM – loess meadow; SeM – serpentinite meadow; MM – marl meadow; SeF – serpentinite forest; MF – marl forest; TF – trachyte forest; ShF – shale forest; *AVG* – average value; *SD* – standard deviation

Bedrock and land use type		Aggregate size, mm					
		> 16	16–8	8–4	4–2	2–1	< 1
LM	*AVG*	0.00	8.9	20.59	27.03	19.5	23.98
	SD	0.00	11.32	9.67	3.82	6.27	11.36
SeM	*AVG*	0.00	6.51	28.58	25.57	21.9	17.44
	SD	0.00	4.92	6.37	3.77	3.5	5.57
MM	*AVG*	0.00	5.27	35.13	24.54	18.7	16.36
	SD	0.00	6.34	7.53	2.11	4.11	6.51
SeF	*AVG*	2.58	9.14	33.45	24.21	19.09	14.11
	SD	6.31	7.57	5.76	4.9	5.33	5.04
MF	*AVG*	0.41	36.92	43.95	12.31	4.73	1.68
	SD	1.01	18.65	13.4	6.89	3.96	1.23
TF	*AVG*	0.00	2.56	23.67	30.84	28.52	14.42
	SD	0.00	3.63	2.41	2.92	6.3	2.65
ShF	*AVG*	0.50	16.01	38.55	23.05	12.03	9.86
	SD	1.22	8.11	7.05	4.17	3.64	3.82

Stability of soil aggregates was investigated for all forest and meadow soil samples.

On average, it was found that forest soils have lower average aggregate stability (51.04 %) than meadow soil (60.05 %), Fig. 1. However, meadow soils have a smaller range of stable aggregates than the forest soils. The content of stable aggregates, regarding geological settings and the land use type is decreasing in the following order: LM > TF > MF > ShF > SeM > SeF (Fig. 1). The ratio of stable/unstable aggregate is lowest for SeF soils (0.24) and highest for LM (2.30).

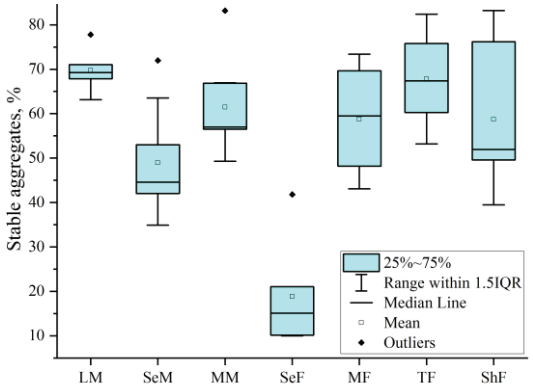

Fig. 1. Content of soil stable aggregates. LM – loess meadow; SeM – serpentinite meadow; MM – marl meadow; SeF – serpentinite forest; MF – marl forest; TF – trachyte forest; ShF – shale forest.

Since the stability of soil aggregates was tested on 4–2 mm size, the analysis of variance (ANOVA) was performed to determine the possible existence of differences between this soil aggregates size depending on: the bedrock type, land use type, and depending on both of these factors simultaneously.

Statistically significant difference ($p < 0.05$) among bedrock type was found between aggregate size of 4–2 mm sampled over shale and trachytes, loess and marls, serpentinites and marls, serpentinites and trachytes, as well as among aggregates of marls and trachytes soils. No significant difference ($p > 0.05$) was found between aggregates size of 4–2 mm among solely meadow soils, while, on the contrary, a significant difference ($p < 0.05$) was found between forest soils on serpentinites and marls, serpentinites and trachytes, as well as among marls and trachytes. ANOVA performed for both of these factors for all soil samples showed that significant difference ($p < 0.05$) exists between aggregates size of 4–2 mm of ShF and MF, ShF and TF, LM and SeF, LM and MF, SeM and MF, SeM and TF, MM and MF, MM and TF, SeF and MF, SeF and TF, MF and TF.

C_{org} was measured in all soil samples, indicating that forest soil covers the range of 1.75–6.08 %, while in meadow soil is in the range of 1.06–1.98 % (Fig. 2). The average value of C_{org} is statistically different ($p < 0.05$) between the given two types of soil, being 2.97 % for forest soils and 1.48 % for meadow

soils. The obtained results show that C_{org} depends on the land use. According to the ANOVA there is a statistically significant difference ($p < 0.05$) in C_{org} in soils on different bedrock types. The organic carbon content decreases in the following order: TF > MF > ShF > SeF > LM > SeM > MF. In comparison with the land use, a smaller impact was established. Thus MF and MM soils have a statistically significant difference ($p < 0.05$) in C_{org}, which can be related to the influence of land use.

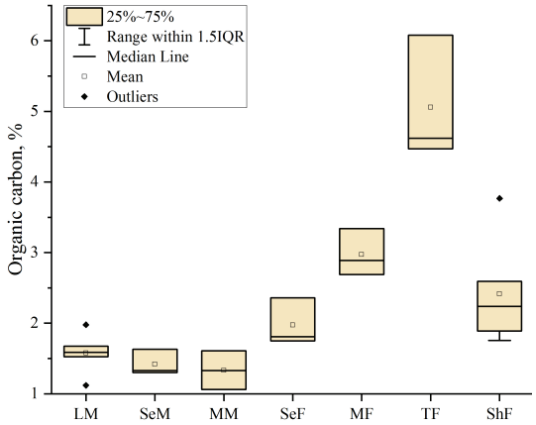

Fig. 2. Organic carbon content in Fruška Gora soils. LM – loess meadow; SeM – serpentinite meadow; MM – marl meadow; SeF – serpentinite forest; MF – marl forest; TF trachyte forest; ShF – shale forest.

EC, *Eh* and pH of all soil samples were measured with the aim to determine the physicochemical properties of soils of different bedrock and land use type.

The pH value of forest soils varies in the range of 6.0–7.13 classifying them as weakly acidic to neutral soils, while the pH of meadow soil varies in the range of 5.77–7.29 classifying them moderately acidic to neutral soil. Mean values and standard deviations of the analysed parameters are presented in Table II. *EC* measured in forest soils vary in the range from 76.8 to 333 μS cm^{-3}, and in meadow soil from 61.2 to 294 μS cm^{-3}, while *Eh* of forest soils varies in the range from 444.4 to 575.8 mV, and meadow soil similarly from 452.8 to 559.7 mV.

TABLE II. Physicochemical properties of soils; *SD* – standard deviation; ShF – shale forest; SeF – serpentinite forest; MF – marl forest; TF – trachyte forest; LM – loess meadow; SeM – serpentinite meadow; MM – marl meadow

Parameter		ShF	SeF	MF	TF	LM	SeM	MM
pH	Mean	6.77	6.79	6.85	6.7	6.9	6.27	6.82
	SD	0.21	0.38	0.22	0.28	0.28	0.37	0.34
Eh	Mean	527.38	517.42	508.65	496.32	498.55	544.09	504.72
mV	*SD*	23.6	39.59	10.91	27.48	5.6	10.41	23.42
EC	Mean	191.53	130.58	197.85	282.4	259.83	89.97	233.39
μS cm^{-3}	*SD*	80.68	42.23	58.58	36.41	21.04	14	37.91
SAR	Mean	0.04	0.12	0.08	0.08	0.02	0.21	0.07
	S*D*	0.01	0.06	0.03	0.00	0.01	0.02	0.04

The difference in soil pH on different bedrock type was tested by one-factor analysis of variance, and it was found that there is a statistically significant difference ($p < 0.05$) between individual soil groups (Table III). Post hoc Fisher's test of the least significant difference (*LSD*) showed that the statistically significant deviations in pH values exist in the following soil pairs: serpentinites – marl and serpentinites – loess ($\Delta = 0.42 > LSD = 0.33$). ANOVA conducted on analysed parameters showed there is no statistically significant difference ($p > 0.05$) between pH in forest and meadow soils which can imply that the land use does not significantly affect the soil pH value. Furthermore, Fisher's *LSD* test proved that the statistically significant differences ($p < 0.05$) exist in the following soil pairs: SeF–SeM; SeM–MF; SeM–MM; SeM–TF; SeM–SeM; SeM–ShF (Δ 0.63––0. 43> *LSD* 0.35–0.30).

TABLE III. One-factor analysis of variance of physicochemical properties of soils

Parameter	*F* factor	Significance
pH	2.71	0.04
Eh / mV	4.95	0.00
EC / μS cm^{-3}	22.23	0.00
SAR	0.51	0.73

ANOVA analysis showed that there is a statistically significant difference ($p < 0.05$) in the values of oxidation-reduction potential between the soils of different bedrock. Fisher's post hoc *LSD* test determined the existence of a statistically significant difference ($p < 0.05$) in *Eh* values in the following soil pairs: serpentinites–marl; serpentinite–trachyte; serpentinites–trachyte; trachyte–shale; trachyte–shale (Δ 37.1–27.12 > *LSD* 28.16–16.98). The result of the *t*-test shows that there is no statistically significant difference ($p > 0.05$) in the values of oxidation–reduction potential between forest and meadow land.

The ANOVA method was used to examine the differences in the *Eh* values of the soil, taking into account the land use and the bedrock. The Fisher's *LSD* test determined the existence of a statistically significant difference ($p < 0.05$) in the following soil pairs: SeF–SeM; SeM–MF; SeM–MM; SeM–TF; SeM–SeM; TF–ShF; MF–ShF (Δ 26.67–47.77 > *LSD* 21.10–27.11).

The result of the *t*-test shows that there is no statistically significant difference ($p > 0.05$) in the values of *EC* between forest and meadow soil. The *LSD* test determined the existence of statistically significant differences ($p < 0.05$) between the following soil pairs: serpentinites–marl; serpentinites–trachytes; serpentinites–loess; serpentinites–shale; marl–trachytes; trachytes–shale; loess––shale (Δ 176.19–63.22 > *LSD* 56.52–34.08). The ANOVA was conducted to examine the *EC* values of the soil. Taking into account the land use and the bedrock type there was a statistically significant difference ($p < 0.05$) between the tested samples. Fisher's *LSD* test the existence of a statistically significant differ-

ence ($p < 0.05$) in the following soil pairs was determined: SeF–MF; SeF–MM; SeF–TF; SeF–LM; SeF–ShF; SeM -MF; SeM–MM; SeM–TF; SeM–LM; SeM––ShF; MF–TF; MF–LM; TF–ShF; LM–ShF (Δ 192.43–60.95 > *LSD* 51.89––47.37). The obtained results show that there are large deviations depending on the parent matrial. The biggest difference comes from serpentinite, both forest and meadow, and this shows a strong influence of the geological substratum on the examined parameter.

In results obtained depending on the bedrock statistically significant difference ($p < 0.05$) was found between the pH value of soil sampled over loess and serpentinites, and serpentinites and marls. Significant differences ($p < 0.05$) in the *Eh* values exist between the soil sampled over shale and loess, shale and trachyte, loess and serpentinite, serpentinite and marl and serpentinites and trachytes. In the *EC* values significant differences ($p < 0.05$) exist between the soils sampled over shale and loess, shale and serpentinites, shale and trachytes, loess and serpentinites, serpentinites and marls, serpentinites and trachytes and marls and trachytes.

ANOVA performed to determine the possible existence of differences between pH, *Eh* and *EC* within the same land use (meadows or forests) over different geological substrates showed certain differences. For meadow soil samples, differences were found in the case of pH values of soil sampled over shale and serpentinites, loess and serpentinites, and marls and serpentinites. In the case of *Eh* values of soil sampled, differences over shale and loess, shale and marl, loess and serpentinites, and serpentinites and marls were found, while analysing the *EC* values, the differences were observed between shale and loess, shale and serpentinites, loess and serpentinite and serpentinites and marls. For the forest soil samples, differences were found for the *EC* values of soil sampled over serpentinites and marls, serpentinites and trachytes and marls and trachytes. At the pH and *Eh* values of forest soil samples there are no significant differences in the 95 % confidence interval.

The average values of *SAR* of forest and meadow soil are presented in Table II. The high concentration of sodium ions in the soil causes the replacement of calcium and magnesium ions, which leads to the dispersion of soil particles and the adhesion of particle aggregates. This process is unfavourable for the soil, because hard soils, which are very poorly permeable to water, are formed and thus become unfavourable for the growth and development of plants. The results show that the *SAR* values of the forest soil vary in the range from 0.03 to 0.19 mmol/L, while in the meadow soil they are in the range from 0.02 to 0.64 mmol/L. The mean *SAR* value is 0.08 mmol/L for the forest soils and 0.11 mmol/L for the meadow soils. The result of the *t*-test showed that there was no statistically significant difference ($p > 0.05$) in *SAR* values between the forest and the meadow soil. ANOVA showed that there is a statistically significant differ-

ence ($p < 0.05$) in *SAR* values between the soils of different bedrock in the following soil pairs: serpentinites–marl; serpentinites–loess; serpentinites–shales (Δ 0.147–0.098 > *LSD* 0.091–0.069).

The ANOVA was also used to examine the *SAR* values of the soil, taking into account both the land and the bedrock. Results showed that there is a statistically significant difference ($p < 0.05$) between the examined samples. *LSD* test determined the existence of a statistically significant difference in the following soil pairs: SeM–MF; SeM–MM; SeM–TF; SeM–ShF (Δ 0.184–0.125 > *LSD* 0.103–0.087). The greatest differences come from serpentinite, namely from the SeM that has the highest *SAR* value. In general, in all tested soil samples, the SAR value is not high, which implies that these soils do not have a high tendency towards dispersion.

The above results show that the characteristics of the soil in the examined area of the Fruška Gora Mt. largely depend on the geological settings, except in the case of organic carbon content, where the greatest impact is the land use. pH has statistically significant positive correlation with *Eh*, *EC* and *SAR*, and *Eh* with *EC* (Table IV). C_{org} is not in correlation with any of the tested parameters, while content of stable aggregates is correlated with *EC* (Table IV).

TABLE IV. Correlations between physicochemical properties of soils; PC – Pearson correlation, Sig. – significance

Parameter	Correlation	pH	*Eh* mV	*EC* μS cm^{-3}	*SAR*	C_{org}	Stable aggregates %
pH	PC	1	–0.47	0.49	–0.38	–0.08	0.16
	Sig.		0.00	0.00	0.01	0.70	0.28
Eh / mV	PC		1	–0.57	0.20	–0.15	–0.09
	Sig.			0.00	0.17	0.46	0.56
EC / μS cm^{-3}	PC			1	–0.21	0.31	0.62
	Sig.				0.16	0.12	0.00
SAR	PC				1	–0.05	0.07
	Sig.					0.80	0.62
C_{org}	PC					1	0.24
	Sig.						0.22
Stable aggregates, %	PC						1
	Sig.						0.00

The relationship between *EC* and *SAR* following the Rengasamy *et al.* (1984)[12] domains indicate that the soil samples are potentially dispersive. This means that in the case of land use change, including the deforestation of tillage, the erosion processes could be expected.

The percentage of variance for the first component is 30.7 % which had large positive eigenvalues for pH, *EC* and stable aggregates, %, but negative for *SAR*, Na^+ and *Eh*. The percentage of variance of the second component explained

24.5 % of variance and it had large positive eigenvector for Ca^{2+}, Mg^{2+} and K^{+} (Fig. 3). The ShF and TF soils are grouped as soils with the most stable aggregates, and serpentinite soils, both with meadow and forest land use, are the most dispersive, grouped around *SAR*.

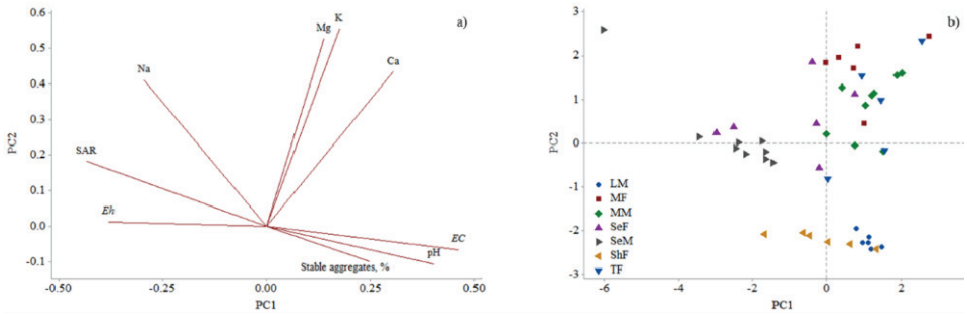

Fig. 3. Principal component analysis of Fruška Gora soils: a) loading plot; b) score plot.

The physical and chemical properties of the soil in the examined area of Fruška Gora Mt. depend on the bedrock type and land use. Statistical analyses have shown that the bedrock has a strong influence on a larger number of analysed soil parameters. Evidence of this are the differences in pH and *Eh* values for meadow and forest serpentinite soils. However, at the same time, no statistically significant difference was found in these parameters between meadow and forest soil on marl.

CONCLUSION

For the purposes of this paper, 47 soil samples (23 forest and 24 meadow samples) were analysed with the aim to determine the impact of land use and geological background on the physical and chemical properties of the soil in the areas of Fruška Gora Mountain.

Based on the obtained results it can be seen that both the examined forest and medow soils belong to the range of slightly acidic to neutral soils. This data, together with values of *Eh*, *EC*, *SAR* and C_{org}, confirms the good soil quality in the study area.

No statistically significant difference in pH, *Eh*, *EC* and *SAR* values exists between the analysed forest and meadow soils, except for the content of C_{org}, implying that the land use does not have a great influence on pH, *Eh*, *EC* and *SAR* values, but that the content of C_{org} largely depends on soil vegetation.

Various parent material affects the measured parameters in different ways. Results indicate that the serpentinite soil differ from the other bedrock type soils. Statistical tests which took into account the bedrock and land use, showed that for all parameters, except for C_{org}, the serpentinite soils, particularly the meadow serpentinite soils, are most vulnerable to land use and possible climate changes.

It can be concluded that both parent matrial, and to a slightly less extent, land use have a great influence on physicochemical properties of the soil.

Of all parent material types, serpentine soils proved to be most sensitive to dispersion and possible soil erosion processes due to land use change. Also, the differences in soil properties between land use types are most prominent for serpentinite soils, while at the same time, the parameters do not show statistically significant differences between meadow and forest soil on marl. This finding should be taken into account in forest management practices, especially in the predicted climate change conditions.

SUPPLEMENTARY MATERIAL

Additional data and information are available electronically at the pages of journal website: https://www.shd-pub.org.rs/index.php/JSCS/article/view/12185, or from the corresponding author on request.

Acknowledgement. This research has been financially supported by the Ministry of Science, Technological Development and Innovation of Republic of Serbia (Contract No: 451--03-47/2023-01/200026).

ИЗВОД

УТИЦАЈ ГЕОЛОШКЕ ПОДЛОГЕ И НАЧИНА КОРИШЋЕЊА ТЕРЕНА НА ФИЗИЧКО–ХЕМИЈСКА СВОЈСТВА ЗЕМЉИШТА ФРУШКЕ ГОРЕ

МИЛИЦА КАШАНИН-ГРУБИН, ГОРИЦА ВЕСЕЛИНОВИЋ, НЕВЕНА АНТИЋ, ГОРДАНА ГАЈИЦА, САЊА СТОЈАДИНОВИЋ, АЛЕКСАНДРА ШАЈНОВИЋ и СНЕЖАНА ШТРБАЦ

Институт за хемију, технологију и металургију, Универзитет у Београду, Његошева 12, 11000 Београд

Ерозија земљишта је проблем који утиче на пределе у различитим размерама и представља озбиљан изазов за управљање земљиштем и очување земљишта како у природним шумама тако и на ливадама. Циљ овог истраживања био је да се утврди како матична стена и начин коришћења утичу на физичко–хемијска својства земљишта на подручју Фрушке горе. Земљишта су подељена на пет типова стена: серпентинит, лапорац, трахит, шкриљац и лес, као и на два начина коришћења терена: шума и ливада. Са Фрушке горе узоркована су 23 шумска земљишта и 24 ливадска земљишта са дубине од 0–20 cm. Одређена су следећа својства: pH, електрична проводљивост (*EC*), редокс потенцијал (*Eh*), садржај органског угљеника (C_{org}), однос адсорпције натријума (*SAR*), величина агрегата и стабилност. Не постоји статистички значајна разлика у вредностима pH, *Eh*, *EC* и *SAR* између анализираних шумских и ливадских земљишта, али постоји статистички значајна разлика у садржају C_{org}. Може се закључити да велики утицај на физичко–хемијске особине земљишта имају изворни материјал и у нешто мањој мери начин коришћење земљишта.

(Примљено 21. децембра 2022, ревидирано 1. марта, прихваћено 3. марта 2023)

REFERENCES

1. D. Karlen, M. Mausbach, J. Doran, R. Cline, R. Harris, and G. Schuman, *Soil Sci. Soc. Am. J.* **61** (1997) 4 (https://doi.org/10.2136/sssaj1997.03615995006100010001x)

2. J. Haas, H. Schack-Kirchner, and F. Lang, *Eur. J. For. Res.* **139** (2020) 549 (https://doi.org/10.1007/s10342-020-01269-5)
3. R. Raison, P. Khanna, in *Soil Health and Climate Change*, B. P. Singh, A. L. Cowie, K. Y. Chan, Eds., Springer, Berlin, 2011, pp. 257–285, ISBN: 978-0-12-818032-7 (https://doi.org/10.1007/978-3-642-20256-8_12)
4. S. Stanchi, G. Falsone, and E. Bonifacio, *Solid Earth* **6** (2015) 403 (https://doi.org/10.5194/se-6-403-2015)
5. B. Wang, F. Zheng, M. J. M. Römkens, and F. Darboux, *Geomorphology* **187** (2013) 1 (https://doi.org/10.1016/j.geomorph.2013.01.018.M)
6. M. Kasanin-Grubin, E. Hukic, M. Bellan, K. Bialek, M. Bosela, L. Coll, M. Czacharowski, G. Gajica, F. Giammarchi, E. Gömöryová, M. del Rio, L. Dinca, S. Đogo Mračević, M. Klopčić, S. Mitrović, M. Pach, D. Randjelović, R. Ruiz-Peinado, J. Skrzyszewski, J. Orlić, S. Štrbac, S. Stojadinović, G. Tonon, T. Tosti, E. Uhl, G. Veselinović, M. Veselinović, T. Zlatanov, R. Tognetti, *Can. J. For. Res.* **51** (2021) (https://doi.org/10.1139/cjfr-2020-0361)
7. A. Cerda, *Soil Till. Res.* **57** (2000) 159 (https://doi.org/10.1016/S0167-1987(00)00155-0)
8. V. Ćirić, M. Manojlović, Lj. Nešić, M. Belić, *J. Soil Sci. Plant Nutr.* **12** (2012) 689 (http://dx.doi.org/10.4067/S0718-95162012005000025)
9. M. Al-Kaisi, in *Proceedings of the Integrated Crop Management Conference*, Digital Repository of Iowa State University of Science and Technology, Ames, IA, 2001, p. 55 (https://doi.org/10.31274/icm-180809-676)
10. M. Manojlović, V. Aćin, *Letopis naučnih radova* **31** (2007) 187 (https://scindeks.ceon.rs/article.aspx?artid=0546-82640701187M) (in Serbian)
11. Z. Jiang, H. Liu, H. Wang, J. Peng, J. Meersmans, S. M. Green, T. A. Quine, X.Wu, Z. Song, *Nat. Commun.* **11** (2020) 2392 (https://doi.org/10.1038/s41467-020-16156-1)
12. P. Rengasamy, R.S.B. Greene, G.W. Ford, A.H. Mehanni, *Aust. J. Soil Res.* **22** (1984) 413 (https://doi.org/10.1071/SR9840413).

Journal of the Serbian Chemical Society
JSCS@tmf.bg.ac.rs • www.shd.org.rs/JSCS
J. Serb. Chem. Soc. 88 (5) S145–S146 (2023) *Supplementary material*

SUPPLEMENTARY MATERIAL TO

The influence of geological setting and land use on the physical and chemical properties of the soil at the Fruška Gora Mountain

MILICA KAŠANIN-GRUBIN, GORICA VESELINOVIĆ, NEVENA ANTIĆ*, GORDANA GAJICA, SANJA STOJADINOVIĆ, ALEKSANDRA ŠAJNOVIĆ and SNEŽANA ŠTRBAC

Institute of Chemistry, Technology and Metallurgy, University of Belgrade, Njegoševa 12, 11000 Belgrade, Serbia

J. Serb. Chem. Soc. 88 (5) (2023) 551–562

SAMPLING DETAILS

The Fruška Gora Mt. is located in the south of the Pannonian Plain and stretches between the Danube and the Sava River. On the south and west, it is framed by the loess plains of Srem. This mountain range has a length of 75 km, and a maximum width of about 15 km. With the highest peak (Crveni Čot) of 539 m, Fruška Gorabelongs to low mountains. The geological diversity, together with the specific microclimate, contributed to the development of a large number of different species of plants and animals that live there, so in 1960 Fruška Gora Mt. was declared a national park.

Geological composition of the Fruška Gora Mt. is heterogeneous and consists of various types of rocks of different ages. The central part of the mountain has peaks with an average height of 440 to 460 m above sea level and mainly consists of serpentinites, while the western part is flat with an average height of about 200 m above sea level built of limestone. The eastern part is at a lower altitude and consists of sedimentary rocks, mainly loess.

Total of 47 soil samples from the Fruška Gora Mt. (Fig. S-1) were analyzed for determining the difference between land use and geological settings. Twenty-three samples of forest soil and 24 samples of meadow land were analyzed. The soils used in this study were developed on five bedrock types: serpentinite (Se), marl (M), trachyte (T), shale (Sh), loess (L) and two land use types forest (F) and meadow (M). Fig. 1 shows sampling locations with the indicated badrock type and land use: MM – marl meadow (9 samples), MF – marl forest (6 samples), SeF – serpentinite forest (6 samples), SeM – serpentinite meadow (9 samples), ShF – shale forest (6 samples), TF – trachyte forest (5 samples), LM – loess meadow (6 samples).

All samples were taken from the depth of 0–20 cm. Samples cleaned of plant residues were dried for seven days in laboratory conditions at room temperature, and then representative samples were selected using the chessboard method.

* Corresponding author. E-mail: nevena.antic@ihtm.bg.ac.rs

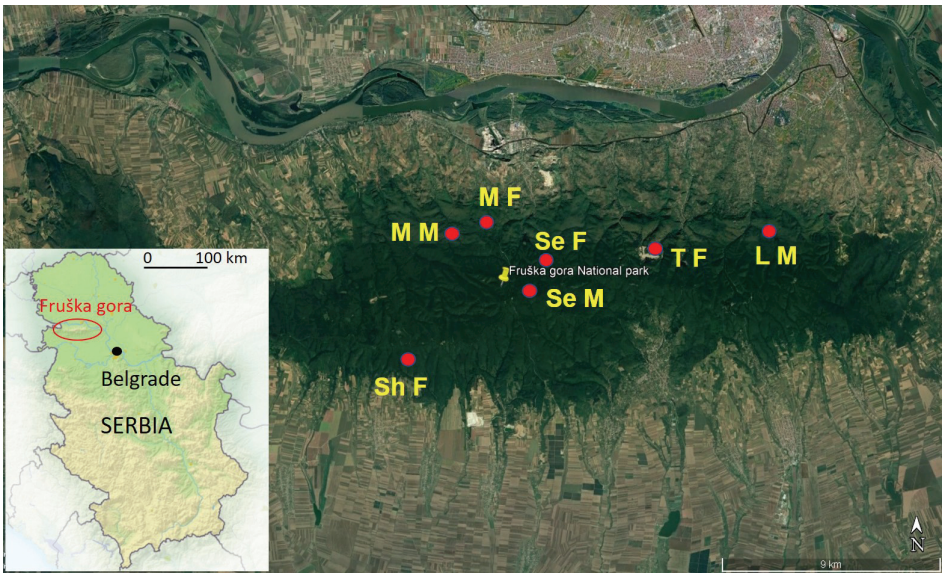

Fig. S-1. Map of Serbia and Fruška GoraMt. with marked sampling locations. MM – marl meadow, MF – marl forest, SeF – serpentinite forest, SeM – serpentinite meadow, ShF – shale forest, TF – trachyte forest, LM – loess meadow.

Journal of the Serbian Chemical Society
JSCS-info@shd.org.rs • www.shd.org.rs/JSCS
J. Serb. Chem. Soc. *88* (5) 563–575 (2023)
JSCS–5646
Original scientific paper
Published 25 March 2023

Using the Escape Room game-based approach in chemistry teaching

ALEKSANDRA NAUMOSKA*, HARI DIMESKI and MARINA STOJANOVSKA

Ss. Cyril and Methodius University, Faculty of Natural Sciences and Mathematics, Institute of Chemistry, Arhimedova 5, 1000 Skopje, Republic of North Macedonia

(Received 28 December 2021, revised 13 December, accepted 15 December 2022)

Abstract: In recent years, the Escape Room approach has been applied in teaching of various content. Aside from being enjoyable, the Escape Room activities actively involve all students in the class and promote their creative, critical and logical thinking, problem solving, communication and cooperation, as well as positive attitude towards the subject. To encourage the engagement and motivation of ninth-grade students, activities were developed regarding the topic of exothermic and endothermic reactions, through the use of Google Forms and Breakout Rooms option in MS Teams. The application of this approach helps students to master the teaching content in a more interesting way, encourages discussion and cooperation among students. 244 9th grade students from five primary schools participated in the research. Apart from encouraging engagement and motivation among students, one of the objectives of the research was to examine their opinions regarding the implemented Escape Room activities. For this purpose, the motivation of students towards Science Learning (SMTSL) and Activity Perception Questionnaire (APQ-ER) instruments were implemented. The research results, positive atmosphere during the classes, and high students' satisfaction after completing the activities indicate numerous benefits of the implementation of the Escape Room approach in chemistry teaching.

Keywords: game-based learning; exothermic and endothermic reactions; IMI; SMTSL.

INTRODUCTION

A game is a type of play where all participants should follow defined rules.[1] They are usually recreational, but can also be used as a pedagogical tool if they are applied to learning in a particular area. Games in education are often used by teachers who have younger students, although it has been proven that older students also enjoy a well-designed educational game that can stimulate them to

* Corresponding author. E-mail: aleksandra.18@hotmail.com
https://doi.org/10.2298/JSC211228088N

be more effectively involved in the class.[2] The application of many educational games is mostly focused on improving critical thinking skills in processing various teaching contents in different subjects. They are an excellent method for developing students' creativity and gaining research and problem-solving skills. Numerous studies have been performed in the past on how the usage of educational games affects students' motivation.[3–7] Many of them refer to mathematical and language cognitive skills,[3,5] and some describe the value of computer games as a motivator.[4] Chemistry is also one of the subjects for which educational games have been developed, and one of the most popular topics for their implementation is the Periodic Table of Elements.[7]

The Escape Room approach has become popular around the world in the recent years.[8–10] It has a relatively short history. The first Escape Room activity was organized in Kyoto, Japan, in 2007, as a single room game for teams of 5–6 players.[11] According to Nicholson,[11] Escape Rooms are live-action team-based games in which players (in this case, students) are given tasks, usually to solve a variety of puzzles, in order to escape from the room. This means that, in a limited amount of time, players should accomplish a specific goal determined by the coordinator of the game. Different versions of this activity can be developed, but the main idea is to create a context where players have to solve different tasks as a group within a given time.[12] Having this in mind, in 2019 seminars for professional development of chemistry teachers were held in the Republic of Macedonia and in the Republic of Serbia,[13,14] the aim of which was to educate teachers on how to apply this approach in chemistry teaching.

In contemporary education, Escape Room activities, which are based on game-based learning, offer opportunities related to active learning, self-regulation, fun and social interaction.[15–18] The teachers need to find a way to motivate their students and keep their attention, while developing their 4C skills (creativity, communication, collaboration, critical thinking). To create a good educational Escape Room activity, the teacher needs to effectively link the goals of the game with the goals of the teaching content. Preparing such activity takes time, but once prepared, games can be used many times with slight modifications.[19] Carefully prepared game-based activities should enable greater students' participation and mental involvement, which would then lead to increased motivation and interest in the subject and development of positive attitude toward chemistry.[19] Game-based lesson promotes much greater student engagement than the traditional lesson because students want to win the game.

This approach can be used for elaboration of teaching content in various subjects or topics, and the effects of its implementation in chemistry teaching have been examined in several studies.[20–22] In recent years, the Escape Room approach has become very popular in STEM classrooms. Chantal and Belova[20] conducted a systematic literature review to gain insight into the prevalence of this

type of educational games and the need for further development in this field. The authors searched the common databases and analyzed 93 journal articles, book chapters, and conference papers that targeted a specific educational level, were designed for formal educational settings and were aimed at STEM education. 15 out of 93 publications dealt with Escape Rooms in secondary and tertiary chemistry education (12 chemistry activities included experiments or lab-based activities), developed either on a specific topic or a combination of several ones. The results of their study showed that there is a need to develop more easily adaptable Escape Rooms, and provide further evidence regarding the effects of their implementation in the classroom. This in-depth research did not uncover studies that dealt with the topic of exothermic and endothermic reactions and, therefore, it is clear that future research should focus on the implementation of Escape Rooms in primary education, which, due to the age of the students, requires simplicity in the solving of the puzzles.

Still, it is worth mentioning that in order to implement the game-based learning approach, teachers in primary and secondary education need to be educated on how to apply it within the teaching process. First of all, the teacher needs to know how to design such an educational game and carefully plan all the details for its application in the classroom. The game should be prepared before the beginning of the classes and the puzzles should be pre-tested. Teachers should also be aware of the lesson time limit and all Escape Room activities must end before the bell rings.[19]

The application of this approach offers many opportunities to master the teaching content elaborated in primary and secondary education. The idea was to develop creative and interactive lessons, which, apart from the enjoyment, would promote the engagement and motivation to master the teaching content through the game, as well as a more positive attitude towards chemistry among students. It is expected that the Escape Room approach would provide a large number of benefits to students. Apart from the advantages, application of this approach also has disadvantages, such as the limited time to answer the puzzles.[8] If this activity is realized online, problems with the internet connection can be mentioned as a disadvantage, especially when the students use this activity for the first time. Therefore, a special challenge was to see if online teaching, which was dominant in schools during the pandemic, enabled better digital competencies for both students and teachers. Furthermore, conducting Escape Room activities in an online environment implies that students will not be able to engage in practical activities, such as experimenting, or make tactile observations.

EXPERIMENTAL

The aim of the research

The objectives of this research were to apply an innovative and creative approach in chemistry teaching to increase the engagement and motivation of 9th grade students in review-

ing the concepts of exothermic and endothermic reactions. The primary idea of the research was to, by using the Escape Room activities, encourage students to participate actively in the classes and to increase their interest and motivation to learn chemistry. The implementation of Escape Room activities, besides helping the students to master the teaching content in a more interesting way, was also aimed at encouraging discussion and collaboration within the group, as well as competition among groups. In this way, students had the opportunity to improve their communicational skills, and develop their creative, critical and logical thinking, as well as a positive attitude toward chemistry classes.

In addition, after the end of the classes, the opinion of the students regarding the conducted activities was examined.

The sample

In order to examine whether the application of Escape Room activities affects the engagement and motivation of 9th grade students in reviewing the topic of exothermic and endothermic reaction, the research was conducted in five primary schools from cities in different regions of the country. The research included a total of 244 9th grade students (13–14-years-old) who attend classes in different languages of instruction, *i.e.*, 195 in Macedonian and 49 in Turkish. The study was conducted in accordance with school rules, and the students and their subject teachers agreed to voluntarily participation. Collection of students' opinions after completing the activities was anonymous using Google Forms. A total of 193 students (123 girls and 70 boys) filled in the APQ-ER items, and 119 students (72 girls and 47 boys) responded to the SMTSL items.

Design

The research was divided into several phases:

1) preparatory phase (preparation and testing of the puzzles),
2) delivering the lesson using Escape Room activities (reviewing relevant concepts from this topic),
3) distribution of Activity Perception Questionnaire for Escape Room activities, APQ-ER (filling in the questionnaire by the students in order to express their opinion regarding the implemented activity),
4) distribution of Students' Motivation toward Science Learning questionnaire, SMTSL (examining students' opinions about their motivation for learning chemistry) and
5) analysis of the obtained data using the SPSS Statistics 26 software package.

This research consisted of reviewing the main concepts related to the last topic of the 9th grade chemistry curriculum regarding exothermic and endothermic reactions by using the Escape Room game-based approach. These activities were conducted during April–May 2021. Considering the fact that the last school year in the Republic of Macedonia took place online, this activity was prepared and realized with the help of MS Teams and Google Forms.

Preparing Escape Room puzzles is time-consuming, whether working face-to-face or online. Thus, for example, if the activities are done in the classroom, boxes, padlocks, envelopes, markers, sheets of paper for solving puzzles, *etc.*, are needed. All of this should be prepared by the teacher before the class starts. On the other hand, these things are not required when working online, but in this case it is necessary to create online puzzles (for example, through Google Forms) and profound skill of the teacher to lead the groups of students (divided into breakout room) is required.

Namely, at the beginning of the class, students were divided into several groups using the breakout rooms option by MS Teams. Depending on the number of students in the class,

they were usually divided into 5–6 groups of 3–4 students. With the help of the subject teacher, the students were previously divided into groups (the selection of students was made prior to the class), depending on their achievement in chemistry. This was done to ensure a fair as competition as possible, and to encourage communication and mutual assistance between students within the group. When all the students were in their group, the researcher sent them the link from the Google Forms and she entered all the groups to check on the students and offer help if needed. One student wrote down the names of all the members in the group and shared his/her screen with other students within a group. The students in the group were able to collaborate, communicate, discuss and share ideas freely. When they were convinced of the correctness of the answers, one member of the group wrote the correct answers in the empty fields of the form (Google Forms) and pressed the submit option. In such a way, a competition between the groups was felt because students had a time limit – they had to finish solving the puzzles in 30 min. In fact, the duration of a school lesson is 40 min, but some time is needed at the beginning and at the end of the lesson for explanations and/or reflection. If students had the whole class at their disposal, they would have more time to think about solving the puzzles.

Description of the games

The Escape Room activities that were prepared for this research consisted of three puzzles the students had to answer to win, *i.e.*, they needed to solve the puzzles and "escape". These puzzles were prepared by the authors taking into account the learning objectives defined in the ninth-grade chemistry curriculum. The Escape Room activity along with these puzzles were piloted among 77 nineth-graders.[23]

The first puzzle (Fig. 1), given as a maze, required an answer to a simple question, but the way the question was posed arouses students' interest.[24]

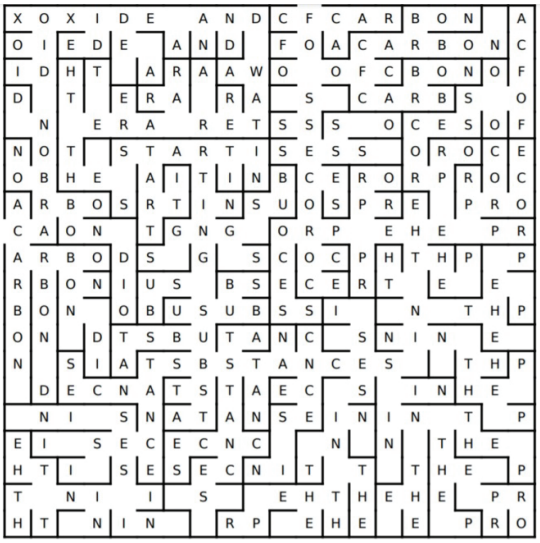

Fig. 1. Puzzle 1 – Maze.

Students had to find the way out of the maze puzzle and, in that way, to discover the question they needed to answer. If the answer was correct, the code had been discovered. In

our case, the question was: Carbon dioxide and water are the starting substances in the process.

In the second puzzle (Fig. 2) chemical formulas of several compounds were given. It was necessary to find the connection between them to discover the code. First, students had to find out which substances are the reactants, and which are products, then they had to write the chemical equation and finally balance it by using stoichiometric coefficients. When they had finished balancing the chemical equation, the inserted numbers revealed the code. The balanced chemical equation was: $2C_2H_6 + 7O_2 \rightarrow 4CO_2 + 6H_2O$.

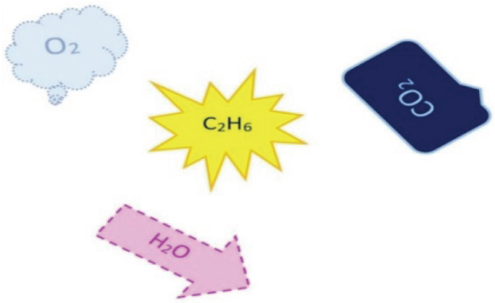

Fig. 2. Puzzle 2 – Chemical formulas of compounds.

The third puzzle consisted of three multiple choice questions. Each question had four options, one of which was the correct answer and other three were distractors (Fig. 3). The aim of this game was to repeat some important segments of the exothermic and endothermic reactions topic. After the students had answered the questions, they were supposed to discover the code using the symbols in the table.

	A	B	C	D
1	@	☼	♫	♥
2	♫	♥	@	☼
3	♥	@	☼	♫

@ = 1 ☼ = 2 ♫ = 3 ♥ = 4

1. An example of an endothermic reactions is:
A. Neutralization
B. Combustion
C. Replacement
D. Electrolysis

2. What is released in the process of photosynthesis?
A. Carbon dioxide
B. Carbon monoxide
C. Oxygen
D. Hydrogen

3. Evaporation is an:
A. Endothermic reaction
B. Endothermic process
C. Exothermic reaction
D. Exothermic process

Fig. 3. Puzzle 3 – Multiple choice questions.

The first question was: An example of an endothermic reactions is: a) neutralization, b) combustion, c) replacement or d) electrolysis. The second question was: Which of these compounds represent a product of photosynthesis: a) carbon dioxide, b) carbon monoxide, c) oxygen or d) hydrogen. The third question was: Evaporation is: a) endothermic reaction, b) endothermic process, c) exothermic reaction or d) exothermic process.

Instruments

One of the aims of this research was to examine students' opinion about the conducted activities during the class. For this purpose, students were administered a questionnaire in which they expressed their opinions on how interesting and enjoyable the activities were, stated the value and the usefulness of those activities in the teaching and learning process, and shared their beliefs about their engagement and effort that they had invested in the activities. Two questionnaires were used: Activity Perception Questionnaire (APQ-ER), as part of the Intrinsic motivation inventory (IMI)[25] and Students' Motivation Toward Science Learning (SMTSL).[26]

The IMI questionnaire was used to assess students' subjective opinions and experiences related to certain activities conducted in the classroom. It was a Likert type questionnaire, where 1 means the respondent does not agree with the statement at all and 7 means that (s)he completely agrees with the statement. The instrument assesses students' interest/enjoyment, perceived competence, effort, as well as the importance of the activity, value/usefulness, felt pressure/tension, and perceived choice while performing a given activity. Recently, a seventh subscale was added to tap the experiences of relatedness. This questionnaire has been used in research in various field, such as: sport,[27] information and communication technology,[28] science education,[29] first language and mathematics learning,[30] *etc.* For the purposes of this study, the APQ-ER was used, which is part of the IMI questionnaire. It was constructed using items from four subscales, each comprised of 4–8 items: interest/enjoyment (*e.g.*, While I was doing this activity, I was thinking about how much I enjoyed it.), value/usefulness (*e.g.*, I would be willing to do this again because it has some value to me.), effort/importance (*e.g.*, It was important to me to do well at this task.), and pressure/tension (*e.g.*, I felt very tense while doing this activity.), and contained a total of 23 items.

The SMTSL questionnaire is also a Likert type questionnaire and contains 35 items, divided into six categories related to students' motivation to study science: self-efficacy (*e.g.*, I am sure that I can do well on science tests.), active learning strategies (*e.g.*, When new science concepts that I have learned conflict with my previous understanding, I try to understand why), science learning value (*e.g.*, I think that learning science is important because I can use it in my daily life.), performance goal (*e.g.*, I participate in science courses to perform better than other students.), achievement goal (*e.g.*, During a science course, I feel most fulfilled when I am able to solve a difficult problem.), and learning environment stimulation (*e.g.*, I am willing to participate in this science course because the students are involved in discussions.). The participants were asked to give their opinions on each of the offered statements, so that they will express the degree of agreement with a certain statement by circling one of the offered possibilities (1–5), as follows: 1, if (s)he does not agree with the statement at all; 2, if (s)he disagrees with the statement; 3, if (s)he does not have an opinion/idea about the statement; 4, if (s)he agrees with the statement, and 5, if (s)he completely agrees with the statement. This questionnaire is well known in the literature and has been used in many studies to examine the students' motivation to study physics,[31] biology,[32] Greek,[33] *etc.*

In the statements of both questionnaires, the word science was replaced by the word chemistry.

Procedure and data analysis

For the purpose of the present research, the SMTSL questionnaire and the four subscales from the IMI questionnaire were translated from English to Macedonian. Five university professors experienced in educational research from two faculties were engaged in the translation procedure. All five versions of the two questionnaires were compared and the disagreements were resolved. The translated questionnaires were then prepared in Google Forms, and the

students filled them out individually and anonymously during the last 5–7 min of the lesson. Students were told that the questionnaire would not affect their grade and that there were no correct and incorrect answers. Furthermore, they were encouraged to give an opinion on each statement and were explained that this will be used for scientific purposes only. The obtained results from both questionnaires were analyzed using the software package SPSS Statistic 26.

RESULTS AND DISCUSSION

In order to examine the internal consistency, taking into account the results of all the items for each subscale, the results were analyzed and the mean, standard deviation and the Cronbach' alpha reliability coefficient were calculated (Tables I and II). To score the APQ instrument, the following procedure was conducted. First, reversed scores were calculated for the items for which an R is shown after them by subtracting the item response from 8. The letter R indicates that the given statement is written with the opposite meaning from that of the other statements in that category. After that, subscale scores were calculated by averaging across all of the items on that subscale and were used in the analyses of this study.

TABLE I. Means, standard deviations and Cronbach's alpha reliability coefficient for APQ--ER instrument

Scale	Number of items	APQ-ER		
		Mean	*SD*	Cronbach's alpha
Interest/Enjoyment	6	6.09	1.46	0.889
Value/Usefulness	8	6.01	1.38	0.994
Effort/Importance	5	5.07	1.90	0.646
Pressure/Tension	4	2.25	1.78	0.647
Total	23	5.17	2.12	0.837

TABLE II. Means, standard deviations and Cronbach's alpha reliability coefficient for SMTSL instrument

Scale	Number of items	SMTSL		
		Mean	*SD*	Cronbach's alpha
Self-efficacy	7	4.00	1.16	0.819
Active learning strategies	8	4.32	0.89	0.879
Science learning value	5	4.12	0.98	0.832
Performance goal	4	3.17	1.52	0.825
Achievement goal	5	4.26	0.97	0.806
Learning environment stimulation	6	3.87	1.19	0.822
Total	35	4.01	1.16	0.901

As can be seen from Table I, the Cronbach' alpha reliability coefficient for the whole APQ-ER instrument was 0.837, ranging from 0.646 to 0.994 for the subscales. Following the cutoff criteria of Cohen,[34] it can be concluded that

Cronbach's alpha reliability coefficient revealed acceptable internal consistency for all four subscales, which was also confirmed by Choi[35] and Monteiro.[30]

From the obtained results of the questionnaire, it could be concluded that most of the students found the activity as fun, enjoyable and interesting. Namely, on a scale from 1 to 7, the agreement with the items from the interest/enjoyment subscale, *i.e*., the mean was 6.09. The mean for the value/usefulness subscale was also high (6.01). The students felt that this activity was important for their success and progress, but it could also enable them to achieve better results and improve their attention during the class. The nature of the Escape Room activities, which is based on teamwork, communication, cooperation and problem solving, certainly contributes to this. This activity affects not only the engagement and motivation of students, but also touches the cognitive and affective domain of leaning.

A lower value (5.07) was observed for the items of the effort/importance subscale. The value is shifted to the right from the mid-point of the scale, but this shift was not as pronounced as in the previous two subscales. Most of these items refer to the students' estimation of how much effort they have put into the activity, *i.e*., in solving the three puzzles. Based on the results, it could be assumed that the puzzles were not too difficult to master, and due to the fun nature of the activity, the students did not feel like they were in a usual" review class. However, an item mean value of 6.20 indicates that it was important for the students to complete the task successfully. It should be mentioned here that negatively formulated items could cause some confusion among students.

Considering the fact that the students were encountering this type of activity for the first time, the aim was to examine whether the students were tense and nervous during this class. The analysis of the students' answers to the questionnaire showed that they were not nervous during the class, but relaxed, in spite of the competitive nature of the activity, as well as the limited working time and problems with the internet connection, could cause some tension. This can be concluded from the mean (2.24) obtained for the last subscale, pressure/tension.

From Table II, the value for the Cronbach' alpha reliability coefficient for the whole SMTSL instrument was 0.901, ranging from 0.806 to 0.879 for the six categories. Dermatzaki[33] and Tsai[31] also obtained high values for the Cronbach's alpha reliability coefficient for this instrument.

Students' motivation was estimated based on the means of their scores for each subscale and for the whole questionnaire.[36] According to the Cavaş's classification system,[37] a high level of motivation includes means between 4.41 and 5.00, a medium level of motivation includes means between 4.40 and 3.39, and a low motivation includes means lower than 3.38. From the results presented in Table II, it could be seen that students had medium motivation towards chemistry learning since their mean score was 4.01. The mean for each subscale were con-

sidered medium as well, except for the performance goal scale where their motivation was low (3.17 < 3.38).

CONCLUSIONS

The Escape Room game-based approach was applied in order to increase the engagement and the motivation of 9th grade students in reviewing the concepts of exothermic and endothermic reactions. In addition, the applied approach was used to improve their communication skills, encourage their creative, critical, and logical thinking, and promote their ability to solve problems. Nowadays this approach is often applied in teaching various subjects, and it arouses additional interest for both the students and the teachers.[38-41]

The research was conducted on a total sample of 244 students from five schools located in different cities. One of the main goals of the research was to examine the students' opinions regarding the implemented activities, and for that purpose the data were collected by SMTSL questionnaire and APQ-ER, which was constructed using items from the IMI questionnaire. The analysis of the collected data showed that this approach in a great extent affects the improvement of teaching. Students were more engaged during the lessons and actively participated in all activities. In this way they were more motivated and more satisfied with the achieved results. Moreover, the atmosphere in the class was very positive and it was visible that students were enjoying the puzzles.

It is worth mentioning some of the limitations of this study. The students participating in the research encountered these Escape Room activities for the first time, so they may have needed some time to cope at first, but the collected data showed that they were not nervous while solving the puzzles. However, the students' answers to the Google Forms in solving the puzzles were received in a relatively short time from the beginning of the class and there was at least one winner in each class. This, in turn, means that the puzzles were solvable within one school class and with a successful strategy and cooperation within the group, the answers could have been reached faster.

In addition, the study was conducted only on 9th grade students on one topic. More such activities related to various topics are needed to obtain more relevant results and to draw more comprehensive conclusions about the applicability of Escape Room activities in chemistry teaching.

ИЗВОД

ПРИМЕНА ПРИСТУПА ЗАСНОВАНОГ НА ИГРИ *ESCAPE ROOM* У НАСТАВИ ХЕМИЈЕ

ALEKSANDRA NAUMOSKA, HARI DIMESKI и MARINA STOJANOVSKA

SS. Cyril and Methodius University, Faculty of Natural Sciences and Mathematics, Institute of Chemistry, Arhimedova 5, 1000 Skopje, Republic of North Macedonia

Последњих година у настави посвећеној различитим садржајима примењује се приступ према правилима игре *Escape Room*. Осим што су активности пријатне, оне у игри

Escape Room активно укључују све ученике у разреду и покрећу њихово креативно, критичко и логично мишљање, решавање проблема, комуникацију и сарадњу, као и позитиван однос према предмету. Да би се подстакло ангажовање и мотивација ученика деветог разреда, развијене су активности на тему егзотермне и ендотермне реакције, помоћу апликације *Google Forms* и *Breakout Rooms* у *MS Teams*. Примењени приступ помаже ученицима да на занимљивији начин савладају наставне садржаје, подстиче њихову дискусију и међусобну сарадњу. У истраживању је учествовало 244 ученика 9. разреда из пет основних школа. Осим подстицања ангажовања и мотивације ученика, један од циљева истраживања био је и испитивање њиховог мишљења о реализованим активностима у оквиру игре *Escape Room*. Примењена су зато два инструмента: упитник за испитивање мотивације ученика за учење науке (SMTSL) и упитник о перцепцији активности (APQ-ER). Резултати истраживања, позитивна атмосфера током наставе и велико задовољство ученика након завршених активности указују на бројне предности примењеног приступа у настави хемије.

(Примљено 28. децембра 2021, ревидирано 13. децембра, прихваћено 15. децембра 2022)

REFERENCES

1. V. S. Zirawaga, A. I. Olusanya, T. Madaku, *J. Educ. Pract*. **8** (2017) 55 (https://files.eric.ed.gov/fulltext/EJ1143830.pdf)
2. M. J. Costa, *J. Chem. Educ*. **84** (2007) 977 (https://dx.doi.org/10.1021/ed084p977).
3. P. M. Noemí, S. H. Máximo, *Univers. J. Educ. Res.* **2** (2014) 230 (https://dx.doi.org/10.13189/ujer.2014.020305)
4. K. Becker, *JCSC* **17** (2001) 23 (https://dx.doi.org/10.11575/PRISM/30356).
5. J. Li, S. Ma, L. Ma, *Phys. Procedia* **33** (2012) 1749 (https://dx.doi.org/10.1016/j.phpro.2012.05.280)
6. J. Hamari, D. J. Shernoff, E. Rowe, B. Coller, J. Asbell-Clarke, T. Edwards, *Comput. Hum. Behav.* **54** (2016) 170 (https://dx.doi.org/10.1016/j.chb.2015.07.045)
7. A. J. Franco-Mariscal, J. M. Oliva-Martínez, M. L. Almoraima Gil, *J. Chem. Educ.* **2** (2014) 278 (https://dx.doi.org/10.1021/ed4003578)
8. Veldkamp, M. Ch. Knippels, W. van Joolingen, *Front. Educ.* **6** (2021) 1 (https://dx.doi.org/10.3389/feduc.2021.622860)
9. Manzano-León, J. M. Rodríguez-Ferrer, J. M. Aguilar-Parra, A. M. Martínez, A. L. de la Rosa, D. S. García, J. M. Fernández-Campoy, *Int. J. Environ. Res. Public Health* **18** (2021) 7304 (https://dx.doi.org/10.3390/ijerph18147304)
10. N. Dietrich, *J. Chem. Educ.* **95** *(*2018) 996 (https://dx.doi.org/10.1021/acs.jchemed.7b00690)
11. S. Nicholson, *Peeking Behind the Locked Door: A Survey of Escape Room Facilities*, 2015 (http://scottnicholson.com/pubs/erfacwhite.pdf)
12. L. H. Taraldsen, F. O. Haara, M. S. Lysne, P. R. Jensen, E. S. Jeensen, *Educ. Inq.* (2020) 1 (https://dx.doi.org/10.1080/20004508.2020.1860284)
13. M. Stojanovska, *Maced. J. Chem. Chem.* **38** (2019) 141 (https://www.mjcce.org.mk/index.php/MJCCE/article/view/1833/711)
14. M. Stojanovska, in *Proceedings of April Days on Chemistry Teaching – 30th Professional training for chemistry teachers and 3rd Conference of methodology in chemistry teaching*, Book of Abstracts, Serbian Chemical Society, Belgrade, Serbia, 2019, p. 3

15. W. Admiraal, J. Huizenga, S. Akkerman, G. ten Dam, *Comput. Hum.* **27** (2011) 1185 (https://dx.doi.org/10.1016/j.chb.2010.12.013)
16. J. C. Burguillo, *Comput. Educ.* **55** *(*2010) 566 (https://dx.doi.org/10.1016/j.compedu.02010.02.018)
17. Y. Orlik, E. Gil, L. C. Hernández, *Nat. Sci. Educ.* **3** (2005) 47 (https://dx.doi.org/10.48127/gu-nse/05.2.47b)
18. R. Peleg, M. Yayon, D. Katchevich, M. Moria-Shipony, R. Blonder, *J. Chem. Educ*. **96** (2019) 955 (https://dx.doi.org/10.1021/acs.jchemed.8b00406)
19. M. Stojanovska, V. Milanović, D. Trivić, *Chem. in Act*. **116** (2020) 49 (https://www.chemistryireland.org/wp-content/uploads/2020/12/Chemistry-in-Action-Autumn-2020-Issue-116.pdf)
20. Lathwesen, N. Belova, *Educ. Sci.* **11** (2021) 308 (https://doi.org/10.3390/educsci11060308)
21. J. W. J. Ang, Y. N. A. Ng, R. S. Liew, *J. Chem. Educ*. **97** (2020) 2849 (https://doi.org/10.1021/acs.jchemed.0c00612)
22. S, Marín, P. R. de Atauri, E. Moreno, S. Pérez-Torras, J. Farràs, S. Imperial, M. Cascante, J. J. Centelles, *Int. J. Eng. Sci. Technol.* **3** (2021) 155 (https://doi.org/10.46328/ijonest.59)
23. K. Rusevska, A. Blazevska, M. Stojanovska, *IPEM J. Innov. Teacher Educ.* **7** (2022) 27 (ISSN 2581-5881)
24. M. Stojanovska, in *Proceedings of the International Conference on Education in Mathematics, Physics and Related Sciences,* Society of Physicists of Macedonia, Skopje, North Macedonia, 2019, 140
25. *Intrinsic Motivation Inventory (IMI), Center for Self-Determination Theory*, https://selfdeterminationtheory.org/intrinsic-motivation-inventory/#:~:text=Scale%20Description,target%20activity%20in%20laboratory%20experiments (assessed March, 2021)
26. H. L. Tuan, C. C. Chin, S. H. Shieh, *Int. J. Sci. Educ*. **27** (2005) 639 (https://dx.doi.org/10.1080/0950069042000323737)
27. M. Gutiérrez, N. Caus, L. M. Ruiz, *J. Leis. Res.* **43** (2011) 355 (https://dx.doi.org/10.1080/00222216.2011.11950241)
28. E. Y. Leng, W. Z. bte Wan Ali, R. Baki, R. Mahmud, *Eurasia J. Math. Sci. Technol*. **6** (2010) 215 (https://dx.doi.org/10.12973/ejmste/75242)
29. Loukomies, D. Pnevmatikos, J. Lavonen, A. Spyrtou, R. Byman, P. Kariotoglou, K. Jauuti, *Res. Sci. Educ.* **43** (2013) 2517 (https://dx.doi.org/10.1007/s11165-013-9370-1)
30. V. Monteiro, L. Mata, F. Peixoto, *Psicol. Reflex, Crit.* **28** (2011) 434 (https://dx.doi.org/10.1590/1678-7153.201528302)
31. C. Tsai, H. L. Tuan, C. C. Chin, J. C. Chang, in *Proceedings of the 2*nd *NICE Symposium*, Graduate Institute of Science Education, National Taiwan Normal University, Taipei, Taiwan, July 30–31, 2007, No. 00057 (https://www.researchgate.net/profile/Hsiao-Lin-Tuan/publication/237634754_Investigating_the_Influence_of_Nested_Inquiry-Based_Instruction_Model_on_8th_Graders%27_Motivation_in_Learning_Physical_Science/links/56c7ed2c08ae96cdd0679db7/Investigating-the-Influence-of-Nested-Inquiry-Based-Instruction-Model-on-8th-Graders-Motivation-in-Learning-Physical-Science.pdf)
32. Mavrakaki, *Int. J. Biol. Educ.* **4** (2015) 78 (https://dx.doi.org/10.20876/ijobed.16761)
33. Dermatzaki, D. Vavougid, K. Kotsis, *Eur. J. Psychol. Educ.* **28** (2013) 747 (https://dx.doi.org/10.1007/s10212.012.0138.1)

34. L. Cohen, L. Manion, K. Morrison, *Research Methods in Education*, Routledge Falmer, London, 2007, p.506 (https://doi.org/10.4324/9780203029053)
35. Choi, T. Mogami, A. Medalia, *Schizophr. Bull*. **36** (2010) 966 (https://doi.org/10.1093/schbul/sbp030)
36. H. Andressa, E. Mavrikaki, I. Dermitzaki, *Int. J. Biol. Educ.* **4** (2015) 78 (https://dx.doi.org/10.20876/ijobed.16761)
37. P. Cavaş's, *Sci. Educ. Int.* **22** (2011) 31 (https://files.eric.ed.gov/fulltext/EJ941653.pdf)
38. Jiménez, N. Aris, A. A. Magreñán, L. Orcos, *Sci. Educ.* **10** (2020) 271 (https://dx.doi.org/10.3390/educsci10100271)
39. A. Kinio, L. Dufresne, T. Brandys, P. Jetty, *J. Surg. Educ.* **76** (2019) 134 (https://dx.doi.org/10.1016/j.jsrug.2018.06.030)
40. B. C. T. Gilbert, M. L. Clapson, A. Musgrove, *J. Chem. Educ.* **97** (2020) 4055 (https://dx.doi.org/10.1021/acs.jchemed.0c00863)
41. Queiruga-Dios, M. J. S. Sánchez, M. Q. Dios, V. G. Martínez, A. H. Encinas, *Mathematics* **8** (2020) 166 (https://dx.doi.org/10.3390/math8020166).